

AD-A071 929

NAVAL POSTGRADUATE SCHOOL MONTEREY CA  
NUCLEAR GIANT MULTIPOLE RESONANCES BY INELASTIC ELECTRON SCATTE--ETC(U)  
MAY 79 F R BUSKIRK  
NPS-61-79-009

F/G 20/8

NL

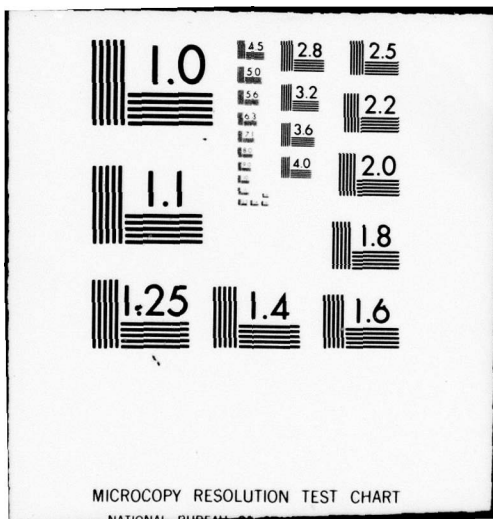
UNCLASSIFIED

| OF |  
ADA  
071929

FFC  
FILM



END  
DATE  
FILED  
8-79  
DDC



~~LEVEL~~

2

NPS 61-79-009

# NAVAL POSTGRADUATE SCHOOL

## Monterey, California

DA071929



DDC  
REPRODUCED  
JUL 30 1979  
REFUGEE

DDC FILE COPY

### NUCLEAR GIANT MULTIPOLE RESONANCES BY INELASTIC ELECTRON SCATTERING

Fred R. Buskirk

Final Technical Report  
Project PHY 76 23886  
(1 Nov 1976 to 31 July 1979)

Sponsor: National Science Foundation

Approved for public release; distribution unlimited

Prepared For: National Science Foundation  
Washington, DC 20550

79 07 27 055

NAVAL POSTGRADUATE SCHOOL  
Monterey, California

Rear Admiral Tyler F. Dedman  
Superintendent

Jack R. Borsting  
Provost

The work reported herein was supported by the National Science Foundation.

Reproduction of all or part of this report is authorized.

This report was prepared by:

*Fred R Buskirk*  
FRED R. BUSKIRK  
Professor of Physics

Reviewed by:

*K. E. Woehler*  
K. E. Woehler, Chairman  
Department of Physics and Chemistry

Released by:

*William M. Tolles*  
William M. Tolles  
Dean of Research

NPS-61-79-009

NATIONAL SCIENCE FOUNDATION  
Washington, D.C. 20550

SUMMARY OF COMPLETED PROJECT

Form Approved  
OMB No. 99R0013

Please read instructions on reverse carefully before completing this form.

1. INSTITUTION AND ADDRESS Dept. of Physics and Chemistry Naval Postgraduate School Monterey, CA 93940		2. NSF PROGRAM Nuclear Physics	3. PRINCIPAL INVESTIGATOR(S) Fred R. Buskirk Professor, Dept of Physics and Chemistry
4. AWARD NUMBER PHY 76 23886	5. DURATION (MOS) 33	6. AWARD PERIOD from 11/1/76 7/31/79	7. AWARDEE ACCOUNT NUMBER 56 928

8. PROJECT TITLE Nuclear Giant Multipole Resonances by Inelastic Electron Scattering			
---	--	--	--

9. SUMMARY (ATTACH LIST OF PUBLICATIONS TO FORM)

→ Inelastic electron scattering experiments were performed with the Naval Postgraduate School 110 MeV Linac. The investigation included  $^{238}\text{U}$ ,  $^{140}\text{Ce}$ ,  $^{89}\text{Y}$ ,  $^{60}\text{Ni}$ ,  $^{58}\text{Ni}$  and  $^{28}\text{Si}$ , which combined with our previous studies (~~PHY 73-21573~~) of  $^{208}\text{Pb}$ ,  $^{197}\text{Au}$  and  $^{165}\text{Ho}$ , form a survey of the giant resonances in many nuclei. The energy resolution of about 0.4% to 0.5%, was usually sufficient for studying these broad resonances; the excitation energy range covered was from 4 to 40 or 50 MeV, and showed giant resonances of energies from 6 to 33 MeV. Forward scattering angles were used resulting in only electric multipole resonances. *Delta?*

The cerium experiment possibly revealed more than any other single nucleus studied. In addition to  $E2(\Delta=0)$  at 10 MeV and  $E1$  at 15.3 MeV, the isovector  $E2$  appears at 25 MeV.  $E3$  resonances appear at 6.0 MeV, 22 MeV and 34638 MeV in general agreement with the model of Bohr and Mottelson.

For Uranium, both quadrupole resonances were observed, but were low in strength unless a transition radius larger than the ground state radius was assumed.

The giant dipole resonance, usually seen with gamma rays, may be studied by  $(e,e')$ , as shown by the case of nickel, where  $\gamma$  absorption does not work and  $(\gamma,n)$  ignores the important  $(\gamma,p)$  cross section. 105% and 110% of the GDR sum rule was observed for  $^{58}\text{Ni}$  and  $^{60}\text{Ni}$ , respectively. Also the GDR form factor was studied as a function of momentum transfer  $q$ , and the Myers-Swiatecki model was seen to be better than the G. T. or S. J. model.

→ Systematics of the resonance at  $^{53}\text{A}^{-1/3}$  MeV showed a smooth and drastic decrease with strength as a function of decreasing  $A$ , a behavior not seen for the GQR at  $^{63}\text{A}^{-1/3}$  MeV. This suggests the former resonance is an oscillation of the excess neutron of a heavy nucleus.

53 cur. r.t. (1/A)

63 cur. r.t. (1/A)

9. SIGNATURE OF PRINCIPAL INVESTIGATOR/ PROJECT DIRECTOR <i>Fred R. Buskirk</i>	TYPED OR PRINTED NAME Fred R. Buskirk	DATE 5/29/79
---	--	-----------------

Unclassified

SECURITY CLASSIFICATION OF THIS PAGE (When Data Entered)

REPORT DOCUMENTATION PAGE		READ INSTRUCTIONS BEFORE COMPLETING FORM
1. REPORT NUMBER <u>(14) NPS-61-79-009</u>	2. GOVT ACCESSION NO.	3. RECIPIENT'S CATALOG NUMBER
4. TITLE (and Subtitle) <u>(6) Nuclear Giant Multipole Resonances by Inelastic Electron Scattering</u>		5. TYPE OF REPORT & PERIOD COVERED <u>Final Report 1 Nov 76 - 31 July 79</u>
7. AUTHOR(s) <u>(10) A. R. Buskirk Fred</u>		8. CONTRACT OR GRANT NUMBER(s) <u>PHY 76-23881</u>
9. PERFORMING ORGANIZATION NAME AND ADDRESS <u>Dept of Physics and Chemistry Naval Postgraduate School Monterey, CA 93940</u>		10. PROGRAM ELEMENT, PROJECT, TASK AREA & WORK UNIT NUMBERS <u>251 450</u>
11. CONTROLLING OFFICE NAME AND ADDRESS <u>National Science Foundation</u>		12. REPORT DATE <u>(11) 29 May 1979</u>
13. MONITORING AGENCY NAME & ADDRESS (if different from Controlling Office) <u>(12) 96 PI</u>		14. SECURITY CLASS. (of this report) <u>Unclassified</u>
		15a. DECLASSIFICATION/DOWNGRADING SCHEDULE
16. DISTRIBUTION STATEMENT (of this Report) <u>Approved for Public Release; distribution unlimited.</u>		
17. DISTRIBUTION STATEMENT (of the abstract entered in Block 20, if different from Report)		
18. SUPPLEMENTARY NOTES		
19. KEY WORDS (Continue on reverse side if necessary and identify by block number) <u>Electron Scattering, Giant Multipole Resonances Nuclear Hydrodynamics</u>		
20. ABSTRACT (Continue on reverse side if necessary and identify by block number) <u>See reverse side</u>		

Unclassified

SECURITY CLASSIFICATION OF THIS PAGE(When Data Entered)

20. Abstract

Inelastic electron scattering experiments were performed with the Naval Postgraduate School 110 MeV Linac. The investigation included  $^{238}\text{U}$ ,  $^{140}\text{Ce}$ ,  $^{89}\text{Y}$ ,  $^{60}\text{Ni}$ ,  $^{58}\text{Ni}$  and  $^{28}\text{Si}$ , which combined with our previous studies (PHY 73 21573) of  $^{208}\text{Pb}$ ,  $^{197}\text{Au}$  and  $^{165}\text{Ho}$ , form a survey of the giant resonances in many nuclei. The energy resolution of about 0.4% to 0.5%, was usually sufficient for studying these broad resonances; the excitation energy range covered was from 4 to 40 or 50 MeV, and showed giant resonances of energies from 6 to 33 MeV. Forward scattering angles were used resulting in only electric multipole resonances.

The cerium experiment possibly revealed more than any other single nucleus studied. In addition to E2( $\Delta T=0$ ) at 10 MeV and E1 at 15.3 MeV, the isovector E2 appears at 25 MeV. E3 resonances appear at 6.0 MeV, 22 MeV and 34638 MeV in general agreement with the model of Bohr and Mottelson.

For Uranium, both quadrupole resonances were observed, but were low in strength unless a transition radius larger than the ground state radius was assumed.

The giant dipole resonance, usually seen with gamma rays, may be studied by  $(e, e')$ , as shown by the case of nickel, where  $\gamma$  absorption does not work and  $(\gamma, n)$  ignores the important  $(\gamma, p)$  cross section. 105% and 110% of the GDR sum rule was observed for  $^{58}\text{Ni}$  and  $^{60}\text{Ni}$ , respectively. Also the GDR form factor was studied as a function of momentum transfer  $q$ , and the Myers-Swiatecki model was seen to be better than the G. T. or S. J. model.

Systematics of the resonance at  $53\text{A}^{-1/3}$  MeV showed a smooth and drastic decrease with strength as a function of decreasing A, a behavior not seen for the GQR at  $63\text{A}^{-1/3}$  MeV. This suggests the former resonance is an oscillation of the excess neutron of a heavy nucleus.

Accession For	
NTIS GRA&I	X
DDC TAB	
Unannounced	
Justification	
By _____	
Distribution/	
Sensitivity Codes	
Mail and/or Special	
A	

Unclassified

SECURITY CLASSIFICATION OF THIS PAGE(When Data Entered)

## Table of Contents

	Page No.
I. Introduction	1
II. Methods	2
III. Summary of Experiments - Survey of Results	9
IV. Results for Individual Nuclei	12
A. $^{238}\text{U}$	13
B. $^{89}\text{Y}$	15
C. $^{28}\text{Si}$	16
D. $^{140}\text{Ce}$	19
E. $^{58}\text{Ni}$ and $^{60}\text{Ni}$	22
V. Conclusion and Remarks	26
VI. Publications and Papers	29
VII. Appendix $^{140}\text{Ce}$ Paper	35

## I Introduction

This report covers experimental determination of giant resonances of various multipolarity in medium and heavy nuclei by inelastic electron scattering using the Naval Postgraduate School Linac. The National Science Foundation grant PHY 76-23886 and PHY 76-2886-01 spanned 1 November 1976 to 31 July 1979, and an earlier grant, PHY 73-21573 covered 15 October 1974 to 31 October 1976. The nuclei investigated included  $^{208}\text{Pb}$ ,  $^{197}\text{Au}$ ,  $^{165}\text{Ho}$ ,  $^{89}\text{Y}$ ,  $^{60}\text{Ni}$ ,  $^{58}\text{Ni}$ ,  $^{238}\text{U}$ ,  $^{140}\text{Ce}$  and  $^{28}\text{Si}$ , divided approximately equally between the two grant periods. Thus the overall program constituted a survey of giant resonance in heavy and medium weight nuclei, starting from the discovery of the electric quadrupole giant resonance in Ce by Pitthan and Walcher in 1971. The broad object has been the investigation of not only the isoscalar electric quadrupole mode but also other modes predicted by Bohr and Mottelson schematic model, including E0, E2, E3 modes of both isoscalar and isovector type, and the study of the dependence of the resonance energy, width and strength of these modes as a function of the nuclear mass A. These experiments covered a wide range of excitation energy, up to 50 MeV, to include the higher angular momentum values, but were not extended to backward angles to measure magnetic states.

The NSF grant supported Dr. Rainer Pitthan for full time research. The operation of the Linac and research time for F. R. Buskirk were provided by the Naval Postgraduate School Foundation Research program.

## II Methods

Inelastic electron scattering ( $e, e'$ ) allows for excitation of electric and magnetic transitions of the nucleus, of both isoscalar and isovector character. The universality of this excitation mechanism makes this method necessary to investigate all possible nuclear excitations, and the knowledge gained may be extended greatly by comparison with other experiments. For example,  $(\gamma, n)$  experiments determine the E1 resonance almost exclusively, while the extremely fruitful hadron scattering experiments such as  $(\alpha, \alpha')$  are insensitive to isovector modes. Identification of modes from  $(e, e')$  alone is based on using backward scattering angles, especially  $180^\circ$ , to isolate magnetic transitions versus forward angles for the electric multipoles. The identification of the electric multipolarity requires inelastic form factor measurements at forward angles but various values of the momentum transfer  $q$  and comparison to DWBA hydrodynamic model calculations, which are shown in Fig. 1 for Ce. This information becomes more useful when combined with hadron scattering, which is sensitive mainly to isoscalar modes, and  $\gamma$  absorption, which singles out the dipole states.

### A. Experimental Apparatus

The giant resonances in ( $e, e'$ ) experiments appear as broad resonances superimposed on a large continuous spectrum called the radiation tail. The main requirements are stability and reproducibility of measurements but not extremely good energy resolution. Thus the rather conventional arrangement of the Naval Postgraduate School Linac shown in Fig. 2 suffices. The energy resolution is typically 0.3% to 0.5%, with a beam of 1 to 2 microamperes on the target. The available beam energy of 110 MeV is sufficient to measure over the first diffraction peak (see Fig 1) for multipolarities up to E3, for the medium and heavy nuclei. For lighter nuclei,  $A < 50$ , the resonances are higher in energy, there is more fine structure and the cross sections are lower so that better current, energy and resolution would help.

$^{140}\text{Ce}(e,e')$   
Goldhaber-Teller model

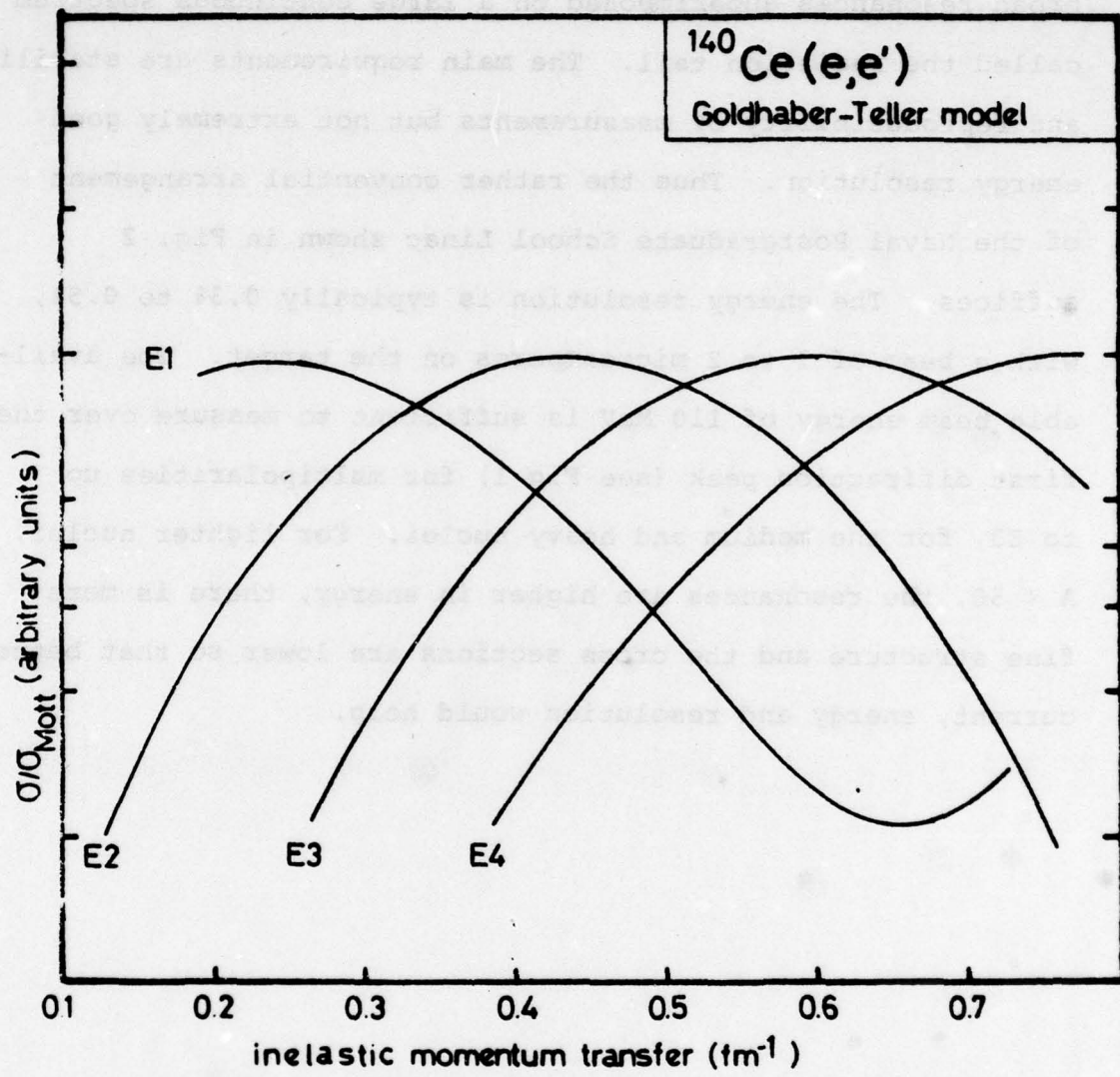


Figure 1  
Comparison of DWBA Cross Sections for E1 to E4  
Transition Divided By The Mott Cross Section

**Naval Postgraduate School  
110 MeV Linear Accelerator**

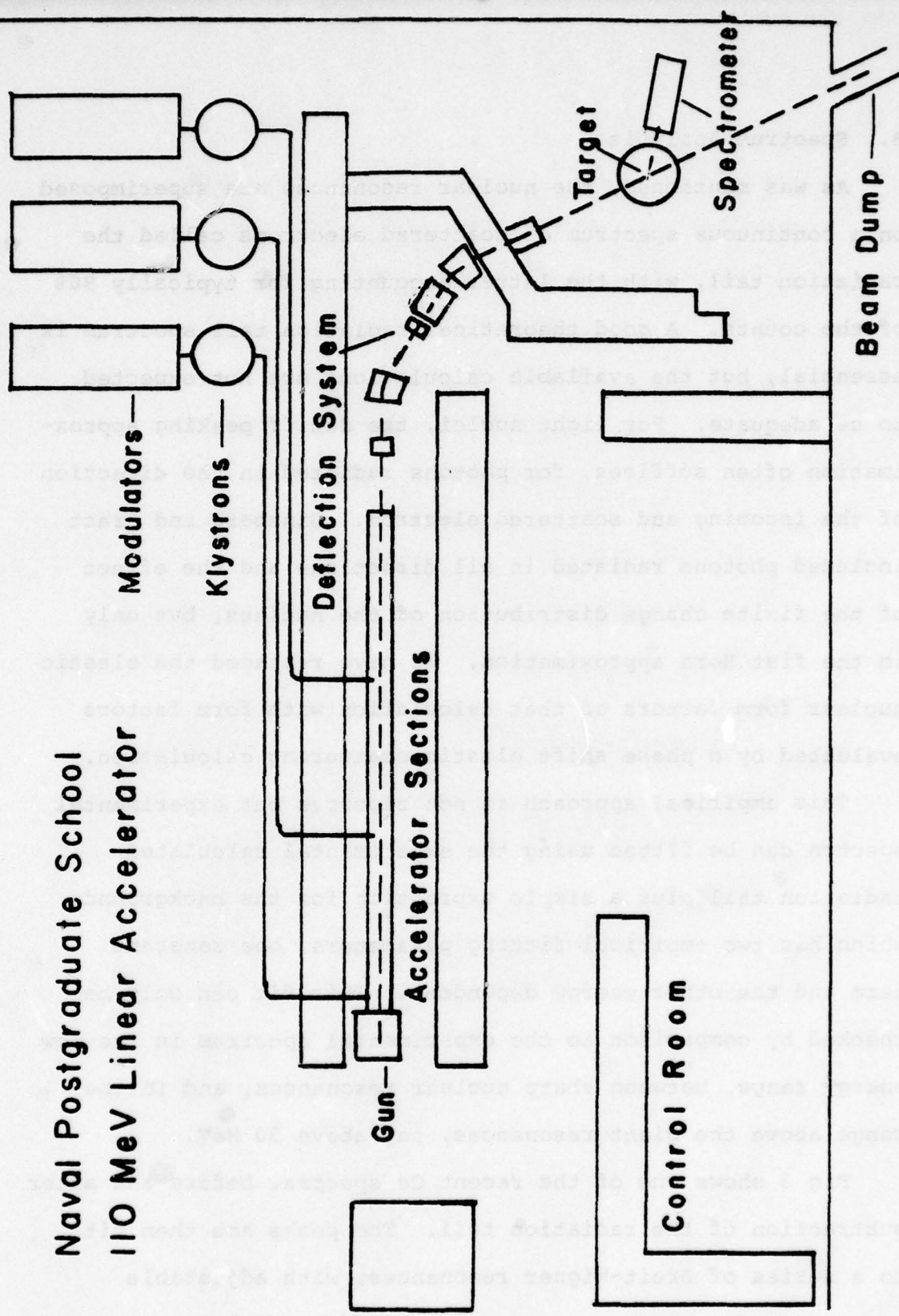


Figure 2 Linac Layout

## B. Spectrum Analysis

As was mentioned, the nuclear resonances are superimposed on a continuous spectrum of scattered electrons called the radiation tail, with the latter accounting for typically 90% of the counts. A good theoretical radiation tail spectrum is essential, but the available calculations are not expected to be adequate. For light nuclei, the Schiff peaking approximation often suffices, for photons radiated in the direction of the incoming and scattered electron. Ginsberg and Pratt included photons radiated in all directions and the effect of the finite charge distribution of the nucleus, but only in the first Born approximation. We have replaced the elastic nuclear form factors of that calculation with form factors evaluated by a phase shift elastic scattering calculation.

This empirical approach is not rigorous but experimental spectra can be fitted using the experimental calculated radiation tail plus a simple expression for the background which has two empirical fitting parameters, one constant term and the other energy dependent. This fit can only be checked by comparison to the experimental spectrum in the low energy range, between sharp nuclear resonances, and in the range above the giant resonances, say above 30 MeV.

Fig 3 shows one of the recent Ce spectra, before and after subtraction of the radiation tail. The peaks are then fit to a series of Breit-Wigner resonances, with adjustable parameters for the resonance energy, width and height. A given resonance must appear in all spectra for a given nucleus,

D. End of path from pulsed (circles) detector see fine line  
 detector. Temperature and voltage used between end to  
 device and end of detector at room temperature. Beam energy

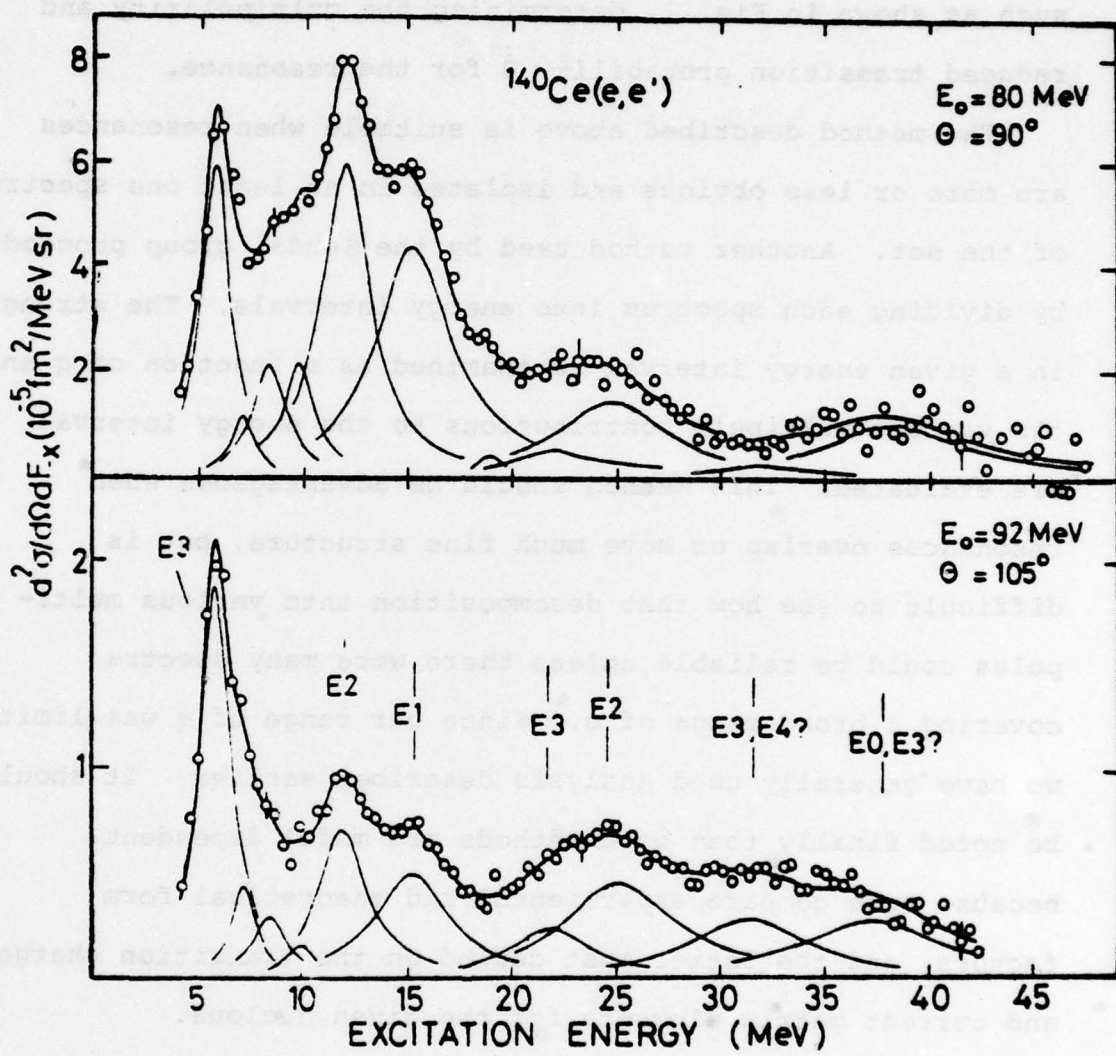


FIGURE 3. Inelastic  $^{140}\text{Ce}$  spectra without background.

with only the strength (height) varying according to the  $q$  of the various runs. Finally, the experimental strength, expressed as a form factor, is compared to the DWBA curves such as shown in Fig. 1, determining the multipolarity and reduced transition probability  $B$  for the resonance.

The method described above is suitable when resonances are more or less obvious and isolated in at least one spectrum of the set. Another method used by the Sendai group proceeds by dividing each spectrum into energy intervals. The strength in a given energy interval is examined as a function of  $q$  and the various multipole contributions to the energy interval are evaluated. This method should be advantageous when resonances overlap or have much fine structure, but is difficult to see how that decomposition into various multipoles could be reliable unless there were many spectra covering a broad range of  $q$ . Since our range of  $q$  was limited we have generally used analysis described earlier. It should be noted finally that both methods are model dependent, because both compare experimental and theoretical form factors, and the latter must depend on the transition charge and current matrix elements for the given nucleus.

### III Summary of Experiment - Survey of Results

The results of this survey of giant resonances are numerous, and the individual publication should be consulted. So here a broad summary of the overall observations will be attempted in Fig. 4 and 5. Then some of the more important results will be discussed in Section IV.

Fig. 4 attempts to represent our results in the form of a plot of the resonance energy observed as a function of mass, with vertical bars representing the widths of the resonances. Not all resonances such as fine structure, are shown; also the representation of the giant dipole resonance is abbreviated for clarity, because  $(\gamma, n)$  experiments usually give the definitive information.

Fig 5 displays the systematics again in a manner which may look the same. However the vertical scale has the energy scaled in units of  $A^{-1/3}$ , so that corresponding resonances strictly following the hydrodynamic model,  $E_r \sim A^{-1/3}$  would appear on a horizontal line. The vertical lines here represent error bars in determining the resonance energy  $E_r$ . The isoscalar quadrupole resonance energy does scale as  $A^{-1/3}$ , while the isovector quadrupole does not. The latter behavior also occurs with the (isovector) dipole resonance so may be a characteristic of isovector modes.

Results from other laboratories are also displayed on Fig 5 to show the general consistancy; in contrast Fig 4 shows only our results.

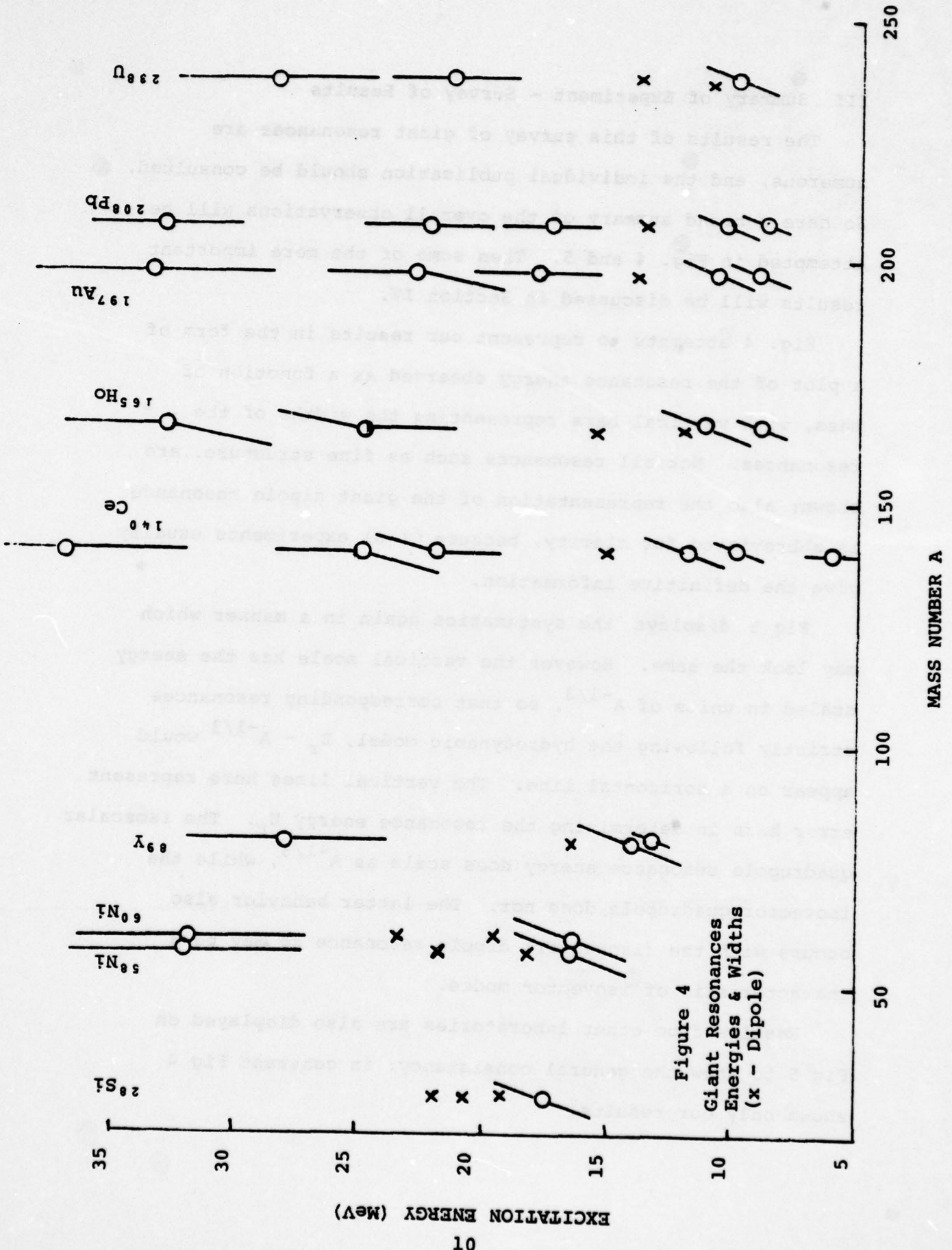
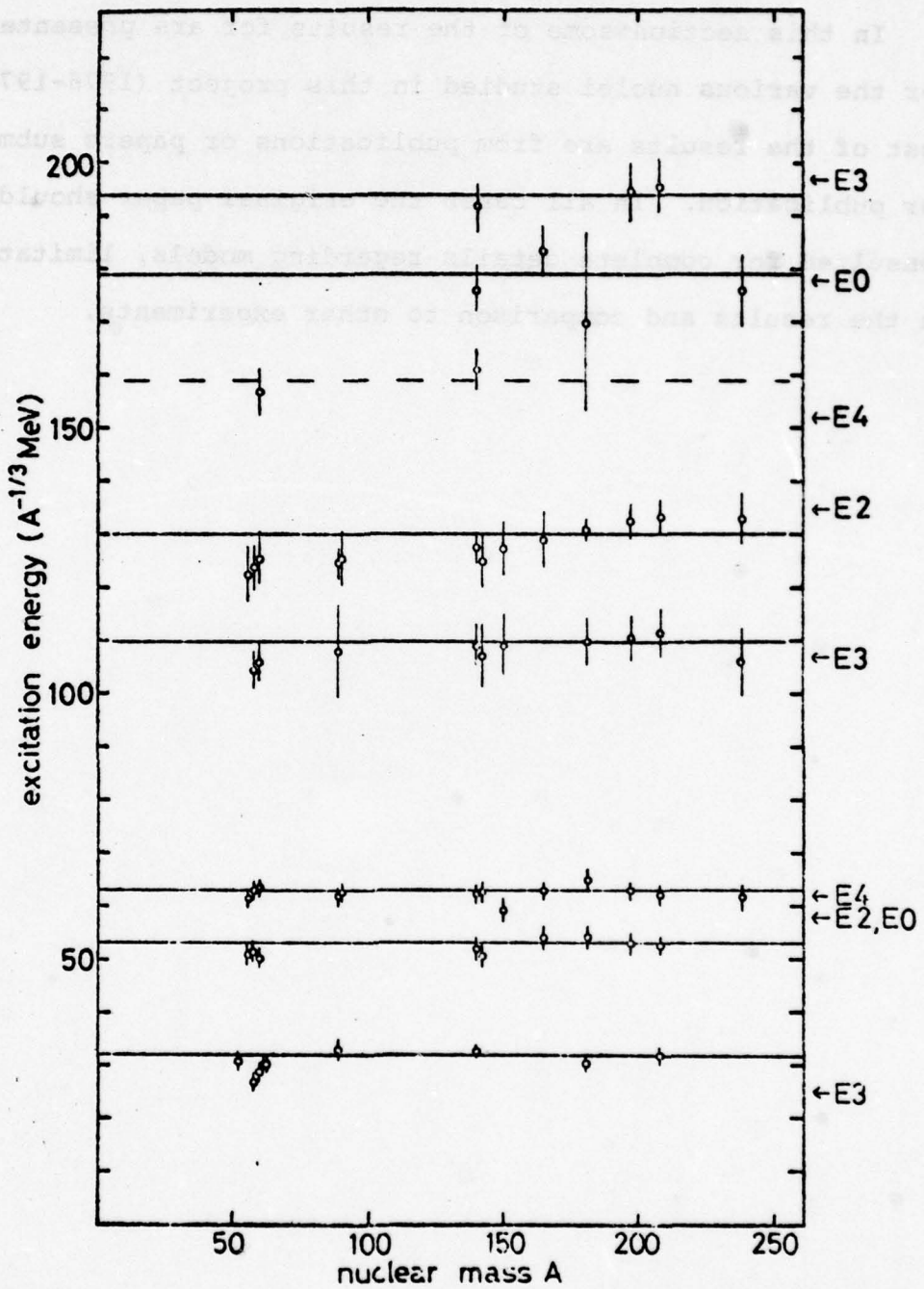


Figure 4  
Giant Resonances  
Energies & Widths  
(x - Dipole)



**Figure 5**  
**Scaled Energy of Observed Giant Resonances As A Function  
 of Nuclear Mass A. Dipole Resonances Omitted.**

#### IV Results for the Individual Nuclei

In this section some of the results for are presented for the various nuclei studied in this project (1976-1978). Most of the results are from publications or papers submitted for publication. In all cases the original paper should be consulted for complete details regarding models, limitations in the results and comparison to other experiments.

### A. Results for $^{238}\text{U}$ .

The splitting of the giant dipole resonance into components at 10.8 and 13.9 MeV is well known from  $(\gamma, n)$  experiments. It is thus possible the E2 giant resonance strength might be broadened or even more widely dispersed in the energy spectrum, and of course, the identification of the various resonances is difficult because of strong overlap. The results may be summarized in the table below which is from the submitted paper.

The unique overall result is that if the usual hydrodynamic (GT) model is employed, the observed E2 resonances account for lower fractions of the sum rule than has been observed in lighter nuclei, using the same experimental and analysis techniques. Assumption of a radius 10% larger than that for the ground state almost doubles the E2 strength which would be in agreement with systematics from lighter nuclei and  $(P, P')$  experiments on  $^{238}\text{U}$ .

TABLE 5 (from publication 9 )

$E_x$ (MeV)	$E\lambda$	Model ( $c_{tr}/c$ )	$E_x^{-1/3}$ MeV	$\Delta T$	$\Gamma$ (MeV)	$B(E\lambda)$ (fm $^2\lambda$ )	$\Gamma_Y^0$ (eV)	SPU	$R(\%)^a$
$9.9 \pm 0.2$	E2	GT(1.0)	62	0	$2.9 \pm 0.8$	3700	56	17	$38 \pm 10$
		GT(1.1)			$-0.4$		114	35	$77 \pm 20$
$10.8 \pm 0.3$	E1	GT(1.24)	67	1	$3.2 \pm 0.4$	28	$1.3 \cdot 10^4$	5	$36 \pm 4$
		MS(1.35) <sup>b)</sup>					30	5	$39 \pm 4$
$13.9 \pm 0.3$	E1	GT(0.9)	86	1	$4.5 \pm 0.3$	49	$4.6 \cdot 10^4$	10	$81 \pm 8$
		MS(1.0) <sup>b)</sup>			$-0.4$		50	$4.7 \cdot 10^4$	10
$21.6 \pm 0.6$	E2	GT(1.0)	133	1	$5.0 \pm 0.6$	3600	$2.7 \cdot 10^3$	17	$51 \pm 8$
		MS(1.1) <sup>c)</sup>					5000	$3.7 \cdot 10^3$	23
$28.4 \pm 1.2$	E3	GT(1.0)	176	1	$8.1 \pm 1.1$	$6.2 \cdot 10^5$	$5.4 \cdot 10^2$	78	$91 \pm 15$
		MS(1.1) <sup>d)</sup>					$5.1 \cdot 10^5$	$6.6 \cdot 10^2$	64

a)  $R = E_x \cdot B(E\lambda) / EWSR(E\lambda, \Delta T)$ b)  $\alpha(238,1) = 0.9$ c)  $\alpha(238,2) = 1.0$ d)  $\alpha(238,3) = 0.5$ 

Summary of the quantitative results of this paper (publication 9). While the excitation energy and the width of the resonant structures found is relatively insensitive to multipolarity and models used, the strength is not. For each resonance, two values are given. The upper value corresponds to a straight application of the GT model to the data. The lower value corresponds to the assumption of an  $^{238}\text{U}$  nucleus which is spatially enlarged by approximately 10% as compared to the ground state. In addition, the MS model was used for the isovector excitations. These assumptions lead to a greater consistency of the strength with other available data in lighter nuclei and for  $^{238}\text{U}$ .

## B. Results for $^{89}\text{Y}$

In addition to the five relatively narrow resonances with energies to 13.5 MeV, the giant dipole was seen, and also the isoscalar and isovector quadrupole resonances. The E1 strength agrees with ( $\gamma, n$ ) results for  $^{89}\text{Y}$  and the strength and width of the E2( $\Delta T = 0$ ) agree with values for  $^{90}\text{Zr}$  as tabulated by Bertrand for ( $e, e'$ ) and ( $\alpha, \alpha'$ ) experiments. High energy octupole strength was not observed, neither was a resonance at  $53 \text{ A}^{-1/3}$  MeV. See Section V for a discussion fo the latter point. Finally, there was no necessity to add strength to the giant dipole resonance region in the form of a monopole resonance as proposed in ( $\alpha, \alpha'$ ) scattering.

Table 6. Compilation of all the results from this experiment (reproduced from publication 4 )

$E_x$ (MeV)	$E_x$ ( $\text{A}^{-1/3}$ MeV)	$\Gamma$ (MeV) <sup>a)</sup>	$B(\text{fm}^{2\lambda})$	$R(\text{s})^b)$	$\Gamma_\gamma^*(\text{eV})$	SPU	$\lambda$	$\Delta T$
2.6	-	$1.0 \pm 0.2$	$(1.12 \pm 0.15) \cdot 10^8$	$15 \pm 3$	$5.3 \cdot 10^{-6}$	34	3	0
4.0	-	$1.0 \pm 0.2$	$700 \pm 140$	$11 \pm 3$	$1.2 \cdot 10^{-1}$	6	2	0
6.75	30	$1.0 \pm 0.2$	$(16.5 \pm 3.0) \cdot 10^8$	$6 \pm 1$	$6.2 \cdot 10^{-6}$	5	3	0
8.05	36	$1.2 \pm 0.2$	$(16.5 \pm 2.5) \cdot 10^8$	$7 \pm 1$	$2.1 \cdot 10^{-1}$	5	3	0
13.5	60	$1.2 \pm 0.2$	$(4.4 \pm 1.0) \cdot 10^8$	$2.5 \pm 0.6$	$2.1 \cdot 10^{-2}$	1.4	3	1
14.0	63	$4.5 \pm 0.4$	$1040 \pm 100$	$56 \pm 6$	$9.0 \cdot 10^1$	8.8	2	0
16.6	74	$3.9 \pm 0.2$	$20.5 \pm 2.0$	$104 \pm 10$	$3.3 \cdot 10^4$	5.3	1	1
28.0	125	$\Gamma = 7$	$565 \pm 65$	$48 \pm 5$	$1.57 \cdot 10^3$	4.8		
		$\Gamma = 8$	$670 \pm 80$	$57 \pm 6$	$1.86 \cdot 10^3$	5.6	2	1
		$\Gamma = 10$	$960 \pm 130$	$82 \pm 10$	$2.67 \cdot 10^3$	8.1		

a) The width may be either the width of the enveloping curve of unresolved discrete states or the width of a coherent resonant state.

b)  $R = E_x \cdot B(E\lambda) / \text{EWSR}(E\lambda, \Delta T) \cdot 100$

### C. Results for $^{28}\text{Si}$

The silicon experiments were undertaken to investigate both the isoscalar and isovector E2 modes in a light nucleus. The first diffraction peak for the E2 mode should be at a value of  $q = 1 \text{ fm}^{-1}$  approximatley, so that no E3 investigation is possible with our Linac which just reaches  $q = 1 \text{ fm}^{-1}$ . Identification of resonances is also hampered by pronounced fine structure; for example, the giant dipole was seen to have four strong peaks. Several ( $e, e'$ ) spectra are shown in Fig. 1 , of publication 7 which clearly show the strong dipole modes. The E2 strengths seen in various broad regions are given in Table 1 . A very interesting possibility results: The weak E2 strength seen below 30 MeV would imply considerable strength at higher energy. But considerable E2 strength above 50 MeV could contribute to the observed  $\gamma$  absorption, which is usually assumed to be only E1. This possible E2 contribution could then help explain why  $\gamma$  absorption experiments considerably exceed the dipole sum rule.

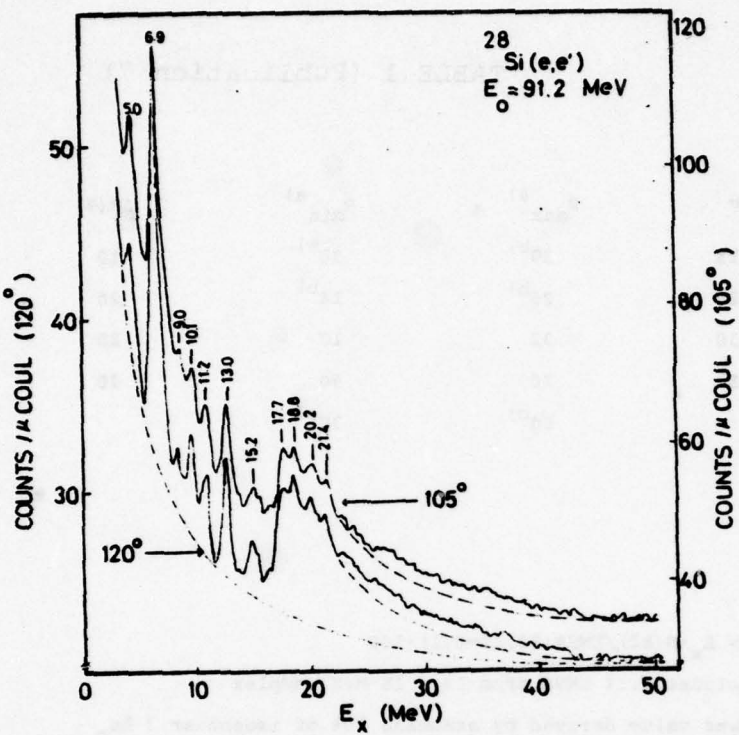


Figure 1 (Publication 7)

Spectrum of 92.2 MeV electrons scattered from  $^{28}\text{Si}$  at  $105^\circ$  and  $120^\circ$  spectrum is the maximum background possible, established with a method similar to the one used in  $(\alpha, \alpha')$ . The dashed lines beyond 22 MeV were extrapolated from the  $(\gamma, \text{abs})$  data and indicate the "excess" (presumably isovector E2) cross section in the region 22-50 MeV. The spectra have been drawn in a way that the peaks (or the peak) at 6.9 MeV coincide. Its prominent rise from  $105^\circ$  to  $120^\circ$ , compared to the others, is indicative of its E3 character. This spectrum has not been corrected for the constant dispersion of the magnetic spectrometer.

TABLE 1 (Publication 7)

$E_x/\text{MeV}$	$R_{\max}^{\text{a})}$	$R_{\min}^{\text{a})}$	$\Delta R(\%)$
0 - 15	30 <sup>b)</sup>	30 <sup>b)</sup>	10
15 - 20	26 <sup>b)</sup>	14 <sup>b)</sup>	20
20 - 30	32	10	20
30 - 50	70	50	30
	50 <sup>c)</sup>	30 <sup>c)</sup>	

a)  $R = E_x \cdot B(E2) / \text{EWSR}(E2, \Delta T=0, 1) \cdot 100$

b) includes 3.5% EWSR from 14 - 16 MeV complex

c) lower value derived by assuming 70% of isoscalar  $3 \hbar\omega_0$   
E3 strength between 30 and 50 MeV (ref. 22).

Distribution of E2 strength in  $^{28}\text{Si}$  into the various regions discussed in the text. Although isospin can not be directly inferred from  $(e, e')$ , the strength below 20 MeV should be predominantly isoscalar and the one above isovector, based on macroscopic and microscopic considerations and comparison with heavier nuclei.

#### D. Results for $^{140}\text{Ce}$

Discoveries concerning the quadrupole resonance had started with the ( $e, e'$ ) experiments with Ce at Darmstadt in 1971. The absence of fine structure and relatively good ratio of spacing to width then made Ce a candidate for new measurements over a wider excitation energy range and at higher values of the momentum transfer. The extensive results are given in the Table 10 from publication 6 reproduced below, along with several spectra. Other noteworthy results which do not show up in the tabulation are:

1. The  $q$ -dependence of the giant dipole resonance fits the Myers-Swiatecki version of the hydrodynamic model. This model is between the extremes of the model of Goldhaber-Teller model of relative motion between rigid neutron and proton spheres) and that of Steinwedel and Jensen (a fixed spherical boundary enclosing n and p density oscillations). If the M.S. model is assumed, there is no necessity to assume a large E0 resonance in this energy range, in agreement with our results for  $^{89}\text{Y}$ .
2. The 10 MeV resonance, at a scaled energy of  $53 \text{ A}^{-1/3}$  MeV but with only one third the strength in terms of the sum rule) for the corresponding resonance for Pb. When the behavior of this resonance for other nuclei is traced out, the strength increases with nuclear mass. Possibly it is associated with oscillation of the excess neutrons (see later discussion).

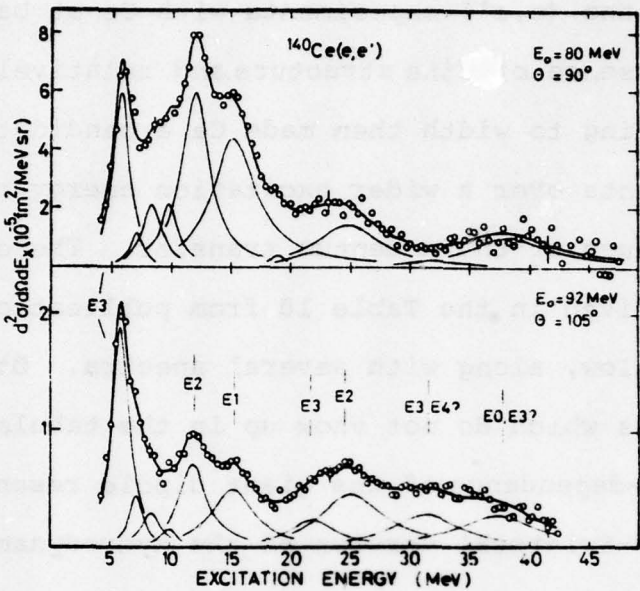


**Figure 5 (Publication 8)**

Data of Figure 2 after the fitted background (consisting of the radiation tail, the general room background and experimental background) and the "ghost peak" as described in the text have been subtracted. These two spectra are shown together so that the shrinkage of smaller multipolarity transitions may be seen. The relative change in peak heights of the single resonances indicate very clearly the various multipoles contributing. Note, e.g., that the E2 cross sections fall off more than a factor of 6 between the 80 MeV and the 92 MeV spectra.

TABLE 10 (Publication 8)

$E_x$ (MeV)	$E_x A^{-1/3}$ (MeV)	$\Gamma$ (MeV)	$E\lambda$	$\Delta T$	$B_{\text{exp}}$ (fm $^{2\lambda}$ ) <sup>a)</sup>	$\Gamma_Y^0$ (eV)	$R$ <sup>b)</sup>	Std. <sup>c)</sup> Dev.	Total <sup>d)</sup> Error
6.0 ± 0.2	31	1.7 ± 0.2	3	0	1.3 10 <sup>5</sup>	2.0 10 <sup>-3</sup>	19	± 3	± 6
10.0 ± 0.2	52	1.8 ± 0.2	2	0	4.30	7.6	9	± 2	± 4
			0	0	7.70		13	± 2	± 6
12.0 ± 0.2	62	2.8 ± 0.2	2	0	2.5 10 <sup>3</sup>	10.0	63 <sup>e)</sup>	± 17	± 13
			2	0	2.0 10 <sup>3</sup>	8.7	50 <sup>f)</sup>	± 5	± 10
15.3 ± 0.2	79	4.4 ± 0.2	1	1	4.1	5.1 10 <sup>4</sup>	122 <sup>g)</sup>	± 12	± 20
			1	1	5.5	6.9 10 <sup>4</sup>	167 <sup>h)</sup>	± 40	± 27
22 ± 1	114	5 ± 1	3	0	3.7 10 <sup>4</sup>	4.9	19	± 2	± 10
25 ± 1	130	6.5 ± 1	2	1	1.3 10 <sup>3</sup>	2.1 10 <sup>3</sup>	50 <sup>i)</sup>	± 8	± 15
			2	1	2.1 10 <sup>3</sup>	3.3 10 <sup>3</sup>	77 <sup>h)</sup>	± 25	± 28
34 - 38	175	7 - 10	3	0	1.2 10 <sup>5</sup>	6.8 10 <sup>2</sup>	75	± 10	± 50
	195		0	1	2.8 10 <sup>3</sup>	—	130	± 20	± 45

a) For the monopole the measured quantity is  $|M_{if}|^2$  (fm $^4$ )

b)  $R = E_x \cdot B(E\lambda) / \text{EWSR}(E\lambda, \Delta T) \cdot 100$

c) The error given (in units of  $R$ ) is the standard deviation of the average sum rule exhaustion and is, therefore, more a measure for the fit to a certain model than a measure for the total uncertainty.

d) The total error (in units of  $R$ ) is based on the maximum and minimum values found for the areas under the curves during the many attempts to fit the spectra.

e)  $c_{tr} = 1.0$  c.

f)  $c_{tr} = 0.95$  c.

g) MS model with  $\alpha = 0.76$ .

h) GT model.

i) MS model with  $\alpha = 1.0$ .

Results in units of the reduced transition probabilities (B-values), ground state radiation width ( $\Gamma_Y^0$ ), and energy weighted sum rule exhaustion, for the major resonances found in this experiment. Some results for weaker states, and those inferred from differences between cross sections and DWBA calculation, are, together with the appropriate discussion, scattered in the text. The isospin assignments are not determined by this experiment, but were taken from comparison with other experiments and theory.

E. Results for  $^{58}\text{Ni}$  and  $^{60}\text{Ni}$  (to be published)

The two tables give some of the results to be published. It is worth noting that some of the most important results concern the dipole resonance, because the usual source of experimental information do not work in this case. ( $\gamma, n$ ) experiments obviously do not measure the  $(\alpha, \gamma)$  cross sections, and the latter are important. The total  $\gamma$  absorption experiments are not expected to work at high  $Z$  and require too much target material to employ separated isotopes.

Note in particular that this experiment results in 110% and 105% of the dipole sum rule for  $^{58}\text{Ni}$  and  $^{60}\text{Ni}$ , respectively, contrasting to 33% and 78% observed for the  $(\gamma, n)$  channel alone.

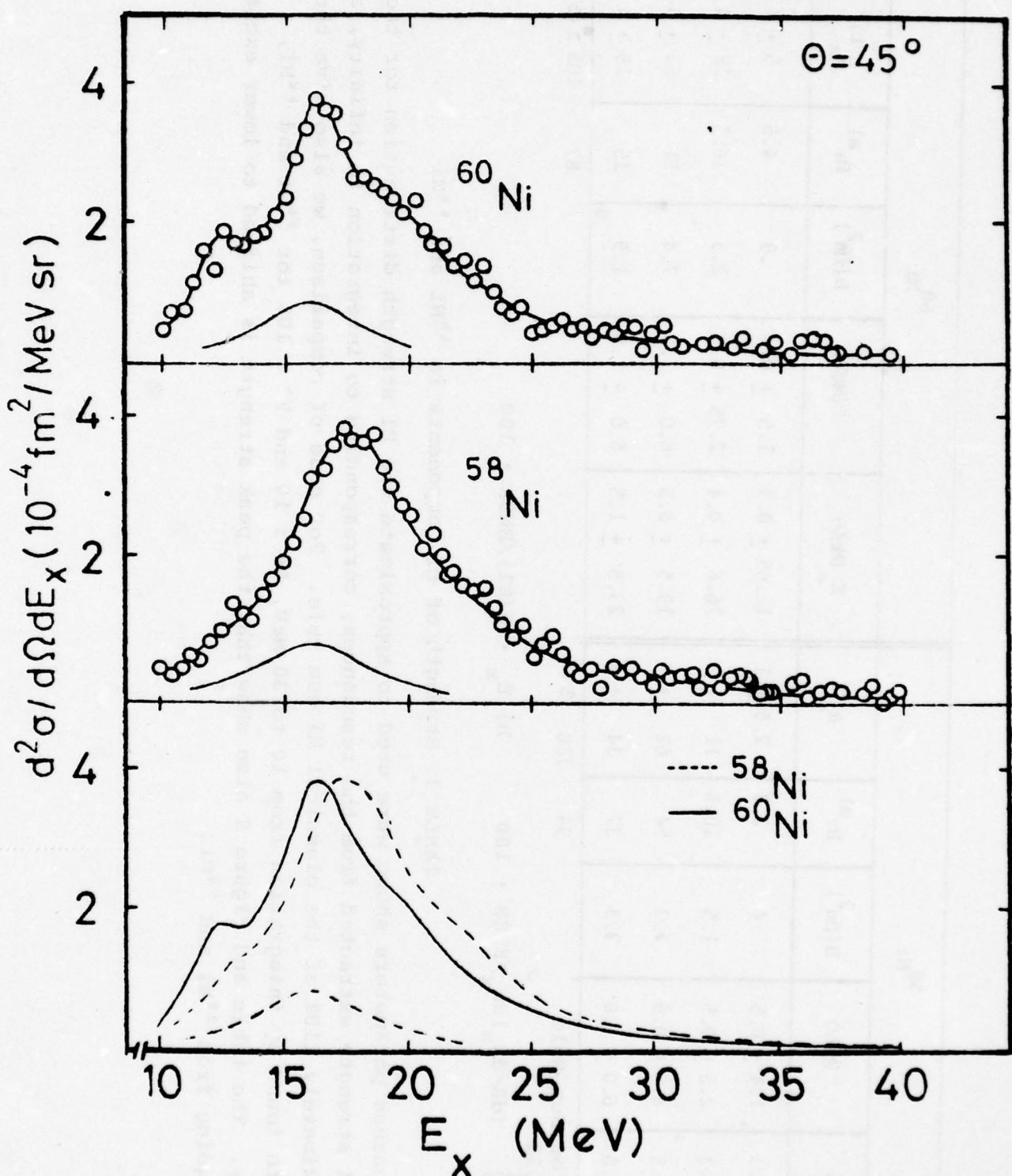


Figure 7 (Publication 9)  
 Spectra For Nickel At Low  $q$  Showing The Dipole State

58Ni				60Ni			
$E_x$ (MeV)	$\Gamma$ (MeV)	$B(\text{fm}^2)$	$R_y^a$	$E_x$ (MeV)	$\Gamma$ (MeV)	$B(\text{fm}^2)$	$R_y^a$
			$R_a^b$				$R_a^b$
13.1 ± 0.3	1.4 ± 0.5	.4	2.3	12.65 ± 0.3	1.5 ± 0.4	.9	4.5
16.2 ± 0.3	2.5 ± 0.5	1.5	10.5	11 ± 2	16.6 ± 0.4	2.75 ± 0.5	16.5
18.3 ± 0.5	4.5 ± 0.5	7.3	54	62 ± 7	19.5 ± 0.5	6.0 ± 1.0	7.4
22.0 ± 1.0	6.0 ± 1.0	3.3	27	34 ± 8	23.5 ± 1.5	6.0 ± 1.5	1.9
Total # of Sum Rule				94	110 ± 11		15
30							19 ± 4
a)	$\int_{10}^{30} (dB/dE_x) dE_x / \text{EWSR} \cdot 100$				b) $E_x \cdot B(E1) / \text{EWSR} \cdot 100$		

24

TABLE 3 Strength of E1 Components in  $^{58}\text{Ni}$  and  $^{60}\text{Ni}$ 

The resonance parameters shown were used to approximate the E1 strength distribution for the  $\chi^2$  fit. The E1 strength extracted from the resonances, corresponding to integration to infinity, adds up to approximately 110 $\pm$ 11 of the classical E1 sum rule. For ease of comparison, we also give the sum rule strength found by integration from 10 to 30 MeV, 94 ± 10 and 87 ± 10 $\pm$ 10 for  $^{58}\text{Ni}$  and  $^{60}\text{Ni}$ , respectively. The table and Figure 8 also show that the peak strength is shifted to lower excitation energy, by going from  $^{58}\text{Ni}$  and  $^{60}\text{Ni}$ .

$^{58}\text{Ni}$			$^{60}\text{Ni}$		
$E_x$ (MeV)	$R$ (MeV) R <sup>a)</sup>	$E_x$ (MeV)	$R$ (MeV) R <sup>a)</sup>	$R$ (MeV) R <sup>a)</sup>	Ref. Method
16.4 $\pm$ 0.3	4.9 $\pm$ 0.2	55 $\pm$ 15	16.6 $\pm$ 0.3	5.0 $\pm$ 0.4	63 $\pm$ 15 17 ( $\alpha, \alpha'$ )
16.5 $\pm$ 0.5	4.2 $\pm$ 1.0	56 $\pm$ 4	16.0 $\pm$ 0.5	3.7 $\pm$ 0.8	52 $\pm$ 3 32 ( $\gamma, \alpha$ )
16.2 $\pm$ 0.3	4.5 $\pm$ 0.4	65 $\pm$ 10	16.3 $\pm$ 0.3	4.5 $\pm$ 0.4	55 $\pm$ 10 PW ( $e, e'$ )

a)  $R = E_x \cdot B(E2)/EWSR(E2, \Delta T = 0)$

TABLE 6 Comparison of E2 Measurements for  $^{58}\text{Ni}$  and  $^{60}\text{Ni}$

## V Conclusion and Remarks

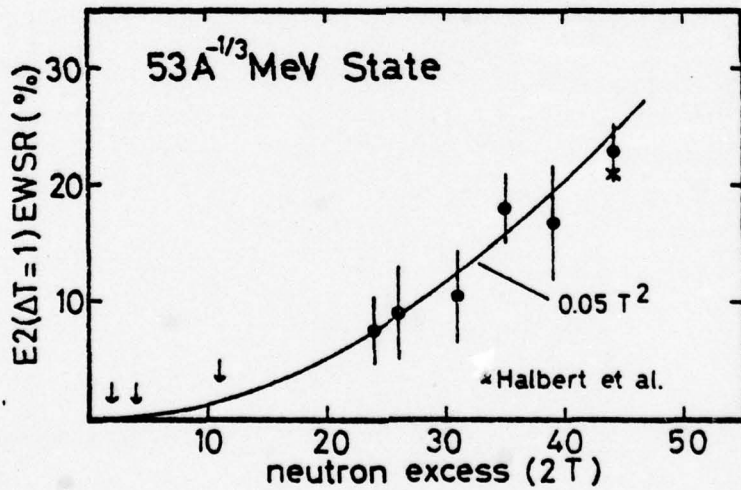
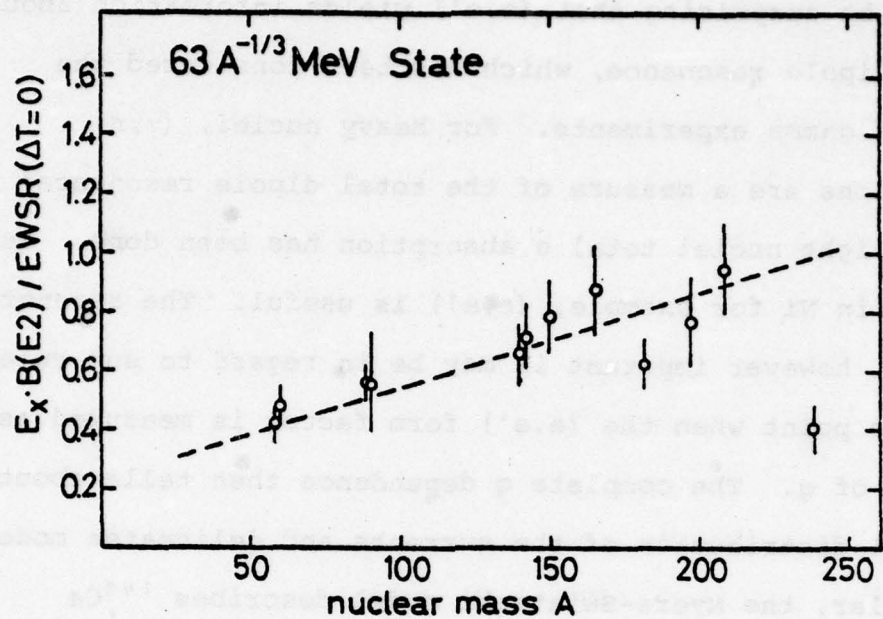
Some conclusions may be made when the experiments reported here ( $^{238}\text{U}$ ,  $^{140}\text{Ce}$ ,  $^{89}\text{Y}$ ,  $^{58}\text{Ni}$ ,  $^{60}\text{Ni}$  and  $^{28}\text{Si}$ ) are considered along with the earlier work ( $^{208}\text{Pb}$ ,  $^{197}\text{Au}$ , and  $^{165}\text{Ho}$ ).

A. The  $E2(\Delta T=0)$  mode is found in all the nuclei, at an energy which scales nicely as  $63A^{-1/3}$  MeV. The strength of about 80% of the sum rule decreases to about 40% for Ni and Y. The unobserved strength for light nuclei may be widely dispersed in energy.

B. The  $E2(\Delta T=1)$  mode is wider ( $\Gamma \sim 8$  MeV) appears at  $E = 130A^{-1/3}$  MeV in heavy nuclei by at somewhat lower energy in lighter nuclei. This behavior is known for the dipole resonance, and may be associated with the isovector character. The observed strength of 80% of the sum rule for heavy nuclei decreases to about 40% in the Ni and Y cases.

C. The state at  $53A^{-1/3}$  MeV lies below the isovector quadrupole state, is weaker, has the ambiguous  $E2$  or  $E0$  behavior as a function of  $q$ , and has not been reported in hadron scattering. But new information emerges when all the nuclei are compared; the strength falls off rapidly for lighter nuclei, leading to the possibility that this resonance may be an  $E2$  (or  $E0$ ) associated with the excess neutrons only. Either an isovector  $E2$  or an  $E0$  mode would be expected to be absent or weak in hadron scattering.

D. It may be surprising that  $(e,e')$  yields information about the giant dipole resonance, which has been considered the territory of gamma experiments. For heavy nuclei,  $(\gamma,n)$  cross sections are a measure of the total dipole resonance; while for light nuclei total absorption has been done. But in between in Ni for example,  $(e,e')$  is useful. The strength or B value, however important is may be in regard to sum rules, is only one point when the  $(e,e')$  form factor is measured as a function of q. The complete q dependence then tells about the spatial distribution of the currents and delineates models. In particular, the Myers-Swiatecki model describes  $^{140}\text{Ce}$  data better than either the Goldhaber-Teller or Steinwedel - Jensen model.



Figures 16 and 24 (Invited Paper 3)  
 Comparsion Of The A-dependence Of The Strength For The  $63A^{-1/3}$  Mev State (Giant Quadrupole Resonance) And The One At  $53A^{-1/3}$  MeV, Indicating That The Latter Resonance May Be Associated With Excess Neutrons Only.

## VI Publications and Papers

### A. Publications

- 1\* Electroexcitation of Giant Multipole Resonances in  $^{197}\text{Au}$  and  $^{208}\text{Pb}$  between 5 and 40 MeV Excitation Energy with 90-MeV Electrons. R. Pitthan, F. R. Buskirk, E. B. Dally, J. N. Dyer and X. K. Maruyama, Phys. Rev. Lett. 33, 849 (1974).
- 2\* The Width of the E2 ( $\Delta T=0$  and  $\Delta T=1$ ) Giant Resonances in  $^{165}\text{Ho}$ . G. L. Moore, F. R. Buskirk, E. B. Dally, J. N. Dyer, X. K. Maruyama, and R. Pitthan, Z. Naturforsch 319, 668 (1976).
3. The Isospin<sup>-</sup> of the Fine Structure between 8 and 12 MeV in  $^{208}\text{Pb}$  and its Implication for the Multipole Assignment of the 8.9 MeV Resonance. R. Pitthan and F. R. Buskirk, Phys Rev. C16, 983 (1977).
4. Giant Resonances and Bound Collective States Observed in the Scattering of 92.3 MeV Electrons from the Closed Neutron Shell Nucleus  $^{89}\text{Y}$  between Excitation Energies from 2 to 55 MeV. R. Pitthan, F. R. Buskirk, E. B. Dally, J. O. Shannon, and W. H. Smith. Phys. Rev. C16, 970 (1977).
5. The Natural Line Shape of the Giant Dipole Resonance. E. F. Gordon and R. Pitthan. Nucl. Instr. Meth. 145 569 (1977).
6. E1 Form Factor and the Existence of Breathing Mode at  $80\text{A}^{-1/3}$  MeV in Heavy Nuclei R. Pitthan, H. Hass, D. H. Meyer, J. N. Dyer, and F. R. Buskirk, Phys. Rev. Lett. 41 1276 (1978).

\* Published under previous grant.

7. Distribution of E2 Strength in  $^{28}\text{Si}$  below 50 MeV Excitation Energy. R. Pitthan F. R. Buskirk, J. N. Dyer, E. E. Hunter, and G. Pozinsky, Phys. Rev. C19 299 (1979).
8. EO, E1, E2, E3, and E4 Giant Resonances in the N=82 Nucleus  $^{140}\text{Ce}$  between 4 and 48 MeV Excitation Energy with Inelastic Electron Scattering. R. Pitthan, H. Hass, D. H. Meyer, F. R. Buskirk, and J. N. Dyer, Phys. Rev. C19 1251 (1979).

Submitted for Publication

9. Giant Multipole Resonances in the Deformed Fissionable Nucleus  $^{238}\text{U}$ . R. Pitthan, F. R. Buskirk, W. A. Houk, and R. W. Moore.
10. Comparison of Giant Multipole Resonances of Multipolarity E1 to E4 in  $^{55}\text{Ni}$  ( $T_0=1$ ) and  $^{60}\text{Ni}$  ( $T_0=2$ ) with Inelastic Electron Scattering. R. Pitthan, G. M. Bates, J. S. Beachy E. B. Dally, D. H. Dubois, J. N. Dyer, S. J. Kowalick and F. R. Buskirk.

B. Invited Papers

- 1\* Evidence of the Isoscalar Monopole and the Electric Dipole Spin Flip Resonance in Heavy Nuclei, R. Pitthan, F. R. Buskirk, E. B. Dally, J. N. Dyer, and X. K. Maruyama, Invited Conference on Nuclear Structure and Spectroscopy, Amsterdam, Vol. 2, (1974).
- 2\* Giant Resonances in Heavy Nuclei Measured by Inelastic Electron Scattering. F. R. Buskirk. Invited Paper, APS Anaheim Meeting, Bull. Am. Phys. Soc. 20, 81 (1975).
3. Some Solved and More Unsolved Problems in Giant Resonance Research. R. Pitthan, Invited Seminar, Masurian Summer School, Masuria, Poland 1978.

\* Presented under previous grant.

### C. Contributed Papers

- 1\* Giant Multipole Resonance in Heavy Nuclei. X. K. Maruyama, F. R. Buskirk, E. B. Dally, J. N. Dyer, and R. Pitthan, Bull. Am. Phys. Soc. 19, 998 (1974).
- 2\* Evidence for the Giant Dipole Electric Spin-Flip Resonance from ( $e, e'$ ) in Heavy Nuclei. F. R. Buskirk, E. B. Dally, J. N. Dyer, K. Ferlic, X. K. Maruyama, R. Waddell, and R. Pitthan, Bull. Am. Phys. Soc. 19, 998 (1974).
- 3\* Comparison of Giant Resonances in  $^{197}\text{Au}$  and  $^{208}\text{Pb}$ . F. R. Buskirk, E. B. Dally, J. N. Dyer, K. P. Ferlic, X. K. Maruyama, R. D. Waddell, and R. Pitthan. Proceedings of the International Conference on Nuclear Structure and Spectroscopy, Amsterdam, Vol. 1, p. 205 (1974).
- 4\* Electroexcitation of  $^{165}\text{Ho}$  in the Giant Resonance Region. G. L. Moore, F. R. Buskirk, E. B. Dally, J. N. Dyer, X. K. Maruyama, and R. Pitthan, Bull. Am. Phys. Soc. 21, 516 (1976).
- 5\* Line Structure and Resonant Structure in  $^{208}\text{Pb}$ . R. Pitthan and F. R. Buskirk, Bull. Am. Phys. Soc. 21, 516 (1976).
- 6\* Practical Improvements in the Calculations of the Radiation Tail of Elastically Scattered Electrons for Evaluation of ( $e, e'$ ) - Experiments in the Nuclear Continuum. F. R. Buskirk, J. N. Dyer, and R. Pitthan, Bull. Am. Phys. Soc. 22, 683 (1976).
7. Electroexcitation of Isovector ( $\Delta T=1$ ) Giant Resonances. D. H. Dubois, G. M. Bates, J. O. Shannon, W. H. Smith, F. R. Buskirk, E. B. Dally, J. N. Dyer, and R. Pitthan, Bull. Am. Phys. Soc. 22, 542 (1977).

8. Isovector Octupole Strength in Heavy Nuclei. W. A. Houk,  
R. W. Moore, F. R. Buskirk, J. N. Dyer, and R. Pitthan,  
*Bull. Am. Phys. Soc.* 22, 542 (1977).
9. El Strength in  $^{58}\text{Ni}$  and  $^{60}\text{Ni}$ . J. S. Beachy, S. J. Kowalick,  
F. R. Buskirk, J. N. Dyer, and R. Pitthan, *Bull. Am. Phys.  
Soc.*, 23, 506 (1978).
10. High Energy Grant Resonance in Ce. H. Hass, E. E. Hunter,  
D. H. Meyer, G. Pozinsky, R. Pitthan, J. N. Dyer and F. R.  
Buskirk, *Bull. Am. Phys. Soc.*, 23, 506 (1978).
11. On the Monopole Breathing Mode in Nuclei, *Bull. Am. Phys.  
Soc.*, 23, 506 (1978).

\* Presented under previous grant.

D. Theses

- 1\* Electroexcitation of Giant Resonances between 5 and 30 MeV Excitation Energy in  $^{165}\text{Ho}$ . G. L. Moore (December 1974).
- 2\* An Investigation of the Natural Line Shape of the Giant Dipole Resonance. E. F. Gordon (December 1975).
- 3\* Electroexcitation of Giant Resonances in  $^{60}\text{Ni}$  between 5 MeV and 30 MeV Excitation Energy. D. H. Dubois II and G. M. Bates (June 1976).
- 4\* Electroexcitation of Giant Resonances between 5.1 MeV and 38 MeV Excitation Energy in  $^{89}\text{Y}$ . J. O. Shannon and W. H. Smith (June 1976).
5. An Investigation of the Nuclear Continuum in the Fissionable Nucleus  $^{238}\text{U}$  with 87.5 MeV Electrons. W. A. Houk and R. W. Moore (March 1977).
6. Electroexcitation of the T=1 Nucleus  $^{58}\text{Ni}$  and the T=2 Nucleus  $^{60}\text{Ni}$  up to 50 MeV Excitation Energy. J. S. Beach and S. J. Kowalick (March 1977).
7. Electroexcitation of Giant Resonances Between 4 MeV and 48 MeV Excitation Energy. E. E. Hunter and G. Pozinsky (June 1978).

\* Experiments done in previous grant period.

## VII Appendix

The recent paper on  $^{140}\text{Ce}$  is reproduced in the following pages. Resonances show up more clearly because the ratio of width to separation of the States is favorable. Also the list of references is up to date so that a separate reference list is not needed for this report.

INVESTIGATIONS OF E0, E1, E2, E3, AND E4  
GIANT RESONANCES IN THE N = 82 NUCLEUS  $^{140}\text{Ce}$  BETWEEN 4 AND 48 MeV  
EXCITATION ENERGY WITH INELASTIC ELECTRON SCATTERING\*

R. Pitthan, H. Hass, D.H. Meyer,  
F.R. Buskirk and J.N. Dyer

Department of Physics and Chemistry  
Naval Postgraduate School  
Monterey, California 93940

$^{nat}\text{Ce}$  (89%  $^{140}\text{Ce}$ ) has been measured with electrons of 80 and 92 Mev at 90 and 105° between 4 and 48 Mev excitation energy. The 9 resonances or resonance-like structures identified at  $E_x = 6$  ( $31 \text{ A}^{-1/3}$ ),  $7.4$  ( $38 \text{ A}^{-1/3}$ ),  $10$  ( $52 \text{ A}^{-1/3}$ ),  $12$  ( $62 \text{ A}^{-1/3}$ ),  $15.3$  ( $75 \text{ A}^{-1/3}$ ),  $22$  ( $114 \text{ A}^{-1/3}$ ),  $25$  ( $130 \text{ A}^{-1/3}$ ),  $31$  ( $160 \text{ A}^{-1/3}$ ), and  $37.5$  ( $195 \text{ A}^{-1/3}$ ) Mev were classified on the basis of their momentum transfer dependence and discussed in the framework of the shell model. Since some of the arguments used are intricate we refer for quantitative particulars to the text. It is shown that the E2 sum rule strength not exhausted in the excitation range of this experiment may contribute up to 50% of the classical dipole sum rule to the photon cross section between 50 Mev and the pion threshold. The resonance at 10 Mev might be due to a separate oscillation of the excess neutrons against the rest of the nucleus.

I. Introduction

Recent years have brought a vastly improved knowledge of the nuclear giant resonances,<sup>1</sup> which are broadly defined as coherent nuclear excitations of the region above the lowest particle threshold. As in any active field of science, as many or more questions have arisen as have been solved. The particular target of this work ( $^{nat}\text{Ce}$  which contains 89% of  $^{140}\text{Ce}$ ) had been chosen for several reasons which we thought made it a particularly interesting and worthwhile nucleus to study. First, the earliest work on giant multipole resonances<sup>2</sup> pointed out several problems with the giant dipole resonance in  $N = 82$  nuclei, problems which do not fit to the normal characterization of this state as well understood. Secondly, a resonance at  $53 \text{ A}^{-1/3}$  Mev, also discovered<sup>3</sup> in  $^{140}\text{Ce}$  and seen in many nuclei by ( $e, e'$ ) in the meantime, exhibits an E2 angular distribution (or momentum transfer dependence). The presence of a second separate E2 branch in addition to the main isoscalar giant quadrupole resonance (GQR) at  $63 \text{ A}^{-1/3}$  Mev, which already carries between 50 and 100% of the isoscalar sum rule in heavy nuclei, is difficult to understand. Thirdly, resonances reported above 25 to 30 Mev, that is above the isovector GQR at  $130 \text{ A}^{-1/3}$  Mev<sup>4</sup> have been found in five nuclei heavier than  $^{140}\text{Ce}$  and have been classified alternatively as E0 or E3 and, in fact, may contain both multiplicities. Lastly, a general reason to choose  $^{140}\text{Ce}$  is based on the observation that  $N = 82$  nuclei have one of the

\*Supported in part by the National Science Foundation and the Naval Postgraduate School Research Foundation.

most favorable ratios of width of the various GR to their energy separation. Since the overlapping of the giant resonances of different multipolarity poses the largest problem in interpretation of observed electro-excitation spectra, the small intrinsic width of the resonances in Ce is of great help in unraveling the complicated structure with a line shape fit.

Giant electric quadrupole resonances have been found to have properties which only slowly vary from nucleus to nucleus and to be not much different in magic and non-magic (especially deformed) nuclei, a property which is understood in the frame work of the shell model<sup>5</sup>. Other resonances like the E3 have been found to show more variance, but have still to be looked at in conjunction with measurements over a wide range of  $\Lambda$ . We will, therefore, shortly describe the general theoretical framework.

Despite early predictions of a hydrodynamical E2 mode in analogy to the E1<sup>6</sup>, the giant multipole resonance region experimentally was found to be flat until 1971. None of the "eagerly expected high-frequency collective modes"<sup>7</sup> could be found. The theoretical foundation for a microscopic understanding of the GMR region has been laid two decades ago by Brown, et al.<sup>8</sup>; the most detailed predictions had been given by Bohr and Mottelson<sup>9</sup> within their self-consistent shell model. One of the best short descriptions of the scheme proposed by Bohr and Mottelson has been given by Hamamoto<sup>10</sup>; results based on a RPA calculation are summarized

in table 1 and can be explained in the following way in terms of the nuclear shell model. Without taking isospin into account, a GR of a certain multipolarity would be found at an excitation energy corresponding to a number of main shell transitions ( $\hbar\omega_0 = 41 \text{ A}^{-1/3}$  MeV) allowed by spin and parity, i.e.,  $2\hbar\omega_0$  for E2,  $1\hbar\omega_0$  and  $3\hbar\omega_0$  for E3, etc. The isospin dependence of the particle-hole interaction, repulsive for isovector excitations<sup>8</sup>, attractive for isoscalar ones,

introduces another degree of freedom. The unperturbed state, i.e.,  $80 \text{ A}^{-1/3}$  MeV for an E2, is thus split in two, with the isoscalar part ( $\Delta T = 0$ ) lowered to  $\approx 60 \text{ A}^{-1/3}$  MeV and the isovector part ( $\Delta T = 1$ ) raised to  $\approx 130 \text{ A}^{-1/3}$  MeV.<sup>11</sup> Figure 1 shows most of the available body of data from inelastic electron scattering<sup>12</sup> for multipolarities  $\lambda \geq 1$ . If one compares with table 1, in general, a good agreement between schematic model and experiment is obvious. The most complete experimental survey of any mode has been made with  $(\alpha, \alpha')$  by Youngblood, et al. for the isoscalar GQR,<sup>13</sup> and for the  $1\hbar\omega$ ,  $\Delta T = 0$  high energy bound octupole state (HEBOS)<sup>14</sup>, predicted early by Bohr and Mottelson<sup>9</sup>, at  $32 \text{ A}^{-1/3}$  MeV.

## II. Experimental Details

The experiment reported here used electrons of primary energy (80 and 92 MeV) at angles of 90 and 105°, from the 120 MeV electron linac of the Naval Postgraduate School, the combination being a compromise between the goals of keeping transverse contribution small (forward angle) but having large cross sections ( $E_0$  small). The forward angle (93°) measurements of ref. 2 with 50 and 65 MeV electrons were included in the analysis because they fulfill these conditions. The momentum transfer thus covered the range from 0.37 fm<sup>-1</sup> to 0.75 fm<sup>-1</sup> for zero excitation energy. nat/Ce metal (89% 140Ce) from Ventron Corporation was rolled into self-supporting targets with a mass density of 126 mg/cm<sup>2</sup> (corresponding to 1.50% radiation length<sup>15</sup>). The inelastic data were measured relative to the elastic cross section, thus eliminating systematic uncertainties arising from determination of solid angle, counter efficiencies, charge integration, etc. The elastic cross section  $\sigma_{el}$  was calculated with the phase shift code of Fischer and Rawitscher,<sup>16</sup> using  $c$ ,  $t$ -values for the charge distribution of the ground state from muonic atoms,  $c = 5.78$  and  $t = 2.31$  fm<sup>2</sup>.

The experimental set-up of the NPS Linac has been described recently<sup>16</sup> and is here only summarized for sake of completeness. The accelerated electrons are momentum analyzed in the symmetry plane of a two 30° sector magnet

achromatic deflection system. The electrons scattered from the target are measured by a ten scintillation counter ladder in the focal plane of a 40 cm, 120° double focusing magnetic spectrometer. The momentum bite of the spectrometer is 38, the stepping width of the magnetic field normally corresponds to 0.1 MeV. The overall resolution of the system is limited by the mechanical dimensions of the scintillators and therefore, maximally 0.3%. It was kept to 0.5%, however, because this value is the optimal compromise between background produced at the energy defining slit system, which rises with better resolution, i.e., narrower slits, and background produced in the beam pipes leading to the spectrometer, which rises with wider slits. The data are sorted into energy bins equal to the stepping width (0.1 MeV). Typical spectra are shown in figure 2. For control purposes the whole excitation range has been measured with a wider stepping width, 2 MeV, before and after each inelastic run. No deviations, indicative of background changes, integrator drifts, etc., were found. The spectrum with the highest momentum transfer, 92 MeV at 105°, was measured twice to achieve a good statistical accuracy. Each run took approximately 100 hours of beam time.

### III. Evaluation

#### A. Background

The general principles of evaluation have been described recently including the various types of background (radiative, general room, target-in) which have to be determined, background function,  $\chi^2$ -tests, reduced transition probabilities, and sum rules. We refer to Section III of ref. 16 for particulars. The radial integrals  $\langle r^{2k} \rangle$ , needed for the evaluation of the sum rules can be calculated from the c,t values by

$$\langle r^k \rangle = c^k / (2k + 6) (6 + (k^2 + 5k)(\pi \cdot t / (4 \ln 3 \cdot c))^2).$$

Our choice for the line shape used for the fit of the strength function (Breit-Wigner) is based on a recent investigation of the line shape of the GDR.<sup>17</sup> Although line shapes for resonances of different multipolarity could differ in principle, it seems unlikely. In any case, using a Lorentz form would not change the results outside the error assigned.

In deviation from earlier procedure<sup>16</sup> we have, however, tried various background forms. The smallest  $\chi^2$  was achieved with

$$BGR4(E_f) = P_1 + P_2/E_f + P_3 \cdot RT \cdot \exp(P_4(E_i - E_f)/E_f);$$

but  $BGR3(E_f) = P_1 + P_2/E_f + P_3 \cdot F_f + RT$  did nearly as well. The simplest form for BGR which still described the data

reasonably well and produced an acceptable  $\chi^2$ , was

$$BGR2(E_f) = P_1 + P_2/E_f + RT.$$

( $E_i$  = elastic energy,  $E_f$  = energy of the scattered electron,  $P_1$  fitted parameters,  $RT$  calculated radiation tail, see below). Other forms used were of the type BGR2 or BGR4 with just more terms  $P_n/E_f^{n-1}$  or  $P_n \cdot E_f^{n-1}$  added. Such terms did not improve the fit.

Naively one would identify in BGR2 the  $P_1$  term with the constant room background and the  $P_2/E_f$  term as a corrective term for the failure of the radiation tail calculation at higher excitation energies. However, the terms are not what they seem to be, a confusion which arises from the effects of the constant dispersion of the magnetic spectrometer. Since the momentum bite becomes smaller with smaller magnetic field ( $E_f$ ) the actual count rates are lower by  $E_f/E_i$  and the spectra have to be dispersion corrected. Quite naturally one takes the elastic energy  $E_i$  as reference point and multiplies the cross sections with  $E_i/E_f$  so that

$$\sigma_{\text{true}} = \sigma \exp(E_i/E_f)$$

Since some of the components which contribute to the total background undergo the dispersion and other don't, a closer look into what happens is necessary. 1. The general room background (GRB) is defined as the electrons which penetrate the counter shielding. Since they do not travel

through the spectrometer they are not affected by the dispersion. As an approximation for GRB we use the count rate 10 Mev above the elastic peak. This value is subtracted from the total spectrum (elastic and inelastic) before any other data handling. Any leftover, due to errors in the determination of GRB would contribute to BGR1 in the form of a constant term  $P_1 \cdot 2$ . That part of BGR that comes through the spectrometer, SB, undergoes dispersion. Two assumptions about the nature of this background are possible; a) SB fills the spectrometer evenly with electrons, if the spectrometer setting is far enough from the elastic peak. In this case it would contribute to  $P_1$ . b) SB is produced by the elastic peak, when it hits the walls of the spectrometer. In this case it will either produce the ghost peak, care of which is taken through the simultaneous fitting of an empirically shaped ghost peak line in the immediate vicinity of the ghost peak at 928 of the elastic energy. A more constant part of the experimental scattering would fall off with  $E_f$ , because the elastic electrons will hit further and further away from the counters. For this latter part we assume the lowest order ansatz  $P_2 \cdot E_f$ .

3. The radiation tail (RT) events come through the spectrometer and have undergone dispersion, but they are trivial to treat because of  $RT = RT_{true} \cdot E_f / E_i$ . Since in the analysis the step after subtraction of GRB (as measured 10 Mev above the elastic peak) is the dispersion correction  $E_i / E_f$ , we have the following ( $E_i$  constant) relations

$$P_1 + P_1' \cdot E_i / E_f + P_1'' / E_f$$

$$P_2 \cdot E_f + P_2' \cdot E_i + P_2''$$

If we rename  $P_1' + P_2'$  and  $P_2'' + P_1''$  we end up with BGR2. In addition we have, in a heuristic manner, to take care of the divergence between calculated and measured radiation tail. We know from experiment that the difference  $RT_D = RT_{exp} - RT_{calc}$  rises with excitation energy  $E_x$ . Since  $E_x = E_i - E_f$  we have the lowest order ansatz possible  $P_1 + P_2 E_x = P_1 + P_2' E_f$ . Again, after dispersion correction this does not change the functional form of BGR2, only  $P_1$  and  $P_2$  have a more complicated meaning. It can easily be shown that BGR3 would correspond to a second order Taylor series for  $RT_D$ . BGR4 was originally tried, because we did not know the order required to fit the difference. In this case it is always advisable to try an exponential ansatz, because in principle it contains all orders. The special form of BGR4 comes from the boundary conditions imposed, namely  $RT_D = 0$  for  $E_i = E_f$  (by definition) and  $RT_D = \infty$  for  $E_f \rightarrow 0$ .

If we express  $P_1$  and  $P_2$  in fractions of the minimum of the radiation tail, typical values for the fit parameters for BGR4 are  $P_1 = 0.30 \pm 0.02$ ,  $P_2 = 0.01 \pm 0.01$  (this term characterizes mainly the accidentals),  $P_3 = (0.95 \pm 1.05) \pm 0.03$ , and  $P_4 = 0.25 \pm 0.05$ . It is important to note that  $P_2$ ,  $P_3$  and  $P_4$  are highly correlated with correlation factors in the range 0.7 to 0.9. This explains why BGR2 does still do a good job when compared to the more complicated BGR4.

### B. Errors

The error assignment to giant resonance cross sections is sometimes difficult. Since many variables enter, the purely statistical error is mostly too small. Most recent hadron scattering experiments seem to apply an overall 20% error to their final results (see, e.g., references 18 and 19), while typical errors in  $(e,e')$  are on the 10% level for the major resonances.<sup>16,20,21</sup> The  $(e,e')$  errors are presumably smaller because there are fewer systematic errors due to the measurement relative to the elastic peak, and the background is known, at least in principle, while inelastic hadron scattering experiments have to work with a totally heuristic background.

The errors quoted in this paper are based on the statistical error for the excitation energy, and on two times the statistical error for halfwidth and B-values (areas), because these values corresponded approximately to the minimum and maximum values of these properties experienced during the numerous fits to the data while maintaining an acceptable  $\chi^2$ . That means, these errors include variations in the areas under the curves due to the use of different background functions, different neighboring lines, etc. The error of the percent exhaustion of the sum rule given later, however, is based on the standard deviation of the average sum rule exhaustion and is, therefore, more a measure for the fit to the models used than a measure for the total uncertainty. This is borne out by the observation

that the standard deviation is always smaller or equal to the total uncertainty. In the table of final results we have given a total error based on the maximum and minimum value of the area under the curve experienced through the fitting procedure and errors from the elastic cross sections, which can be considerable, close to the minima in the elastic form factor.

### C. Radiative Corrections

Any scattered electron loses, with a certain probability, energy through emission of photons. It thus ends up in an energy bin it does not belong to, giving rise to the radiation tail. This subsection concerns itself with the loss due to these processes which occurs, because the spectrum  $d^2\sigma/dE dE$  is integrated to an energy cut-off  $\Delta E$ , and electrons with a loss greater  $\Delta E$  will not be counted in the elastic peak, for example. This correction is different for photon emission which occurs in the field of the same nucleus as the scattering event itself (internal Bremsstrahlung, giving rise to the Swinger<sup>22</sup> correction  $\delta_g$ ), and photon emission which occurs in the field of another nucleus (external Bremsstrahlung, giving rise to the Bremsstrahlung<sup>23</sup> correction  $\delta_B$ ). The cross section for internal Bremsstrahlung is proportional to the target thickness, the one for external Bremsstrahlung is proportional to the square of the target thickness and puts, therefore, a limit on the target thickness which may be used.

The expression for the Schwinger correction is<sup>22,24</sup>

$$\delta_S = \frac{2a}{\pi} \ln \frac{E_i}{q} (\ln q^2 - 1) ,$$

( $q$  = momentum transfer) under neglect of terms smaller than 0.01.

The Bremsstrahlung correction is<sup>15,25</sup>

$$\delta_B = t \cdot \frac{4}{3} (1 + \frac{1}{g \ln 1842/173} \ln \frac{E_i}{\Delta E})$$

( $t$  = target thickness) with neglect of terms smaller ~0.01.

When applied to the measured and integrated elastic cross section both  $\delta$  are exponentiated to account for multiple photon emission and thick target effects, respectively.

The true integrated cross section then is related to the measured one by

$$\frac{d\sigma}{dt} \text{ true} = e^{(\delta_S + \delta_B)} \cdot \frac{d\sigma}{dt} \text{ exp}$$

With a cut-off energy of approximately 1 MeV (~ half-width (FWHM))  $e^S \approx 1.2$ , and  $e^B \approx 1.1 - 1.2$ , depending on effective target thickness. Radiative corrections were only applied to the elastic area, because the area under an inelastic resonance is determined from resonance parameters by Area =  $\pi/2 \cdot r \cdot \text{Height}$  and corresponds thus to integration

to infinity so that no cut-off energy is defined.<sup>2</sup>

It can be shown that it is justified to neglect the inelastic corrections for giant resonances if one follows Tait's method<sup>26</sup> and divides the resonances in energy intervals with a width  $\Delta E$ , e.g., equal to the width of the elastic line, and treats each interval as an isolated level with the excitation energy of the middle of the interval. One finds that the electrons which are scattered out of the interval through emission of photons are measured in intervals with lower electron energy (higher excitation energy).

Since the inelastic radiation tail falls off very fast and does, in contrast to the elastic one, not rise again,<sup>27</sup> the radiative corrections which were neglected influence the value of the integrated area measured very little (<3%).

However, the above radiative effects result in an overall shift of the whole resonance to higher excitation energies. The influence on the relative strength of the same resonance in different spectra is even smaller than 3%, because the radiative corrections for the same resonance are nearly identical in different spectra, and do not influence, therefore, multipolarity assignments. Quite generally, it may be stated that radiative corrections in (e,e') do not pose a fundamental problem, when the overall accuracy of the experiment is not better than 1 or 2%.<sup>28</sup>

#### D. Radiation Tail

Three processes contribute to the radiation tail of the elastic peak, which is produced by the elastic electrons which have lost energy through these processes and are, therefore, measured at a lower electron energy  $E'_e$  instead of  $E_i$ .

These processes are (1) radiation during scattering (internal Bremsstrahlung) leading to the radiation tail proper; (2) radiation before or after scattering in the field of another nucleus (external Bremsstrahlung); and (3) electron-electron (Möller) scattering. Landau straggling and ionization is only important close to the elastic peak and does not concern measurements of the continuum. The relative contribution of external Bremsstrahlung and Möller scattering grow with target thickness  $t$ ; they are called  $t^2$ -effects.

We feel that the difficulty in subtracting the radiation tail has been vastly overemphasized, as long as one aims at a final error of (10-15%) (excluding model dependence). This is borne out by the essential agreement between experiments in various laboratories which used quite different approaches, ranging from a free heuristic polynomial fit<sup>29</sup> to a very constraint background fit under inclusion of a calculated radiation tail.<sup>16</sup> In our experience it is more the fact that the resonances overlap which poses a problem. Nevertheless the radiation tail of the elastic peak contributes somewhere between 50 and 90% to the total

cross section and any improvement would be helpful.

While reviewing the systematic body of data measured in Monterey between  $^{28}\text{Si}$  and  $^{238}\text{U}$  we found evidence that it is not the radiation tail proper (internal Bremsstrahlung) which poses a problem, but radiation before and after scattering, because the deviation between fitted total background after subtraction of constant room background and the calculated radiation tail using the formalism by Ginsberg and Pratt<sup>30</sup> was larger for thicker targets ( $t > 1.0$  radiation length) instead for larger  $Z$ . This may, in part, be due to our energy range. It has been pointed out by Tsai<sup>31</sup> that some assumptions which enter the derivation of the formalism for the radiation tail (e.g., screening) do not work particular well between 10 and 100 MeV. For completeness, we give below the expressions for the effects which contribute to the radiation tail of the elastic peak.

The expression given by ref. 30 for the charge radiation tail is

$$\frac{d^2\sigma}{dE_f dE_i} = \frac{1}{m_O c^2} \frac{z^2 r_Q^2}{4\pi a} \frac{p_f}{p_i} \int_{x_{\min}}^{x_{\max}} \frac{dx}{x^2} F^2(x) R_{\text{CH}}$$

with  $r_Q = 2.82$  fm (classical electron radius),  $p_i, p_f$  initial and final electron momentum,  $x = \frac{1}{2} q^2$  ( $q$  three momentum transfer),  $F^2(\frac{1}{2} q^2)$  elastic form factor, and  $R_{\text{CH}}$  a lengthy kinematical expression.<sup>30</sup>

Since this expression has been derived in first order Born approximation (one photon exchange) it is not strictly valid for heavy nuclei, but the influence of the nuclear electric potential (multi-photon exchange) can, somewhat heuristically, be taken into account by replacing  $p^2 (\frac{1}{2} q^2)$  by  $p^2 (\frac{1}{2} q^2, \theta)$  from experiments, in practice calculated with phase-shift codes from experimental  $c.t.$  values (only in DWBA is the cross section simply a function of  $q$  alone, if  $\alpha \cdot z$  is no longer small compared to unity, it becomes a function of two of the three variables  $E$ ,  $\theta$  and  $q$ ).<sup>32</sup>

Sometimes Schiff's peaking approximation is used, which leads to a simple analytical expression

$$\frac{d^2\sigma}{dQ dE_f} = \frac{1}{m_e c^2} \frac{t}{E_i - E_f} \left\{ \left( 1 + \frac{E_f}{E_i} \right) I_m(2E_i \sin \theta/2) - \frac{1}{2} \right\} \times \left\{ \frac{d\sigma}{dE_i}(E_i) + \frac{d\sigma}{dE_i}(E_f) \right\}$$

However, for 90 MeV electrons the peaking approximation only gives reasonable results for  $E_x \leq 10$  MeV.

The cross section for external Bremsstrahlung

$$\frac{d^2\sigma}{dQ dE_f} = \frac{1}{m_e c^2} \frac{t}{E_i - E_f} \left\{ \frac{E_f}{E_i} + \frac{3}{4} \frac{(E_i - E_f)^2}{E_i} \right\} \left\{ \frac{d\sigma}{dE_i}(E_i) + \frac{d\sigma}{dE_i}(E_f) \right\}$$

$$b = \frac{4}{3} \left\{ 1 + \frac{1}{9} \ln \frac{1}{4\pi^2 \chi_0^2} \right\}$$

was taken from Mo and Tsai,<sup>26</sup>  $\chi_0$  radiation length.

Möller scattering finally is given by<sup>23</sup>

$$\frac{d^2\sigma}{dQ dE_f} = \frac{1}{m_e c^2} \frac{2\pi r_0^2 N_A}{2} \frac{\frac{2}{A} \left\{ \frac{1}{E_i^2} - \frac{2E_i - 1}{E_f(E_i - E_f)(E_i + 1)} + \frac{1}{(E_i + 1)^2} \right\}}{\left\{ \frac{d\sigma}{dQ}(E_i) + \frac{d\sigma}{dQ}(E_f) \right\}}$$

with  $2\pi r_0^2$  being the cross section of a classical electron and  $N$  Avogadro's number.

#### **IV. Results**

##### **A. General**

In Plane wave Born approximation (PWBA), only valid for  $z \alpha \ll 1$ , the form factors are proportional to  $q^\lambda$  for low momentum transfer  $q$  (see, e.g., ref. 33). While for  $z = 58$  PWBA evidently no longer is applicable quantitatively the  $q^\lambda$ -dependence still is qualitatively useful. Figure 4 shows the DWBA cross section divided by the Mott cross section (in light nuclei equivalent to the square of the form factor) as a function of momentum transfer. Since form factors are not a unique function of  $q$  in heavy nuclei, the curves are interpolations between cross sections taken from DWBA calculations with the correct primary (= elastic) energy,  $E_1$ , used at the appropriate momentum transfer. This procedure is possible, because despite the breakdown of PWBA in general, we found that for constant primary energy  $E_1$  calculations of the form factors with different energy of the outgoing electrons  $E_f$  agree within 3% for the same  $q$  over an angular range from  $30^\circ$  to  $175^\circ$  (only  $135^\circ$  for the  $E_1$ ).

immediately evident. If we identify<sup>2,3</sup> the  $12$  MeV ( $63 \text{ A}^{-1/3}$  MeV) and  $25$  MeV ( $130 \text{ A}^{-1/3}$  MeV) resonance with E2, the states at  $6$ ,  $22$ , and  $31$  MeV have a higher multipolarity. If we compare the energies in  $\text{A}^{-1/3}$  units ( $31$ ,  $114$ ,  $160$  respectively) with table 1, the first two are good candidates for an E3 assignment, while the latter lines up best with an E4 prediction. The resonance at  $37$  MeV is the most cumbersome to evaluate, because it is highest in energy and has therefore the largest width. Comparison with table 1 leads to an E3 assignment, but estimates based on sum rule considerations make E0 possible as well. The final assignment from DWBA calculations are indicated in figure 5, the ambiguities with the  $31$  and  $37$  MeV resonance will be discussed in detail later.

One also sees, that the ratio of E1 to E2 peak height (equal to the cross section ratio) does change very little, in agreement with figure 4, if taken at the correct  $q$ .

##### **B. The Giant Dipole Resonance and the Nuclear Breathing Mode**

More than 30 years ago Migdal<sup>34</sup> explained the nuclear photoeffect results of Bothe and Gentner<sup>35</sup> by assuming the existence of a dipole oscillation of the "protons against the rest of the nucleus" (the neutrons), an assumption leading to an average excitation energy for this mode of  $24 \text{ A}^{-1/3} \sqrt{\beta z/A}$  MeV, with  $\beta$  the coefficient of the symmetry term  $\beta (N - 2)^2/A$  in the Bether-Weizsäcker mass formula.<sup>36</sup> Several years later, independent developments led to

The broken vertical lines in figure 4 indicate the inelastic momentum transfer covered by the data used, for an excitation energy of  $5$  MeV. The method employed by us (interpolation of the calculated DWBA cross section) has the advantage of not changing the measured values. Comparing figure 5 with figure 4 some qualitative results are

the papers of Goldhaber and Teller<sup>37</sup> ( $E_x \sim A^{-1/6}$ ) and Steinwedel and Jensen<sup>38</sup> ( $E_x \sim A^{-1/3}$ ). Experimental evidence (see the review article by Berman and Fultz<sup>39</sup>) has shown, in the meantime, that neither model describes the energy of the dipole mode, the correct single  $\alpha$  exponential law being  $E_x \sim A^{-0.23}$ .

The difficulty posed by the existence of two models for the GDR rests with the fact that they lead to quite different transition charge densities, which in turn, when used in DWBA calculations, produce form factors  $F(q, E) = [(d\sigma/d\Omega)_{DWBA}/(d\sigma/d\Omega)_{Mott}]^{1/2}$  which are different up to a factor of 2 in heavy nuclei.

The transition charge densities associated with Goldhaber-Teller (GT) and Steinwedel-Jensen (SJ) models are  $\mathcal{G}_{tr}^{GT}(r) = C^{GT} A^{-1} d\mathcal{G}_o(r)/dr$  and  $\mathcal{G}_{tr}^{SJ} = C^{SJ} \cdot J_1(r \cdot 2.08/c) \mathcal{G}_o(r)$ . Photoabsorption measurements are practically model-independent, consequently they can not decide between different charge densities. While there have been many generalizations of the Goldhaber-Teller model (see, e.g., ref.<sup>40</sup>) only very recently a new detailed macroscopic approach to the problem has been tried by Myers, Swiatecki and co-workers<sup>41</sup>, who applied the framework of Myers' and Swiatecki's droplet model<sup>42</sup> to the problem of the giant dipole resonance. In short, their approach yielded a mixture of both modes,

$$\mathcal{G}_{tr}^{(r)} = \frac{C^{HS}}{1+\epsilon} \left\{ \mathcal{G}_{tr}^{GT}(r) + \alpha \mathcal{G}_{tr}^{SJ}(r) \right\},$$

with the constant  $\alpha$  being a function of  $A$ , rising from approximately 0.5 for the Ni region to 0.8 for  $^{208}\text{Pb}$ . Myers, et al.<sup>41</sup> give three solutions to their model, the super-simple solution, the droplet mode, and the exact solution, with the parameter  $\alpha$  being 0.80, 0.74, and 0.64, respectively, for  $A = 140$ .

Aside from the fundamental importance of the macroscopic description of the giant dipole resonance, it has a very actual importance. There has been mounting evidence recently of the existence of a giant monopole resonance at  $80 \text{ A}^{-1/3}$  MeV in heavy nuclei, exactly under the GDR. This excitation energy has been originally proposed by Marty, et al.<sup>43</sup>, the strongest support coming from  $(\alpha, \alpha)$  scattering at very forward angles.<sup>44</sup> This evidence is very convincing, but not conclusive, because it is based on the assumption that  $(\alpha, \alpha')$  does not excite the isovector GDR resonance, the  $\alpha$ -particle being a  $T = 0$  particle. However, the  $\alpha$ -particle does have a charge and, therefore, breaks isospin selection rules, and, probably more importantly, the nuclei where this mode has been investigated by  $(\alpha, \alpha')$ ,  $^{208}\text{Pb}$  and  $^{144}\text{Sm}$ , have a large neutron excess, giving rise to isospin impurities in  $\alpha$ -scattering of the order  $(N - Z)/A$ . In addition, isospin impurities in the GDR have even been found with capture reactions in light self-conjugate<sup>45,46,47</sup> nuclei and in nuclei with small neutron excess<sup>46,48</sup> up to  $A = 52$ . Unfortunately, in heavier nuclei capture reactions

cannot be used to investigate the GDR, because of the rising Coulomb threshold and the falling energy of the dipole resonance. Little is known, therefore, about isospin impurities in these nuclei.

Electron scattering is very suited to exciting a monopole oscillation, but is hampered in general by the well-known property of an E0 excitation to exhibit the same momentum transfer (or angular) dependence as the E2, and in particular, that is for a monopole mode at  $80 \text{ A}^{-1/3}$  MeV, by the presence of the GDR. Any ( $e, e'$ ) experiment which attempts to investigate the problem of the monopole, has first to solve the problem of the model for the GDR, because the latter has to be subtracted in order to get the monopole cross section and the choice of the model determines the result. In our opinion this problem is mainly a question of good enough statistical and systematic accuracy over a wide enough range of momentum transfer in order to pin down the experimental form factor. Past ( $e, e'$ ) experiments, including our own, have not achieved this goal.

Despite these uncertainties, the existence of a monopole resonance at  $80 \text{ A}^{-1/3}$  MeV has been supported by ( $e, e'$ ) measurements at high primary energy and forward angles, using multipole expansion<sup>49</sup>, the result being that 100% of the monopole sum rule are exhausted if one uses the GT model for the GDR but finding only 10% when using the SJ model. It might be noted, that these results are in contrast to

earlier evaluation of the same data using a line shape fit by the same authors. Similar results<sup>50</sup> have been given for 208 pb.

Since the multipole expansion introduces a nuclear model before the cross sections are extracted, it is not possible to make a decision between the models with this method. The low primary energy electron scattering experiments<sup>2,51</sup> ( $E_0 \lesssim 70$  MeV), on the other hand, are unsuited to explore this problem, because in order to reach the necessary momentum transfer, backward angle ( $\theta \geq 120^\circ$ ) scattering has to be used. Two problems enter here. The DWBA code 52 with retardation (excitation energy  $> 0$ ) fails for the E1 at backward angle<sup>2</sup> (that it converges at all at more forward angles is due to accidental cancellation of two terms).<sup>53</sup> As can be clearly seen in the form factor,<sup>3,29,51</sup> an unphysical upswing occurs at backward angles. A way around this is to neglect retardation (excitation energy = 0), and to take the form factor at the correct inelastic momentum transfer

$$q_{\text{in}} = (E_i^2 + E_f^2 - 2E_i E_f \cos\theta)^{1/2}/\hbar c$$

instead.<sup>54,55</sup>

In addition, to add one more layer of ambiguity, there are transverse contributions to the cross section in the GDR regions. This is evident when one uses DWBA calculations without retardation as described before, because a

large cross section remains at backward angles in excess of the B-value, expected from forward angle  $-(e,e')$  at the same momentum transfer, and from  $(\gamma,n)$ . Assumption of a transverse electric spin flip  $E_1$  is compatible with the data<sup>2,3,4</sup>, but the experimental evidence is not conclusive, or there might be an M2 (ref.2) or M3 (ref. 21) resonance in the GDR region. Since both effects (failure of DWBA at large angles, transverse contributions) go in the same direction the problem has apparently not been recognized in recent low energy electron scattering experiments.<sup>21,51</sup> The conclusion drawn, namely the model independence of  $E_1$  excitation at momentum transfers  $q < 0.7 \text{ fm}^{-1}$ , does not stand up to scrutiny. Although GT and SJ model in the case given<sup>21,51</sup> do give approximately the same B-value, the standard deviation of the SJ model fit is much larger than that due to the GT model, that means, the SJ model does not describe the data and the assignment of a B-value is meaningless.

In order to convince ourselves that there is a real problem with the DWBA formalism in its present form,<sup>53,55</sup> and not a problem of suitable choice of integration parameters, we have done extensive  $E_1$  calculations with the program of 'van, et al., which to our knowledge is the basis for most calculations performed in various laboratories<sup>56,57</sup>. The standard test for  $(e,e')$  DWBA is to compare the DWBA results for  $z = 0$  with PWBA, because the latter can be solved in closed form. Both should be identical. The subroutine which selects the integration parameters depending

on primary energy, number of partial waves, etc., gave for 65 MeV agreement only up to approximately  $140^\circ$ . Since series of spherical harmonics have poles at the origin, we used the reduction method of Ravenhall, et al.<sup>58</sup> to improve upon the convergence. The program, which has one reduction built-in, was changed to allow for multiple reductions. Using more reductions made the convergence at forward angles worse, which is understandable because more poles are removed at the origin than exist<sup>55</sup>, but it improved the backward convergence for  $z = 0$  dramatically. With four reductions DWBA ( $z = 0$ ) and PWBA agreed to better  $1/2\%$  up to  $180^\circ$ , but only when the radial integration was extended to greater than 500 fm, instead of 50 to 100 fm which are sufficient for higher multipoles. However, this work turned out to be nearly for naught because DWBA ( $z \neq 0$ ) still diverged at backward angles,  $\theta > 150^\circ$ , the divergence becoming more pronounced with lower primary energy, that is, with a rising  $E_x/E_i$  ratio.

As a reference cross section for testing the divergence, we have used DWBA ( $z \neq 0$ ) calculations with  $E_x = 0$  (no retardation). Since for multipolarities greater one, as already described above, form factors for the same primary energy agree within 3% as a function of (inelastic) momentum transfer, independent of the actual energy of the outgoing electron used in the calculation, one may assume the same to be true for  $E_1$ .<sup>55</sup>

In the attempt to solve the problem of the E1 form factor we have only used measurements with  $90^\circ \leq \theta \leq 105^\circ$  thus avoiding the whole complex of transverse contributions. DWBA calculations show (figure 6) that in order to be able to differentiate between GT, SJ and MS model for  $^{140}\text{Ce}$ , an accuracy of 25% or better for the single measurement is necessary. To differentiate between the various solutions of Myers, et al., one needs an accuracy of better than 10%. While the latter is difficult to achieve in general, it is possible for the E1 in the case of  $^{140}\text{Ce}$ . For once, the line shape of the GDR is known from  $(\gamma, n)$ <sup>59</sup> and secondly, the already described separation of E1 and E2 resonance in  $N = 82$  nuclei is important. The essential element, however, is the fit over a very wide range of excitation energy, which puts a strong constraint on the freedom in the background fitting. In addition, our finding that radiation tail calculations are good up to 20-25 Mev agrees with Szalata, et al.<sup>60</sup>, who used comparable primary energies for  $^{20}\text{Ne}$ . Sasao and Torizuka<sup>50</sup> even claim 80 Mev as limit for  $^{208}\text{Pb}$ , which might be possible, because of their much higher primary energy (see remark in Section III.D.). Since the GDR in  $^{140}\text{Ce}$  is well below 20 Mev, the cross section turned out to be little background sensitive, much less so than for the resonances below 10 Mev, where the accuracy in our installation is hampered by the ghost peak, and the ones above 20 Mev, due to their large width.

We have employed a fitting procedure described

recently<sup>17</sup> to the  $(\gamma, n)$  data<sup>59</sup> for  $^{140}\text{Ce}$  resulting in  $E_\gamma = 14.95 \pm 0.05$ ,  $\Gamma = 4.20 \pm 0.05$  and  $\sigma = 384 \text{ mb}$ . The difference in cross section to the values given by Berman<sup>61</sup> is mainly due to the inclusion of the isovector GQR at 25 MeV. The difference in excitation energy is due to the fact that we have fitted the E1 strength function rather than the  $(\gamma, n)$  cross section<sup>17</sup>. Our result for the  $(\gamma, n)$  cross section corresponds to an  $B(E2, q = k) = 41 \text{ fm}^2$  or  $B(E1, q = 0) = 43 \text{ fm}^2$ , the latter quantity to be used in electron scattering.

Nevertheless we have fitted the GDR parameters in the  $(e, e')$  spectra, despite the knowledge about the line shape  $(E_x, \Gamma)$  from  $(\gamma, n)$ . The results are  $E_x = 15.3 \pm 0.1$ , and  $\Gamma = 4.4 \pm 0.2$ . The excitation energy is higher than the  $(\gamma, n)$  energy outside the error. A similar shift has been reported earlier for  $N = 82$  nuclei<sup>2,62</sup>. Since due to our unified approach of fitting the strength distribution rather than the cross section in  $(e, e')$  and  $(\gamma, n)$  data, the explanation given in ref. 2 for an even larger shift now no longer applies for the shift found.

We believe that the remaining difference in excitation energy is due to the shift produced by the radiation tail, described in Section III.C., but this assumption could only be proven by applying Tsai's unfolding procedure<sup>26</sup>, which we have not done, because this would add one more layer of data manipulation without improving the accuracy in cross section determination.

Figure 6 shows the final result for the resonant cross section found at 15.3 MeV. We must emphasize that the curves shown (GT, SJ, MS) are not fitted to the data. They were normalized to  $B(E\lambda, q = 0) = 43 \text{ fm}^2$  from the  $(\gamma, n)$  data.<sup>59</sup> There is a small inconsistency in our procedure insofar as we have measured on a nat Ce target, while the  $(\gamma, n)$  data were taken on enriched isotopes, but the  $^{142}\text{Ce}$  resonance values 59.61 are so close to  $^{140}\text{Ce}$ , that the change is negligible for our purposes.

In order to investigate the three solutions of the MS model, we have fit the model parameter  $\alpha$  to our data, while keeping the B-value to  $43 \text{ fm}^2$ , resulting in  $\alpha = 0.74 \pm 0.04$ , thus corresponding to the droplet mode.<sup>41</sup> While at first glance our result seems to rule out a monopole under the giant dipole resonance, more discussion is needed.

Figure 6 clearly rules out the SJ model, however, because it is higher than the experimental points by nearly a factor of two. But because the GT form factor is lower than the data, the difference between GT and MS models could be due to a resonance of different multipolarity. Figure 7 shows, therefore, the difference between the experimental points and the GT curve of figure 6. The difference is nicely described by an E2 or E0 form factor. If one chooses the latter,  $(45 \pm 15)\%$  of the EWSR ( $E0, \Delta T = 1$ ) would be exhausted, in near agreement with<sup>44</sup>, which gives  $(100 \pm 20)\%$ , the GT curve itself in figure 6, that it would have a peak

but reports a model dependence of a factor of two. For the monopole calculations the model by Schucan<sup>63</sup>

$$\frac{E_0}{S_{tr}}(r) = -3\beta_0(r) + \frac{d\beta_0(r)/dr}{r}$$

was used, which is identical with one of two used by Satchler<sup>63</sup> and Youngblood, et al.,<sup>44</sup> except for the difference between charge and nuclear matter oscillation in  $(e, e')$  and  $(\alpha, \alpha')$ , respectively. The DWBA code used by us is a version of that of Tuan, et al.<sup>52</sup> written by Kawazoe<sup>57</sup>. We have also tried the second model of Satchler<sup>63</sup>; differences between the two are below 10% in the momentum transfer region covered by our experiment, quite in contrast to ref. 44. Table 2 shows the parameters for monopole resonances reported in  $N = 82$  nuclei. In contrast to the E1 results, shown for  $^{140}\text{Ce}$  and  $^{142}\text{Nd}$  in table 3, there is a wide variation in strength and excitation energy. Especially for the excitation energy, not model-dependent like the strength, the difference is difficult to explain for a giant resonance, which is expected to change slowly with  $A$ .

There are two arguments against the interpretation that the difference between experiment and GT model shown in figure 7 is due to a monopole or quadrupole excitation.

1. Since the claimed monopole has a width of 2.5 - 3.0 MeV in heavy nuclei<sup>43,44,65</sup>, it can be seen from the difference between experiment and GT curve, compared to the value of the GT curve itself in figure 6, that it would have a peak

height greater than the E1 at  $q = 0.52$  and  $q = 0.61 \text{ fm}^{-1}$ .

The apparent width of the composite line ( $E1 + E0$ ) then should be noticeably smaller in our fits than the width known from ( $\gamma, n$ ). If we make the conservative estimate that the peak heights are equal,  $\Gamma(E0 + E1) = 3.5 - 3.7 \text{ MeV}$  compared to  $\Gamma_{\text{fit}} = (4.4 \pm 0.2) \text{ MeV}$ . However, due to the problems encountered with the choice of background in hadron scattering, we would not put too much emphasis on this argument.

2. More convincing, therefore, is the independent confirmation of the MS model through the single power A-law for the GDR. The MS model reproduces  $E_x \sim A^{-0.23} \text{ MeV}$  known from experiment and consequently rules out the GT model unambiguously. Use of the MS model instead of the GT model in other  $(e, e')$  experiments which find monopole strength at  $80 \text{ A}^{-1/3} \text{ MeV}$  will eliminate most or all of the E0 strength within the errors given.

As outlined earlier in this subsection, isospin is not necessarily conserved in a (and d) scattering from  $(N - 2) > 0$  nuclei and rather large isospin impurities have been found in the GDR in such nuclei accessible to capture reactions, which mostly do not have a large neutron excess. For example, comparing the  $(e, e')$   $^{40}\text{Ca}$  data of Goldmann<sup>66</sup> and the  $^{36}\text{Ar}(a, \gamma_0)$   $^{40}\text{Ca}$  data of Watson, et al.<sup>47</sup>, with the  $E0$  data of Marty, et al.<sup>43</sup>, a very close agreement of width and position of the E1 GR with the proposed monopole is found ( $E_x = 20 \text{ MeV}$ ,  $\Gamma = 4 \text{ MeV}$ ). If we would apply the background procedure of hadronic scattering, and of ref. 66 (matching of a linear background to the data at the energy

where the spectra start to be flat) to our data, an apparent width of the 15.3 MeV resonance of  $2.5 - 3.0 \text{ MeV}$  would result. The position of the monopole claimed in  $^{40}\text{Ca}$  gives even more reason to believe that the E1, and not the monopole, is seen in  $(a, a')$ <sup>44</sup> and  $(d, d')$ <sup>43</sup> scattering, because its excitation energy ( $68 \text{ A}^{-1/3} \text{ MeV}$ ) scales exactly with the GDR, down from  $81 \text{ A}^{-1/3} \text{ MeV}$  in  $^{208}\text{Pb}$ . From the very constant  $A^{-1/3}$  dependence (fig. 1) of the isoscalar E2 one would not expect such a strong variation for the isoscalar breathing mode.

On the other hand, the excitation mechanism for E0 and E1 excitation is well understood for  $(e, e')$  and  $100\text{e}$  EWSR ( $E0, \Delta T = 0$ ), as proposed, would be visible. We think, therefore, that more work is needed at the understanding of the excitation mechanism of  $T = 0$  hadronic particles beyond the argument that they just do not excite the  $\Delta T = 1$  GDR. Since we did not measure backward angles, we cannot experimentally contribute to the solution of the question, whether the 'excess' strength of the GDR at backward angles are due to electric E1 spin-flip<sup>67</sup> or M2 or M3 contributions<sup>2,51</sup>. However, we can rule out that they are due to anything but transverse excitations.

### C. Quadrupole Excitations and the Total Photon Cross Section

The giant isoscalar quadrupole resonance in nuclei ( $QQR, \Delta T = 0$ ) is probably the best investigated of the 'new' (how long have they been there?) resonances. It corresponds to a jump between single particle orbits which have quantum numbers different by 2. In contrast to the case of the GDR, the hydrodynamic models completely fail to predict this mode of excitation. The flood of information produced in recent years, following the first discovery of the  $E2 (\Delta T = 0)$  mode,<sup>7</sup> have, in contrast, shown that the ideas of Bohr and Mottelson concerning the interplay between single particle and collective coherent motion in the nucleus and especially including the role of isospin, were correct.<sup>11</sup> The scattering of strongly interacting particles, especially alphas<sup>13</sup> have played an essential role in the systematic investigation of the isoscalar giant quadrupole resonance, but the potential structural richness of the giant resonance region has, up to now, mainly been fully open to electro excitation, because isovector excitations are suppressed in hadron scattering.<sup>18</sup> Capture reactions, while one of the most versatile tools in light nuclei,<sup>1,68</sup> are hampered by the rising Coulomb threshold in heavy ones.

In general, good agreement has been found for the sum rule strength extracted from  $(\alpha, \alpha')$  and  $(e, e')$ , e.g.,  $(92 \pm 25)\%$  (ref. 13) vs  $(92 \pm 10)\%$  (ref. 69) in the case of  $^{208}\text{Pb}$ , or  $(54 \pm 15)\%$  (ref. 13) vs  $(56 \pm 6)\%$  (ref. 16) the case of  $^{90}\text{Zr}$  and  $^{89}\text{Y}$ . There has been some controversy

concerning position and width in  $N = 82$  nuclei<sup>13,70</sup>, but this discrepancy has been resolved with  $\alpha$ -scattering of higher energy, which showed a satellite at  $80 \text{ A}^{-1}/3 \text{ MeV}$ ,<sup>44</sup> interpreted as E0 (see discussion in the previous subsection, but also ref. 71). A closer look into  $N = 82$  nuclei shows some inconsistencies, which occur very systematically, although they are not in all cases outside the range of overlapping errors. To find these discrepancies one has to look into the method of evaluation. The  $(e, e')$  spectra have mostly been evaluated with a line shape fit using either Lorentz lines for the cross section (e.g., ref. 2, 62, 72), or Breit-Wigner curves for the  $B$ -value distribution (strength function),<sup>16</sup> and it has been shown that the two approaches are nearly equivalent to each other, at least they do not change the resulting areas under the strong resonances noticeably.<sup>17</sup> In contrast,  $(\alpha, \alpha')$  data could not be described as well by a Lorentz curve as by a Gaussian.<sup>13</sup> Positions and width from a direct evaluation of the data (rms-energy, rms-width) agreed within 100–200 keV with width and centroid position from Gauss or Lorentz fits, but the Lorentz fits resulted in 20–30% increase in peak yield, because more strength is under the tails, which do not fall off as rapidly as for the Gaussian.<sup>13</sup>

Since the areas under a Lorentz and a Gauss curve of equal width and height are different by a factor of  $\ln 2$ ,<sup>17</sup> the  $(e, e')$  results should be 44% larger, everything else equal (that the effective yield going from Gauss to Lorentz

curves changes only 20 - 30% as reported in ref. 13 and not by 44%, is understandable, because line shape fits have a tendency to conserve the area). In fact, as table 4 shows, just the opposite occurs, namely the ( $a, a'$ ) data are systematically higher, even the introduction of the  $80 \text{ A}^{-1/3}$  MeV resonance in the analysis reduces the sum rule strength only from 91% to 85% (ref. 13 vs 44 for  $^{144}\text{Sm}$  in table 4). The last value in table 4, from the current measurement, under inclusion of the 93° spectra of ref. 2 is markedly lower than the old analysis for  $^{140}\text{Ce}$  or any of the other low energy ( $e, e'$ ) results<sup>29,62,70</sup>, although it agrees within the errors with the others (except  $^{142}\text{Nd}$  (ref. 29,70) which is marginally outside the errors). Figure 8 shows why. The lower energy measurements span too small a momentum transfer region at forward angles to be able to recognize the systematic behavior of the cross sections, namely a deviation from the Goldhaber-Teller (GT) model. If one, not considering the standard deviation of the experimental points from the curve, does a fit of the 'strict' ( $c_{tr}/c = 1.0$ , nomenclature of ref. 73) GT model to the data, a strength of 65% EWSR results. But obviously, the data do not fall on this curve. The solution to this discrepancy is ambiguous. Either the model fails, or another (or several) underlying higher multipoles (figure 4) contribute. Figure 8 shows the solution to the first possibility, namely a fit of the model parameter  $c_{tr}/c$  to the data, which reduces the B-value from 2500 fm<sup>2</sup> to 2000 fm<sup>2</sup>. Since it has

been shown, both with microscopic calculation<sup>74</sup> and with more fundamental consideration,<sup>11,75</sup> that an E2 state which carries a major fraction of the sum rule should follow the hydrodynamical model closely, we prefer the alternative explanation. Figure 9 thus shows the difference between the experimental points and the GT model of figure 8, clearly favoring an E3 assignment for the assumed underlying cross section. Despite this ambiguity in interpretation the B(E2) would be reduced in either case to approximately 2000 fm<sup>2</sup>. But an E4 cannot be ruled out, especially if one realizes that the result is doubly model dependent, insofar as the "experimental points", too, depend on the DWBA calculations used in figure 8.

Table 5 shows the E2 strength up to 12 MeV from ( $e, e'$ ), a total of 67 to 77% of the EWSR is exhausted depending on whether or not the 10 MeV state<sup>2</sup> is counted. Since the latter coincides with the  $53 \text{ A}^{-1/3}$  MeV state in  $^{208}\text{Pb}$ , which may or may not be part of the monopole GR, 69,76 we will come back to that point in a separate section later. There is a corresponding number of microscopic calculations to the experimental attention the isoscalar E2 (and isovector) mode has had in recent years. Historically the first such calculation has been published by Kamerdzhev<sup>77,78</sup> followed by Ring and Speth<sup>79</sup> and Bertach<sup>80</sup>. We would like to point out that ref. 77, being submitted at the same time as ref. 3, is the only microscopic calculation which truly predicted very accurately both isoscalar and isovector E2 in  $^{208}\text{Pb}$  and  $^{120}\text{Sn}$ . The most detailed results have been

published by Liu and Brown.<sup>81</sup> Though they do not treat <sup>140</sup>Ce explicitly, their results show a regularity concerning A-dependence and we have interpolated their <sup>90</sup>Zr and <sup>208</sup>Pb calculations (table 6) to compare with our data. Although it would be easily possible with our DWBA code to use the microscopic transition densities from one author or the other, we have abstained from doing so, not only for the reason already given above, but also to preserve compatibility between different laboratories. (Transition densities from macroscopic models are easily available and comparable, microscopic ones are not.) The (u,u') data show convincingly, that the Goldhaber-Teller model describes the isoscalar E2 and E3 data over many maxima and minima, even though there is an inherent difficulty to extract the electromagnetic strength unambiguously from strong interacting particle scattering.<sup>82</sup>

In contrast to the isoscalar E2 is not expected from the isovector mode to simply follow a surface oscillation<sup>11</sup>. The Goldhaber-Teller and Steinwedel-Jensen model has been applied separately to the isovector mode in <sup>208</sup>Pb by Sasao and Torizuka within their multipole expansion. The same argument as for the dipole mode is valid; since the multipole expansion introduces a model already for the extraction of the cross sections, a model dependence can not be investigated. Our line shape fit shows a resonance at  $25 \pm 1$  MeV with a width of  $6.5 \pm 1$  MeV (FWHM). As in the case of the isoscalar resonance we find a deviation between cross sections

and DWBA GT calculations. Figure 10 shows, among transitions to other resonances, which will be discussed later, that the strict GT model does not describe the 25 MeV data, but also, that an E3 form factor does even worse. Although there has not yet been a quantitative extension of the work by Myers, et al. for description of the E2 mode, we have fitted a parameter  $\alpha(E2)$  in analogy to the E1 resonance<sup>41</sup>

$$\mathcal{S}_{tr}(r) = \frac{C^{MS}}{1+\alpha} [\mathcal{S}_{tr}^{GT}(r) + \alpha(E2) \mathcal{S}_{tr}^{SJ}(r)]$$

with  $\alpha(E2) = 1.0 \pm 0.2$  determined experimentally. Table 10 shows that the 'Myers-Swiatecki' model reduces the standard deviation compared to the GT model.

Figure 11 shows the alternative interpretation: analogous to figure 9 the difference between experimental points and GT model is plotted as a function of momentum transfer and compared to DWBA form factors. Either E3 (-20% EWSR) or E4 (~40% EWSR) strength, or both, may be hidden under the 25 MeV resonance. Table 6 shows that both multipoles would be compatible with the microscopic calculations.<sup>81</sup> As in the case of the isoscalar E2 both interpretations result in a lower B(E2) value, 50% EWSR ( $\Lambda T = 1$ ), compared to 80% for the strict GT model. It is clear from the foregoing that in this case we favor the MS model interpretation over the interpretation of underlying other multipoles, but clearly a more thorough investigation in terms of the droplet model, as done in ref. 41 for the E1, is needed.

This leaves us with the overall result that only approximately 50% of isoscalar and isovector strength are concentrated in form of a coherent resonant state of 12 and 25 MeV, respectively. The question of where the missing E2 strength might be is of great importance. It could be either dispersed into a non-resonant background, or it could be pushed up to higher excitation energies through short range correlations<sup>5,11</sup> as already mentioned. If we assume the latter, an interesting possibility opens up. Intrigued by the total  $\gamma$ -absorption measurement of the Mainz group<sup>83</sup> and small percentage of E2 strength found in a concurrent measurement on  $^{28}\text{Si}$  (ref. 84) we have calculated for  $^{28}\text{Si}$  the amount of photon cross section which could be due to E2 absorption at high excitation energy.

The total photon absorption measurements<sup>83</sup> found that two times the classical E1 sum rule 60-NZ/A MeV mb (Thomas-Reiche-Kuhn<sup>85</sup>) were exhausted up to the pion threshold. No disentangling into different multipolarities has yet been possible (see, e.g., Editors Comments in ref. 86, Part VI). While our measurement<sup>84</sup> in  $^{28}\text{Si}$  does not disentangle multipolarities above 50 Mev either, it is nevertheless illuminating to calculate how much of the E2 strength missing below 50 MeV would contribute if it is located higher in excitation energy. It was found that nearly all the excess  $\gamma$ -cross section in excess of the Gell-Mann - Goldberger-Thirring sum rule<sup>87</sup> ( $GTR = 1.4$  times the classical E1 sum rule) under certain conditions might be due to E2 absorption.

Since the  $\gamma$ -cross section and the reduced transition probability  $B(E2, k)$  are connected by<sup>17</sup>

$$\int \sigma_\gamma dE_\gamma = 3.1 \cdot 10^{-6} E_x^3 B(E_x, k) [\text{MeV mb}]$$

( $k$  photon momentum transfer,  $E_x/\hbar c$ ), it is evident that the actual contribution depends on the excitation energy. Effectively the dependence does not scale with  $E_x^3$  due to the effect of the energy weighted sum rule and the fact that  $k$  is no longer small. Since

$$B(E_x, k) = (2\lambda+1) \left| \frac{(2\lambda+1)!!}{k^{\lambda}} \int d_k(kr) S_{kr}(r) r^2 dr \right|^2$$

(which transfers into the familiar  $(2\lambda+1) \int |\int \delta_{tr}(r) r^{\lambda+2} dr|^2$  for  $k \rightarrow 0$ ),  $B(E_x, k)$  falls off with rising excitation energy. For example,  $B(E2, k = 0.25) \approx 0.8 B(E2, 0)$ . Table 7 shows for  $^{140}\text{Ce}$  some examples of possible contributions of E2 strength to the photon cross section in units of the Thomas-Reiche-Kuhn sum rule under the assumptions specified in the caption.

A recent monochromatic ( $\gamma, n$ ) measurement<sup>88</sup> which extended an earlier one<sup>59</sup> to  $E_\gamma = 100$  MeV, found for  $^{nat}\text{Ce}$  the total cross section up to that energy to be 1.7-TRK. The cross section in excess of a Lorentz line extrapolation of the GDR at 15 MeV rises to approximately 8 mb at 55 MeV and stays relatively constant out to 100 MeV.<sup>88</sup> Table 7 shows that (1) the isovector E2 strength at 25 MeV (50%

EWSR) already contributes 0.05  $\gamma$ TRK to the total photon sum and (2) that the missing isoscalar (308 EWSR) and isovector (508 EWSR) E2 strength easily can contribute another 40 - 50% of the TRK sum rule between 50 and 100 MeV (see caption to table 7). That means that in  $^{140}\text{Ce}$  as well as in  $^{28}\text{Si}$  all of the cross section in excess of the GGT sum rule could be (but does not necessarily have to be) of E2 nature.

Since nothing in the derivation of the GGT sum rule limits the contributing multipolarities to E1, the fundamentally important discrepancy between experiment and GGT sum rule still prevails.<sup>89</sup> But we think the actual nature and nuclear origin of the cross section up to the pion threshold merits more investigations. Perhaps future ( $e, e'$ ) coincidence experiments will shed some light on this question.

#### D. Octupole and Isovector Monopole Strength

In contrast to the quadrupole strength expected from the Bohr and Mottelson self-consistent shell model<sup>7,9,11</sup>, the octupole strength has been more elusive. This is understandable for once, because (table 1) there are two main shell transitions allowed by spin and parity, namely  $1 \hbar\omega$  and  $3 \hbar\omega$ . Although many E3 states at  $\sim 30 \text{ A}^{-1/3}$  MeV have been known from electron scattering in the  $A \approx 50$  mass region since many years (see table 27 in ref. 40), a systematic investigation has only recently been undertaken by Moss, et al. with  $(\alpha, \alpha')$ <sup>90</sup>. Although these states are below particle threshold, they are generally regarded as belonging to the giant resonance region and were called low energy octupole

resonance (LEOR). The main feature of these high lying bound octupole state(s), HEBOs, as evolved from the  $(\alpha, \alpha')$  experiments in nuclei between  $^{90}\text{Zr}$  and  $^{154}\text{Sm}$ , is a concentration of many E3 levels in a relatively narrow range ( $\Gamma \sim 2 - 3$  MeV), exhausting approximately 20% of the isoscalar EWSR in spherical nuclei, but much less in the deformed  $^{154}\text{Sm}$ . The essential conclusions of Moss, et al.<sup>90</sup> have been verified for a wider range of nuclei in a more extended survey by the same group,<sup>91</sup> covering 18 nuclei between  $^{40}\text{Ca}$  and  $^{208}\text{Pb}$ , with a notable weak strength in the double closed shell nucleus  $^{40}\text{Ca}$  and a total absence in  $^{208}\text{Pb}$ . Table 8 shows a comparison between nuclei for which results are available from both alpha and electron scattering. While there is some agreement for 3 nuclei, the a result for  $^{208}\text{Pb}$  is in disagreement with Ziegler and Peterson,<sup>73</sup> who find 6% of the sum rule in one level at 5.6 MeV and perhaps 8% more in another one at 5.25 MeV.

In  $^{140}\text{Ce}$  we were able to fit the HEBOs envelope with a Breit-Wigner shape of width  $\Gamma = 1.7 \pm 0.2$  MeV at  $E_X = 6$  MeV ( $31 \text{ A}^{-1/3}$  MeV) and a strength of  $19 \pm 6$  EWSR, which agrees with the  $(\alpha, \alpha')$  data for  $^{142}\text{Nd}$  (see table 8). The topmost part of figure 12 shows this state to clearly follow an E3 form factor and table 6 shows that our result agrees also very well with the RPA calculations of Li and Brown.<sup>81</sup> From table 1 we learn finally that together with the E3 state at 2.46 MeV ( $12 \pm 2$  EWSR, ref. 2) all the strength expected from the schematic model for the  $1 \hbar\omega$  E3 transition (isoscalar)

is exhausted.

The situation is more difficult for the higher E3 excitations. The isovector  $1 \hbar\omega$  E3 is expected to exhaust only a minor fraction of the sum rule (table 1) and can, therefore, probably not be distinguished in shape from the E2 resonance at 12 MeV. But this state may be partially responsible for the deviation of the measured 12 MeV cross section from the E2 form factor (figure 8 and 9).

The isoscalar E3 state is predicted to occur at  $-105 - 115 \text{ A}^{-1/3}$  MeV (table 1, table 6). Figure 1 shows, that indeed a resonance occurs in this energy region. It is also apparent from figure 1, that this mode will be difficult to measure because it is bracketed between the much stronger E1 at 15 MeV and the isovector E2 at 25 MeV. In addition, its strength may be fragmented, as indicated by the RPA calculations (table 6) and the behavior of the resonance at 25 MeV discussed in Section IV.C. Similar conclusions about the fragmentation have been drawn earlier for the closed shell nucleus  $^{89}\text{Y}$  (ref. 16). Despite these difficulties figures 3 and 5 show most clearly that cross section at 22 MeV becomes stronger with rising momentum transfer and is best described by an E3 form factor (figure 10). It has a width of  $5 \pm 1$  MeV and exhausts (only) 19% of the EWSR whereas the schematic model 10 predicts 72% and RPA calculations<sup>81</sup> 19%. But if we interpret the difference between experiment and GT form factor for the 25 MeV resonance as E3, additional 20% strength are located in

this region (table 6).

The only nucleus where all the expected strength has been observed so far is  $^{208}\text{Pb}$  (ref. 4) where  $90 \pm 42\%$  EWSR has been reported. In  $^{197}\text{Au}$ , within the same experiment<sup>4</sup>, only  $45 \pm 21\%$  were observed. This change in sum rule exhaustion does not necessarily mean that the strength is not there at all, it may just be differently distributed. The apparent greater dependence of the E3 strength on the (shell model) configuration of the nucleus gives hope that one will be able to learn more about nuclear structure from the octupole residual interaction than has been possible to date from the quadrupole. The very regular appearance of the latter does not reveal too much about the structure of the nucleus in which it occurs. This hope is especially justified for the HEBOS, since these states occur in the bound region of the excitation response.

The last member of the E3 continuum state family, the  $3\hbar\omega$  isovector state is even more difficult to accurately determine. It is high in the continuum, i.e., it has presumably a large spreading width, and relatively small B-values will exhaust considerable amounts of the sum rule. Consequently, one has to expect very small peak cross sections.

The schematic model<sup>10</sup> predicts  $195 \text{ A}^{-1/3}$  MeV ( $37 - 38$  MeV in  $^{140}\text{Ce}$ , table 1) which carries nearly all the isovector strength (97%). The RPA calculation<sup>81</sup> finds nearly the same amount centered at 36 MeV, with tails ranging from 13 to 60 MeV. As figure 1 shows, there have been resonances

seen in five nuclei heavier than  $^{140}\text{Ce}$  ( $^{165}\text{Ho}$  (ref. 71),  $^{181}\text{Ta}$  (ref. 72),  $^{197}\text{Au}$  (ref. 4),  $^{208}\text{Pb}$  (ref. 4) and  $^{238}\text{U}$  (ref. 93)). The excitation energy scatters considerably in  $\text{A}^{-1/3}$  units, thus, it is difficult to believe that this is the same state in all nuclei, and, in fact, the interpretation oscillates between E0 (isovector)<sup>4</sup>, E3 (isovector) 71, 93 and E2 + E4 in ref. 72. Although the  $^{181}\text{Ta}$  experiment of Hicks, et al. 72 is by far the best ( $e, e'$ ) measurement of any nucleus, what concerns statistical accuracy and momentum transfer covered, direct use of their data is hampered by the following. First, the angle was varied between 40 and 150°, giving rise to difficulties with transverse contributions (see discussion in Section IV.B). Secondly, the authors did not use a strict hydrodynamical model ( $c_{tr}/c = 1$ , see above), but chose to generally fit the model to the data, making a direct comparison with their data impossible, with the exception of the E2, in which case the conversion factors can be extracted from ref. 72. Our conclusion is, that their lower  $q$  data, which are also the more forward angle spectra, are compatible with E3 as well.

Since the isovector monopole has been predicted (ref. 94, see caption of table 1 for details) at  $178 \text{ A}^{-1/3}$  MeV, the structure seen in this region may indeed be a mixture of both isovector monopole and  $3\text{hu}$  octupole. The scatter of excitation energy, in addition, can be explained consistently if we assume the higher resonance to be E3. Similar to the lower octupole states 16, 90-93, it might be spread

out sufficiently in deformed nuclei as to disappear in the background (the spreading process presumably can be thought of as a quadrupole-octupole coupling). Therefore in the deformed nuclei one sees the lower-lying monopole state, which in spherical nuclei cannot be recognized in resonant form because it is bracketed between the isovector E2 ( $135 \text{ A}^{-1/3}$  MeV) and the E3 ( $195 \text{ A}^{-1/3}$  MeV). While it should be clear, that most of the interpretation given above is inferred from a skimpy data basis, it also might be pointed out that it is the only interpretation which is consistent both with theory and experiment.

In  $^{140}\text{Ce}$ , finally, we have encountered the same ambiguities as apparent from the systematics in figure 1, amplified in our evaluation procedure through a chance happening in our experiment. In Section II we mentioned that the spectrum with the highest momentum transfer was measured twice in order to achieve sufficiently good statistical accuracy in a tolerable time ( $\leq 100$  hours). In fact a machine failure of several hours duration in the first of the two runs produced an obviously unphysical discontinuity in the spectrum beyond 42 MeV. The 37 MeV form factor in figure 10 shows two sets of points. The filled circles, favoring an E2 (or E0) form factor, correspond to a fit of the composite spectra up to 42 MeV. The open circles, favoring an E3 interpretation, correspond to a fit to the second run only, but up to 48 MeV in excitation energy. Correspondingly, the apparent maximum shifted from 37 to

38 MeV ( $195 \text{ A}^{-1/3}$  MeV) to 34 MeV ( $175 \text{ A}^{-1/3}$  MeV). This is evident in figure 5, where the lower spectrum clearly shows that the resonance at the highest excitation energy (fixed at 37 MeV) does not describe the data very well; a relative maximum appears to be at 34 MeV. Our interpretation is that the  $\chi^2$  fit, attempting to achieve the lowest possible  $\chi^2$  (per degree of freedom) mismatches the background, verifying our rule of thumb, that in order to fit the continuum resonances reliably the spectra have to extend at least one full halfwidth beyond the last resonance fitted. Naturally it would be possible to insert two resonances in this region, one at 34 and one at 37 MeV, and attempt to disentangle the spectra that way. However, to do so would pretend that a greater accuracy is achievable, than justified by the data basis and our method of fitting the background together with the resonances. The latter obviously leads to difficulties at high excitation energies. The values given in table 9 for the 34 - 38 MeV region thus should be interpreted as upper limits with any mixture of monopole and octupole possible. Within the errors both microscopic  $0^1$  and macroscopic  $10, 94$  predictions can be accommodated.

#### E. Hexadecupole Strength

There has been little convincing evidence for  $E4$  excitations into the continuum. Similar to the  $E3$  states, they are fragmented into four transitions ( $2\hbar\omega$ ,  $4\hbar\omega$ , and these into isoscalar and isovector), and since they are even higher in excitation energy, they will be more spread out

and smaller cross sections will exhaust the sum rule. As outlined earlier, to determine a certain multipolarity with certainty, on the basis of the form factor alone, one has to have a momentum transfer which covers the maximum of the form factor. This is not the case for the  $E4$ . However, for the states believed to be  $E4$  a classification with  $\lambda > 4$  would lead to multiple exhaustion of the sum rule. Table 4 shows the results from our laboratory for  $^{58,60}\text{Ni}$  (ref. 92) and  $^{140}\text{Ce}$ . For the Ni isotopes a line shape fit for all the  $E4$  contributions was possible; in  $^{140}\text{Ce}$ , as already discussed, some are inferred from differences to form factors and thus might be due to failures of models. The table shows a certain regularity concerning strength and position (in  $\text{A}^{-1/3}$  MeV), surprising for nuclei that far apart in the nuclear system. Comparison with table 1 shows some agreement with the schematic model prediction for both isoscalar  $2\hbar\omega$  and  $4\hbar\omega$  transitions what concerns the excitation energy, but clearly more work and better data are needed to establish a systematic behavior. The states at 7.4 MeV and 31 MeV, however, could be fitted by a line shape; figure 12 and 10, respectively, show that an  $E4$  assignment is favored by the form factor.

It is clear that the sum rule would be approximately twice overexhausted if all the states in table 9 indeed would be  $E4$ . Figure 9 shows for the 12 MeV region that  $E3$  is favored in explaining the difference in cross section to the GT E2 DWBA calculation (Figure 8), for the 25 MeV region

(figure 10) we have argued above that one would not expect the Goldhaber-Teller model to fit the isovector E2. That means, together with the 2.08 MeV state (4% EWSR, ref. 2) some 90% of the isoscalar sum are exhausted, but the distribution seems to be different than predicted by the schematic model<sup>10</sup>, or the microscopic calculations.<sup>81</sup> However, the large uncertainties preclude more definite conclusions.

#### F. The $53 \text{ A}^{-1/3}$ MeV State

All the results discussed so far have been categorized according to certain multipolarities and straight forward macroscopic and microscopic considerations. The  $53 \text{ A}^{-1/3}$  MeV (10 MeV) state defies such treatment. Discovered in the experiments described in ref. 2 and 3 and correctly recognized as of electric character, it was regarded as an unwelcome nuisance, forced upon the unhappy authors<sup>2,3</sup> by a pitiless  $\chi^2$  fit, giving rise to many a malicious conference question. More seriously, its systematic occurrence was first recognized by (e,e') on  $^{197}\text{Au}$  and  $^{208}\text{Pb}$ .<sup>4</sup> Although ref. 2 does not give a multipolarity, it is clear from the spectra that it scales with the GQR at 12 MeV. Consequently, it was a natural candidate for a monopole assignment.<sup>4</sup> Since this assignment in  $^{208}\text{Pb}$  was based on some intricate argument concerning finestructure visible (and not visible) in both ( $\gamma, n$ ) and (e,e'), it was argued it might as well be quadrupole<sup>76</sup>, or the monopole assignment was even ruled out.<sup>95</sup> Since we did not agree with this conclusion, we have given a detailed account of history and arguments

recently,<sup>69</sup> to which we refer for particulars. There are two new elements which make it possible and necessary to amend the weasleword statement in the abstract of ref. 69 that "the new analysis makes any assignmnet for the 8.9 MeV resonance other than monopole difficult to understand". Despite that sentence, arguments in favor of an isovector E2 resonance were given,<sup>69</sup> and understood.<sup>96</sup>

The two new elements are:

1. A  $^{207}\text{Pb}$  ( $n, \gamma$ ) experiment by Raman, et al.<sup>96</sup> shows, based on the technique developed in ref. 17, that the 8.9 MeV resonance in  $^{208}\text{Pb}$  has to be E2 in order to explain the slope of primary E2 transitions (monopole states decay only in higher order through  $\gamma$  emission).
2. The availability of more (e,e') data for the  $53 \text{ A}^{-1/3}$  MeV region in a number of nuclei between  $^{58}\text{Ni}$  and  $^{208}\text{Pb}$ . The systematics of this resonance is indeed different from any other electric resonance found so far. Generally, the strength of giant resonances varies very slowly with A, dropping from approximately 80 to 100% EWSR for the isoscalar GQR in the heaviest nuclei, to 50 to 60% in the  $A \approx 60$  region.<sup>12,13</sup> This is quite different for the  $53 \text{ A}^{-1/3}$  MeV state. If we express its energy in units of the isoscalar sum rule, because it undoubtedly follows an E2 (or E0) form factor, its strength drops from 35% in  $^{208}\text{Pb}$  (ref. 4, 69, 76) to 9% in  $^{140}\text{Ce}$  and below 3% in  $^{58}\text{Ni}$ . Figure 12 shows that an E2 form factor explains the  $^{140}\text{Ce}$  data best.

There are many possibilities to display the strength of the  $53 \text{ A}^{-1/3}$  MeV resonance as a function of various parameters. The one which produced the greatest consistency is shown in figure 13 and displays the isovector E2 strength as function of the neutron excess. Clearly the strength rises in proportion to  $T$ . The most important case is  $^{208}\text{Pb}$ . Not only has this state been measured by several experiments, or different evaluation of the same data have been made,<sup>4,69,76,96,97</sup>, it is also the only case where applicable RPA calculations have been performed.<sup>82</sup> Halbert, et al.<sup>82</sup> have calculated with RPA wavefunctions that the  $T = 1$  and  $T = 0$  sums in the region of the isoscalar giant quadrupole resonance in  $^{208}\text{Pb}$  should be in the ratio 0.23.

Figure 13 shows this calculation to be in close agreement with the strength of the  $53 \text{ A}^{-1/3}$  MeV state. From the context of the discussion in ref. 82 it appears that this strength is thought to be due to the excess neutrons, although a simple mass oscillation model would only produce isovector strength of the order  $(N - Z)^2/A^2$ , or  $1/5$  of the microscopic result.<sup>82</sup> Similar considerations by Bohr and Mottelson (ref. 11, page 513) must not be interpreted as suggesting a special mode of oscillation associated with the excess neutrons,<sup>98</sup> because it would be difficult to imagine a force which holds together the excess neutrons in a separate

oscillation against the rest of the nucleus.<sup>98</sup> On the other hand, it seems clear from the experimental evidence (see discussion in ref. 69, especially the apparent non-excitation in hadron scattering) that this mode is not just a simple second branch of the GQR at  $10.5 (63 \text{ A}^{-1/3})$  MeV. Despite the objections raised, the explanation as a separate excess neutron isovector E2 shape oscillation seems to be the only one which explains all the data in a consistent manner.

Summary

This work covers a large range of the nuclear continuum, which contains many resonances. Since they have been discussed in detail, often with complicated arguments, in the text, we do not want to give a short version of our paper here, open to misinterpretation. For a short overview concerning the major resonances, table 10 may be consulted. Rather we want to state the shortcomings. We have measured  $^{140}\text{Ce}$  up to 48 MeV in excitation energy. The full use of the data has been hampered by two problems.

First, the continuum states are wide and overlap and are, therefore, difficult to disentangle with the overlapping resonances. This difficulty is a principle one and cannot be helped. Coincidence experiments are sometimes proposed as remedy, but they do not measure the total cross section, and, as additional difficulty, will produce interference between resonances of different multipolarity.<sup>40</sup> Secondly, the radiation tail fails at higher excitation energy, where those resonances lie which are open mainly to investigation by  $(e, e')$  (the isovector states). Little theoretical progress has been made here since the pioneering work of ref. 27 and 30. Experimentors have made some heuristical improvements, first by inserting correct elastic cross sections into the peaking approximation<sup>73</sup>, and then by extending this method<sup>32</sup> to the formalism of Ginsberg and Pratt.<sup>30</sup> A greater theoretical effort to overcome this problem is clearly needed.

Coincidence experiments may be, however, the only method to decide whether or not the total photon cross section below pion threshold contains a large E2 contribution, or not. From our experiment we can only show that it might be possible.

If the 10 MeV state ( $53 \text{ A}^{-1/3}$  MeV) is indeed a neutron oscillation, coincidence experiments may also help here. On the other hand, they may not, because neutrons are the only particles which come out of the nucleus at this excitation energy in heavy nuclei anyhow.

**Figure 1** Excitation energy of resonant cross section above approximately  $30 A^{-1/3}$  MeV as a function of  $A$ . The lines have been drawn solely to guide the eye. Although this plot does not enable one to decide on the multipolarity of the states found, certain systematic features are apparent. Excitation energies seem to be fairly constant for resonances at  $\sim 30$ , 63 and  $105 A^{-1/3}$  MeV, but drop distinctly over the range of  $A$  covered for the resonances grouped around  $130 A^{-1/3}$  MeV. Since this behavior is reminiscent of the GDR, an isovector state, and since the  $130 A^{-1/3}$  MeV state has also been identified as isovector (E2), one may conclude that isovector states fall off in excitation energy with  $A$ , while isoscalar rates do not, at least between  $A \approx 50$  and 208. Some irregular features, concerning the  $53$  and  $\sim 190 A^{-1/3}$  MeV states are discussed in the text. Only results from  $(e, e')$  are shown. Not presented is the GDR because its energy is much better known from  $(\gamma, n)$  results.<sup>61</sup>

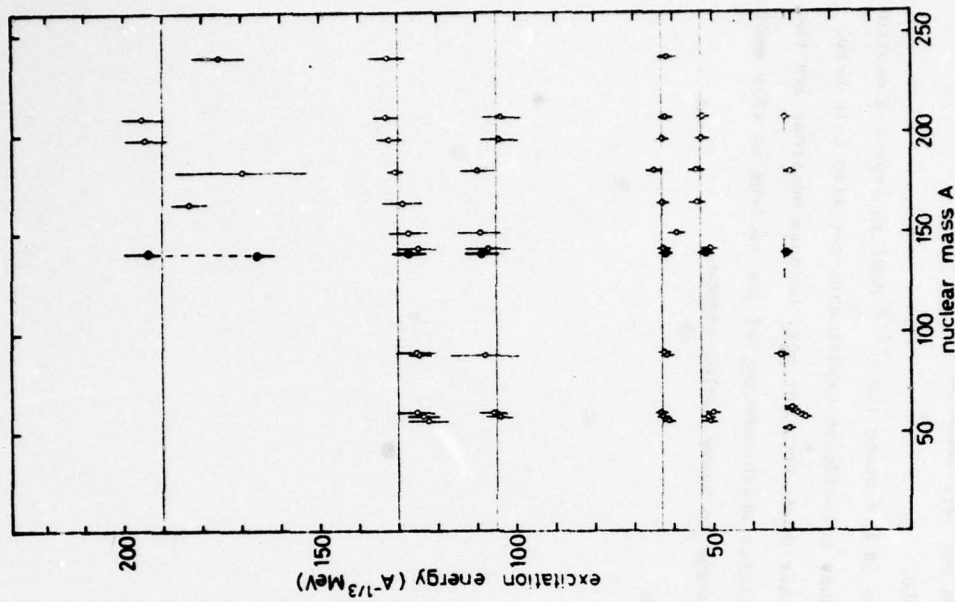


**Figure 1**

Figure 2 Spectra of 80 and 92 MeV electrons scattered inelastically from  $^{140}\text{Ce}$ . Resonances (or envelopes of discrete states) are indicated and discussed in more detail in the text. The bottom curved line in both parts is the fitted total background. Note that zero in the lower spectrum is not suppressed. The ghost peak has not been subtracted from the data, neither are the cross sections corrected for the constant dispersion of the magnetic spectrometer. The spectra were taken and fitted with 10 points per MeV, which were reduced for graphical purposes by a factor of 4. Resolution was 500 keV, approximately 1/3 of the width of the smallest resonance found; the statistical error is shown on selected points in the lower spectrum; it was smaller than the circles in the upper one. The fitted range of the spectra shown was 4 - 48 MeV for the upper, and 4 - 42 MeV for the lower spectrum (see discussion in text in conjunction with the 37 MeV state).

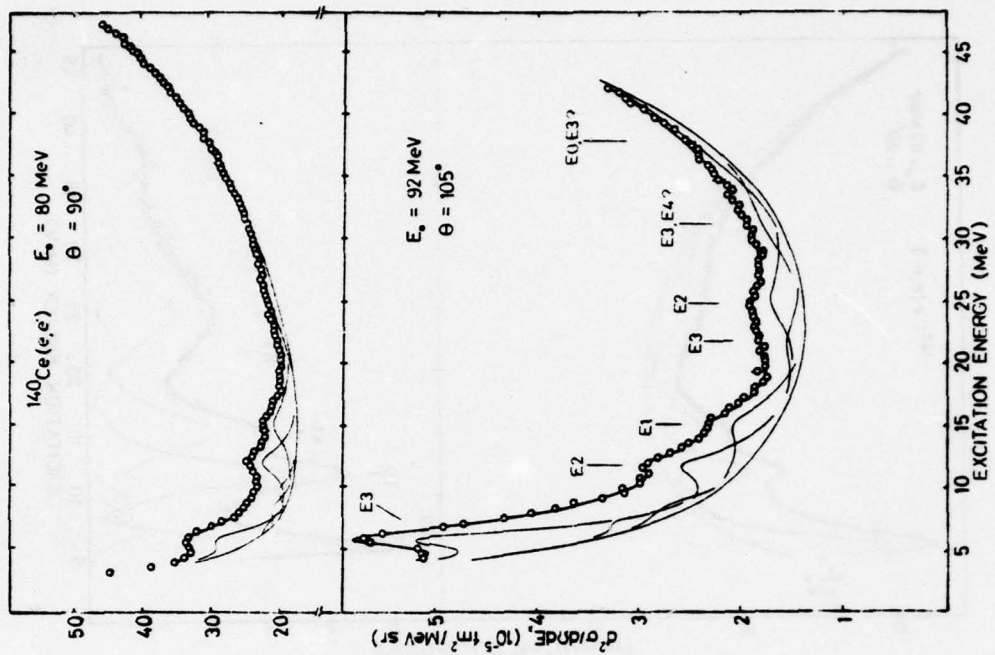


Figure 2

Figure 3 Spectrum of 92.1 MeV electrons scattered inelastically from  $^{140}\text{Ce}$  at  $90^\circ$ . The spectrum with and without the background is shown together so that the difference between the two may be seen. The resonances which were used for fitting the spectrum and the background as described in the text are drawn. The "ghost peak" is not subtracted from the upper graphs. The spectrum was taken and fitted with 10 data points per MeV. For graphical purposes the number of points for the spectrum was reduced by a factor of 4. The fitting range was 4 - 48 MeV; the broken lines are drawn to guide the eye. The statistical error is shown on selected points. While the upper part has not been corrected for the constant dispersion of the magnetic spectrometer and thus shows the data points as measured, the subtracted spectrum has been corrected, in order to show the cross sections of the resonances in their true relation.

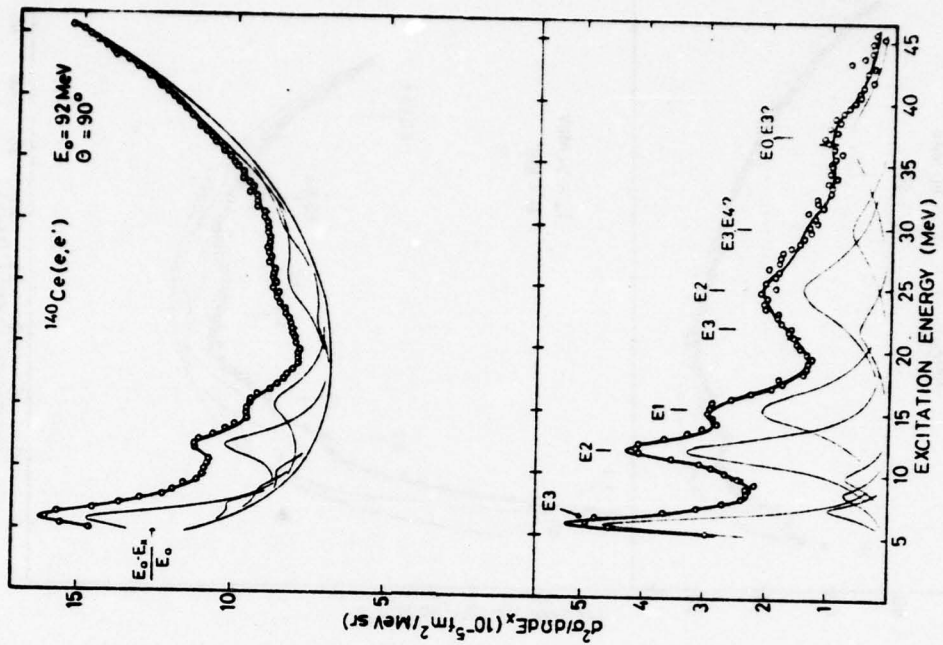


Figure 3

Figure 4 Comparison of DWBA cross sections for E1 to E4 transitions divided by the Mott cross sections. The curves are interpolations between calculations for the correct energy and angle of the five measurements used, since the data in this work and from ref. 2 vary greatly in electron beam energy. The curves were normalized so that the first maxima are equal. The program of Tuan, et al.<sup>52</sup> was used with a transition charge density  $\rho_{tr}(r) = C r^{\lambda-1} d\phi_0(r)/dr$ .

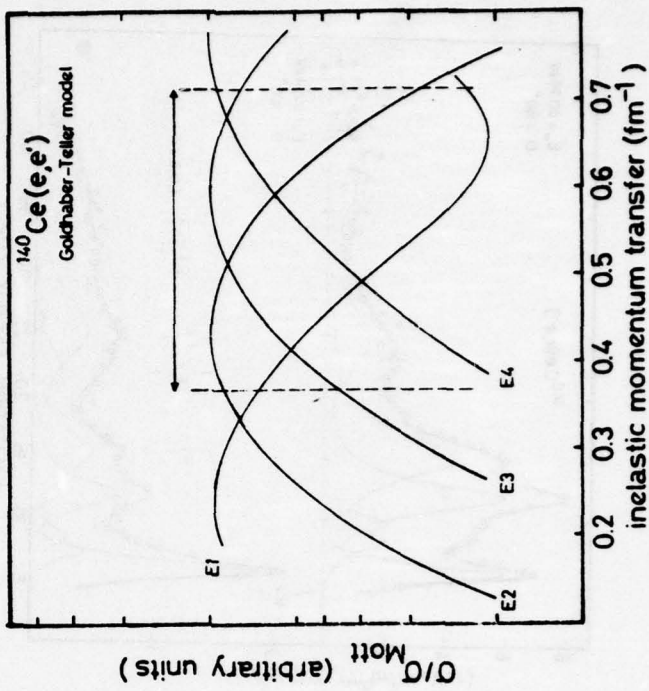


Figure 4

Figure 5 Data of figure 2 after the fitted background (consisting of the radiation tail, the general room background and experimental background) and the "ghost peak" as described in the text have been subtracted. These two spectra are shown together so that the shrinkage of smaller multipolarity transitions versus the growth of higher multipolarity transitions may be seen. The relative change in peak heights of the single resonances indicate very clearly the various multipoles contributing. Note, e.g., that the E2 cross sections fall off more than a factor of 6 between the 80 MeV and the 92 MeV spectra.

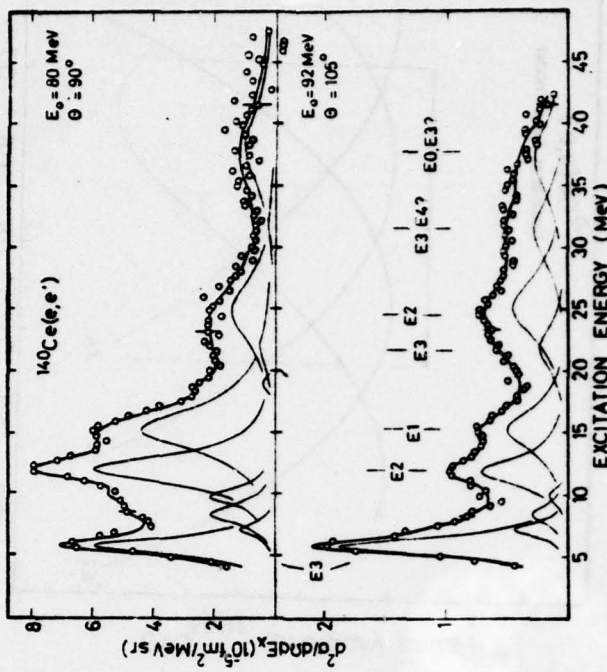
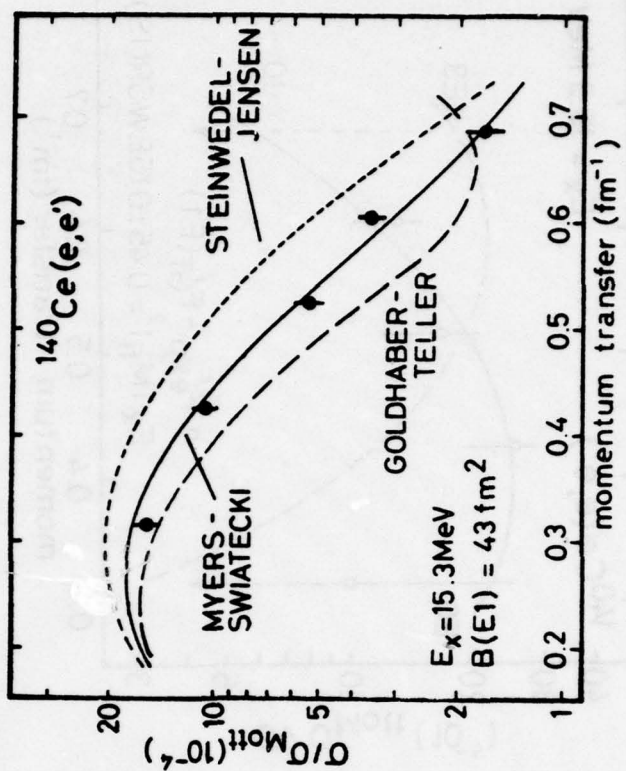


Figure 5

**Figure 6** Comparison of the DWBA and experimental form factors for the resonance found at 15.3 MeV. The experimental form factors are compared to the Goldhaber-Teller, Steinwedel-Jensen and Myers-Swiatecki models. The mixed model of Myers, Swiatecki, et al.,<sup>41</sup> explained in the text, fits the experimental data best. A mixture ratio of GT mode to SJ mode of  $0.76 \pm 0.04$  was found, corresponding to the droplet mode of ref. 4. The curves are not fitted to the ( $e, e'$ ) data, but to the photon measurement of ref. 59.



**Figure 6**

**Figure 7** Comparison of the difference between the experimental form factors and the Goldhaber-Teller model (see figure 6) and the DWBA form factors for the resonance found at 15.3 MeV. The difference shows that the possibility of an E0 transition with  $45 \pm 15\%$  of the monopole isoscalar sum rule lying beneath the dipole exists only if the Goldhaber-Teller model is assumed to be correct.

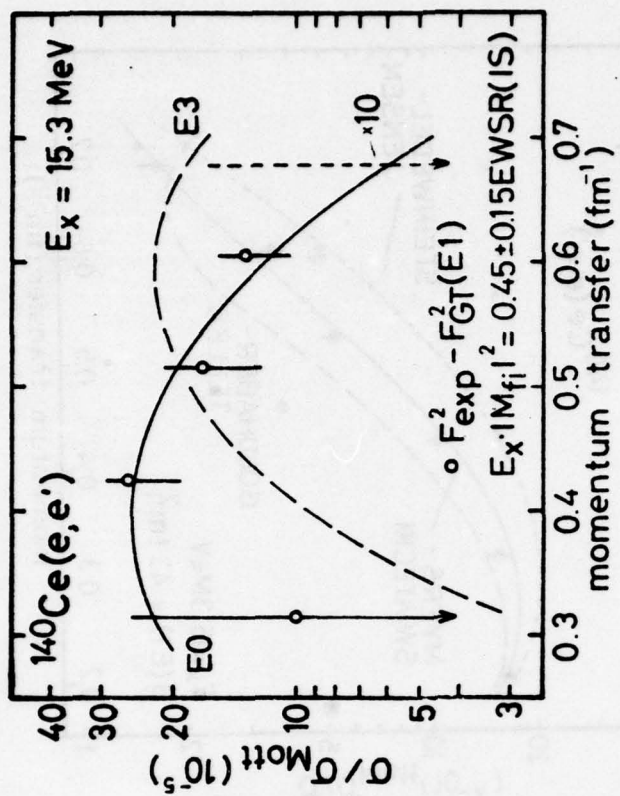


**Figure 7**

**Figure 8** Comparison of the DWBA and experimental form factors for the resonance found at 12 MeV. The Goldhaber-Teller model for an E2 transition was fit to the experimental data (table 10) first using as the half density radius  $c_{tr} = c$  and secondly  $c_{tr} = 0.95c$  as explained in the text.

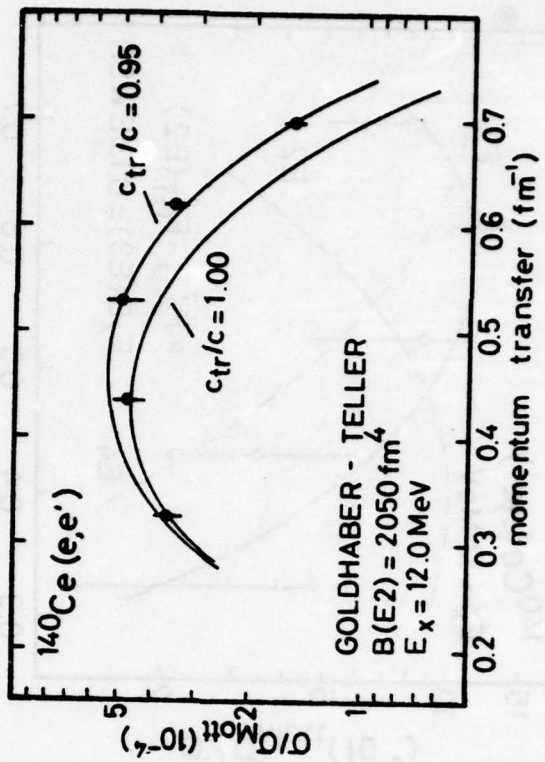


**Figure 8**

Figure 9 Comparison of the difference between the experimental form factor and the Goldhaber-Teller model DWBA form factor with  $c_{tr} = c$  (see Figure 8) for the resonance found at 12 MeV. The difference shows that an E3 transition beneath the E2 transition found at 12 MeV may exist if the Goldhaber-Teller model is assumed to be correct. A sizable E4 contribution may not be ruled out.

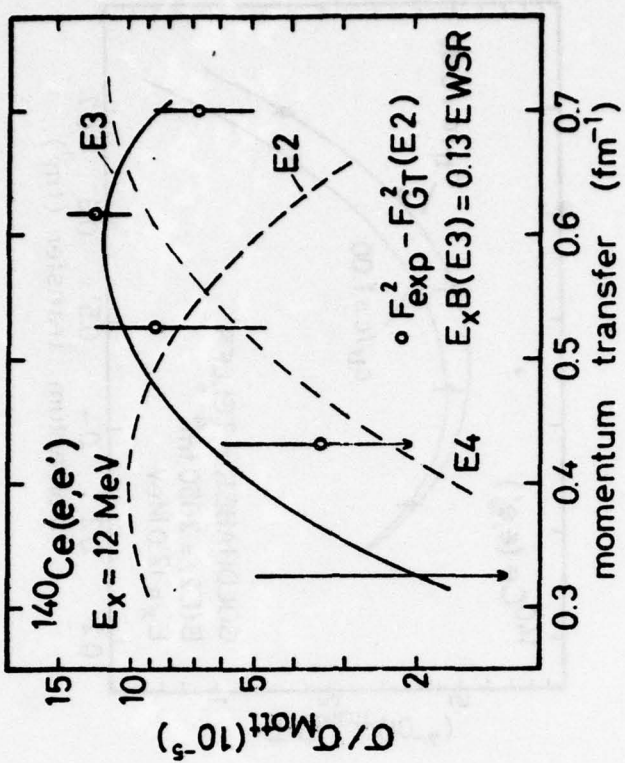


Figure 9

**Figure 10** Comparison of the DWBA and experimental form factors for the resonances found at 22, 25, 31 and 37 MeV. The Goldhaber-Teller model for an E3 transition fits the experimental form factors of the resonance found at 22 MeV. Both the Goldhaber-Teller and the Myers-Swiatecki E2 models were fit to the experimental form factors for the resonance found at 25 MeV (table 10). The Myers-Swiatecki model with a mixture ratio of 1.0 was found to fit the data better than the Goldhaber-Teller model as explained in the text. The assignment of an E3 transition can be clearly ruled out. The experimental form factor of the resonance found at 31 MeV fit the Goldhaber-Teller model for both E3 and E4 transition. An upper value could only be estimated for the form factor obtained from the 80 MeV/90° experiment, based on the statistical error of the measurement. The assignment of an E2 transition can be ruled out. The assignment of the resonance around 37 MeV is the most difficult. Because of the intricate arguments, we refer to the text.

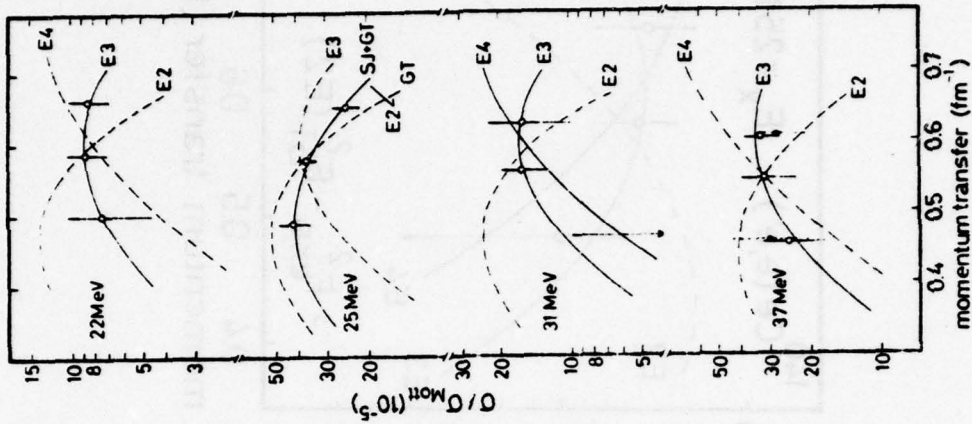
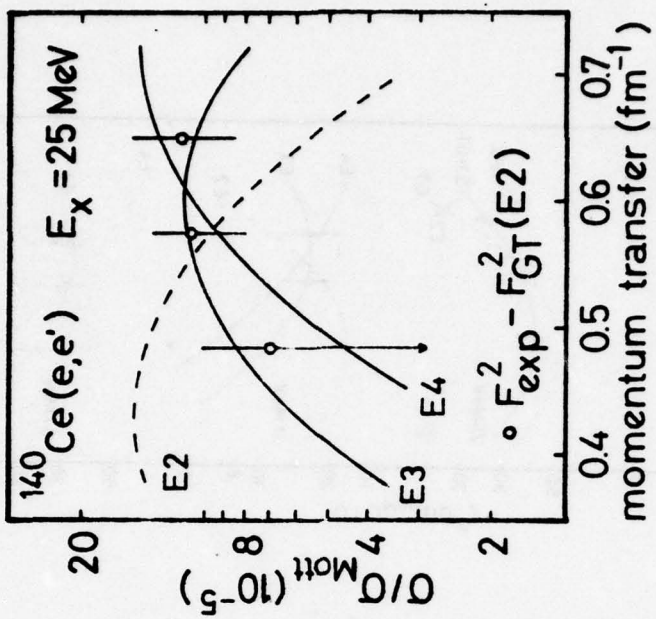


Figure 10

**Figure 11** Comparison of the difference between the experimental form factors and the Goldhaber-Teller model (see figure 11) and the DWBA form factor for the resonance found at 25 MeV. The difference shows that the possibility of an E3 or an E4 transition lying beneath the E2 transition exists if the Goldhaber-Teller model is assumed to be correct.



**Figure 11**

**Figure 12** Comparison of the DWBA and experimental form factors for the resonances found at 6.0, 7.4, and 10 MeV. The Goldhaber-Teller model for an E3 transition fits the experimental form factors of the 6.0 MeV resonance (table 10) while an E2 or E4 assignment of form factors can clearly be ruled out. The Goldhaber-Teller model for both an E3 and for an E4 transition fits the experimental form factors for the resonance found at 7.4 MeV. An E2 assignment of the form factor, though, can be clearly ruled out. The Goldhaber-Teller model for an E2 (E0) transition fits the experimental form factors of the resonance found at 10 MeV but the results depend on the interpretation of this mode (see table 5).

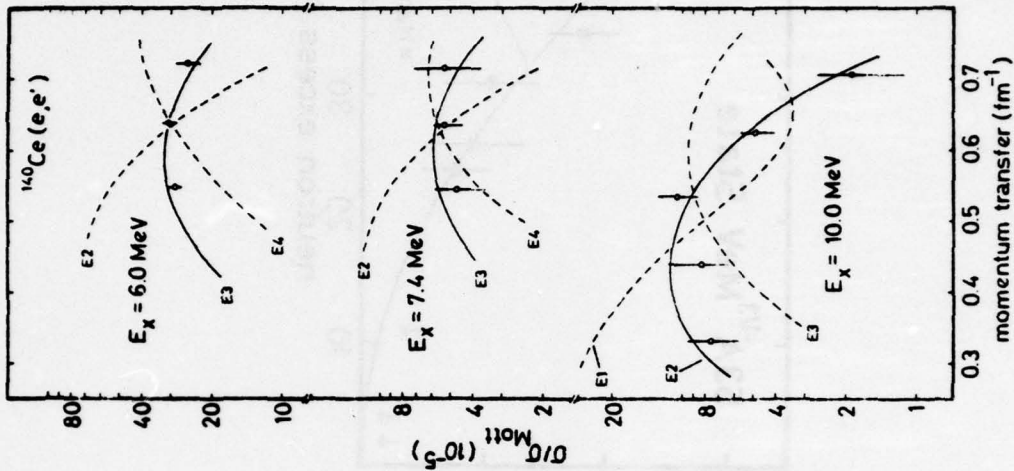


**Figure 12**

Figure 13 Strength of state at  $53 \text{ A}^{-1/3}$  MeV in nuclei between  $^{58}\text{Ni}$  and  $^{208}\text{Pb}$  expressed in units of the isovector sum rule. The calculation of Halbert, et al.<sup>82</sup>, normalized to the strength found experimentally for the isoscalar E2 in  $^{208}\text{Pb}$  (92% EWSR), is indicated. The experimental points are from ref. 92 ( $^{58,60}\text{Ni}$ ), ref. 16 ( $^{89}\text{Y}$ ), this work ( $^{140}\text{Ce}$ ), ref. 29 ( $^{142}\text{Nd}$ ), ref. 71 ( $^{165}\text{Ho}$ ), average of ref. 20 and ref. 72 [which had to be renormalized, see discussion in connection with the 37 MeV resonance]  
 $(^{181}\text{Ta})$ , ref. 4 ( $^{197}\text{Au}$ ), average references 4, 69, 76, and 97 ( $^{208}\text{Pb}$ ). For the three lightest nuclei only upper limits for the E2 strength can be given. A resonance with a width of 1 - 2 MeV in the Ni isotopes at this energy is predominantly E3, in  $^{89}\text{Y}$  no resonant cross section could be identified at all.

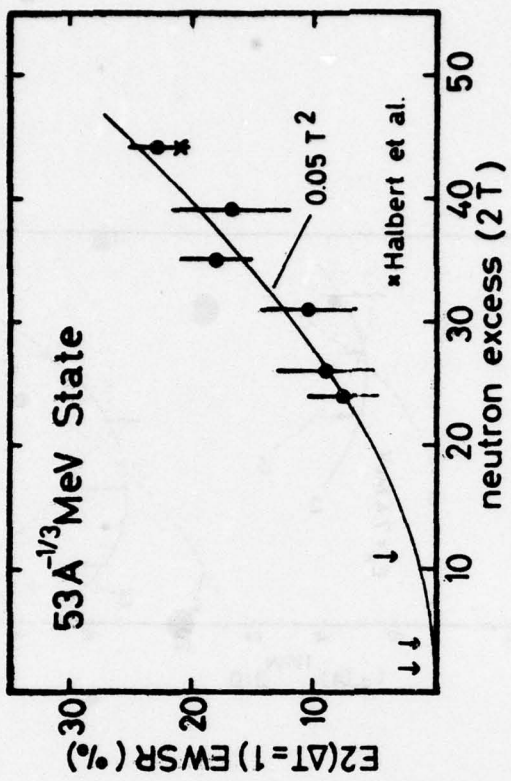


Figure 13

TABLE 1

Random Phase Approximation (RPA) calculations of Hamamoto<sup>10</sup> for the principal main shell transitions into the continuum. While this simple model naturally can not account for finer details, like the fine structure found in <sup>208</sup>Pb (ref. 32), it describes the giant resonances found to date very well. A different approach by Susuki<sup>94</sup> based on sum rule considerations predicts in addition the monopole strength to be located at 58 and 178  $\text{A}^{-1/3}$  MeV for the isoscalar and isovector part, respectively.

TABLE 1

$\lambda$	$\hbar\omega_0$ <sup>a)</sup>	$\Delta T = 0$		$\Delta T = 1$	
		$E_x$ ( $\text{A}^{-1/3}$ MeV)	$R^b)$ (%)	$E_x$ ( $\text{A}^{-1/3}$ MeV)	$R$ (%)
2	2	58	100	135	100
3	1	25	28	53	2
	3	107	72	197	98
4	2	62	51	107	3
	4	152	49	275	97

a)  $\hbar\omega_0 = 41 \text{ A}^{-1/3}$  MeV

b)  $R = E_x \cdot B(E\lambda, q = 0) / E_{NSR} (E\lambda, \Delta T) \cdot 100$

Table 2 E0 Strength at  $80 \text{ A}^{-1/3}$  MeV in N = 82 Nuclei

Nucleus	Reaction Method	$E_x$ (MeV)	$\Gamma$ (MeV)	$R^a)$	Ref.
$^{140}\text{Ce}$	(e,e')		$45 \pm 15^b)$	this work	
$^{142}\text{Nd}$	(e,e')	$16.2 \pm 0.2$	$3.00 \pm 0.15$	$28 \pm 10^c)$	21
$^{144}\text{Sm}$	(e,e')	$14.8 \pm 0.2$	$2.40 \pm 0.15$	$20 \pm 10^c)$	21
$^{144}\text{Sm}$	(e,e')	$15.1 \pm 0.5$	$2.9 \pm 0.5$	$100 \pm 20^c)$	44

Table 3 E1 Strength in N = 82 Nuclei

Nucleus	Method	$E_x$ (MeV)	$R^a)$	Model	Ref.
$^{140}\text{Ce}$	( $\gamma$ ,n)		$14.95^b)$	124	MR <sup>e)</sup>
$^{140}\text{Ce}$	(e,e')		$(15.1)^d)$	121	GT
$^{140}\text{Ce}$	(e,e')		$(15.3)^b)$	$124^e)$	MS <sup>e)</sup> this work
$^{142}\text{Nd}$	( $\gamma$ ,n)		$14.90^b)$	130	MI
$^{142}\text{Nd}$	(e,e')		$15.4^f)$	129	GT

a)  $R = E_x \cdot B(E1,0) / EWSR(E1,AT = 0) \cdot 100$

b) Strength based on difference between experiment and GT form factor

c) line shape fit

d) was taken from ( $\gamma$ ,n)

e) With  $\alpha = 0.74$

f) peak of the cross section

TABLE 4

TABLE 4

Comparison between ( $\alpha, \alpha'$ ) and ( $e, e'$ ) experiment for the 12 MeV resonance in different  $N = 82$  nuclei show the alpha results to be systematically higher. A detailed look at the different evaluation procedures and line shapes used, as discussed in the text, shows that the ( $\alpha, \alpha'$ ) results should be 20 to 30% lower than the ( $e, e'$ ) data, because this would be the effective difference of the yield of a Lorentz or Breit-Wigner fit vs. a Gaussian line shape. Effectively, the ( $e, e'$ ) sum rule values are 20 to 30% lower, making the difference even more markedly. The new ( $e, e'$ )  $^{140}\text{Ce}$  value,  $(50 \pm 10)\%$  EWSR, is lower than the older  $^{140}\text{Ce}$  and  $^{142}\text{Nd}$  data because a wider range of momentum transfer was covered. Figure 8 and 9 show that there is an ambiguity in the interpretation as to whether the difference to the strict Goldhaber-Teller model ( $g_{tr} - dg_{tr}/dr$ ) is due to other multipolarities (E3 and E4), or to a failure of the model. However, the low value of the sum rule results independent of this ambiguity. The newest ( $\alpha, \alpha'$ ) position and width for  $^{144}\text{Sm}$  (ref. 44) is now in essential agreement with the electron data.

Nucleus	$E_x$ (MeV)	$\Gamma$ (MeV)	$R^a)$	Model	Method	Ref.
$^{140}\text{Ce}$	$12.0 \pm 0.2$	$2.8 \pm 0.2$	$66 \pm 20$	GT	( $e, e'$ )	2
$^{142}\text{Nd}$	$12.0 \pm 0.2$	$2.8 \pm 0.2$	$65 \pm 13$	GT	( $e, e'$ )	62
$^{142}\text{Nd}^b)$	$13.2 \pm 0.4$	$3.6 \pm 0.3$	$110 \pm 30$	GT	( $\alpha, \alpha'$ )	13
$^{142}\text{Nd}$	$12.0 \pm 0.2$	$2.9 \pm 0.3$	$73 \pm 9$	GT	( $e, e'$ )	29,70
$^{144}\text{Sm}$	$11.9 \pm 0.2$	$2.9 \pm 0.2$	c)	GT	( $e, e'$ )	70
$^{144}\text{Sm}^b)$	$13.0 \pm 0.3$	$3.9 \pm 0.2$	$91 \pm 25$	GT	( $\alpha, \alpha'$ )	13
$^{144}\text{Sm}$	$12.4 \pm 0.4$	$2.6 \pm 0.4$	$85 \pm 15$	GT	( $\alpha, \alpha'$ )	44
$^{140}\text{Ce}$	$12.0 \pm 0.2$	$2.9 \pm 0.2$	$51 \pm 10^d)$	GT <sup>e)</sup>	( $e, e'$ )	this work

a)  $R = E_x \cdot B(E2, q = 0)/\text{EWSR}(\Delta T = 0) \cdot 100$

b) Energy, width, and strength not corrected for assumed monopole at 15 MeV

c) Strength not given

d) Total error. Standard deviation results in  $(51 \pm 5)\%$  EWSR

e)  $c_{tr}/c = 0.95$ , see text

TABLE 5

$E_x$ (MeV)	$B$ ( $\text{fm}^4$ )	$r_Y^0$ (eV) ( $10^{-3}$ )	$R^a$	Ref.
1.60	$2.71 \cdot 10^3$	4.6	9.2	2
2.90	$2.87 \cdot 10^2$	9.5	1.6	2
3.12	$5.44 \cdot 10^2$	26	3.6	2
3.32	$2.92 \cdot 10^2$	19	2.0	2
10.0 b)	$4.30 \cdot 10^2$	7590	9.1	this work
12.0	$2.01 \cdot 10^3$	80700	51	this work

Strength of all identified E2 states up to 12 MeV as determined by  $(e, e')$  (ref. 2). They sum up to 77% of the isoscalar sum rule if one includes the 10 MeV state, and to 67% without. The assignment for 10 MeV state is ambiguous for two reasons. First  $(e, e')$  can not easily distinguish between E0 and E2, and secondly, this state has not been seen in hadron scattering, possibly indicating either monopole or isovector character. Thus, this resonance might be (1) a second branch of the isoscalar GR at 12 MeV, (2) part of the monopole resonance with 13% of the EWSR  $(E_0, \Delta T = 0)$  or, (3) due to an oscillation of the excess neutrons.<sup>11</sup> While a force which produces a separate excess neutron oscillation is difficult to imagine,<sup>98</sup> the same is true for case (1). Against the monopole interpretation speaks mainly the low sum rule value,

leaving the nature of this state as unsolved question, with the excess neutron oscillation slightly favored, because it is the only explanation which consistently explains the data.

a)  $R = E_x \cdot B(E2, 0) / \text{EWSR}(E2, \Delta T = 0) \cdot 100$

b) Interpretation ambiguous

TABLE 6

Table 6

		Theory (ref. 81)			Experiment	
$\lambda$	T	R <sup>a)</sup>	E <sub>x</sub> MeV	R <sup>a)</sup>	E <sub>x</sub> MeV	
0	0	34	19	45	15	
		55	21-27			
1	1	9	11-21	(13) <sup>b)</sup>	10	
		80	21-50	130 <sup>c)</sup>	37	
				1.5-3.4		
2	0	15	6	16		
		65	12	50	12	
1		10	17-27			
		13	0-23	(9) <sup>b)</sup>	10	
		65	23-32	50	25	
		20	32-50			
3	0	18	6	19	6	
		7	10	(5)	7.4	
		12	12-18	(8) <sup>d)</sup>	12	
		39	18-28	19,(20) <sup>d)</sup>	22,(25)	
		13	28-37			
1	14	13-28				
		65	28-43	75 <sup>c)</sup>	37	
		15	43-60			
4	0	26	0-18	4*(7)*(20) <sup>d)</sup>	2.1,7.4,12	
		40	18-40	(60, <sup>d)</sup>	25	
1	17	17	0-30			
		70	30-70	80	31	

## Footnotes for Table 6

a)  $R = E_x \cdot B(\lambda, q = 0) / E_{MSR}(\lambda_A, \alpha_T) \cdot 100$ 

b) ambiguous, see caption to table 5

c) data compatible with both E0 and E3

d) difference to GT E2 form factor, compatible with both E3 and E4

TABLE 7

TABLE 7

Contribution of E2 strength to the photon cross section. For the calculation it was assumed that all the sum rule strength (isoscalar plus isovector =  $1.14 \cdot 10^5$  MeV fm<sup>4</sup>) would be distributed in the form of a Breit-Wigner curve with resonance maximum  $E_X$  and width  $\Gamma$ . The result is expressed in units of the classical sum rule<sup>85</sup> and was calculated by integration from 10 MeV to 100 MeV and 140 MeV, respectively. To get possible contributions from E2 to the total photon cross section,  $\sigma_{100}$  (or  $\sigma_{140}$ ) has to be multiplied by the sum rule fraction measured or assumed, and additionally by Z/A and N/A for isoscalar and isovector strength. For example, if we assume the 50% EWSR (AT = 1) missing at 25 MeV to be localized at 60 MeV, with  $\Gamma = 20$  MeV,  $\sigma_{max}^{int} = 9$  mb,  $\sigma_{100}^{int} = 124$  TRK and  $\sigma_{140}^{int} = 154$  TRK would result.

While the assumption of Breit-Wigner form may not be justified, a constant E2 distribution with a width of 30 to 40 MeV at 60 to 80 MeV excitation energy would be in agreement with Ahrens, et al.<sup>88</sup> and contribute even more to the photon cross section (since the Breit-Wigner curve contains only 50% of the area within its halfwidth, assumption of a box-like distribution would raise  $\sigma_{100}^{int}$  and  $\sigma_{140}^{int}$  by some 50 to 80% of its value, depending on location and width).

$E_X$ (MeV)	$\Gamma$ (MeV)	$\sigma_{max}$ (mb)	$\sigma_{100}^{int}$ /TRK	$\sigma_{140}^{int}$ /TRK
1.2	2.8	1.2	.06	.08
25	6.5	21	.16	.18
25	13	10	.20	.24
40	15	21	.29	.34
60	20	30	.42	.50
80	20	43	.49	.62
		30	.39	.50
		40	.22	.38

Table 8 Comparison of  $1\hbar\omega$  isoscalar octupole strength from  
( $a, a'$ ) and ( $e, e'$ ).

Nucleus	$E_x$ (MeV)	Method	$R^a$	Ref.
$^{58}\text{Ni}$	-6.8 b)	( $a, a'$ )	$8 \pm 2$	91
$^{58}\text{Ni}$	6.95	( $e, e'$ )	$13 \pm 2$	92
$^{89}\text{Y}$	7.1	( $a, a'$ )	$-20 \pm 5$	91
$^{89}\text{Y}$	7.4 c)	( $e, e'$ )	$12 \pm 2\text{c})$	16
$^{142}\text{Nd}$	6.2	( $a, a'$ )	$22 \pm 6$	91
$^{140}\text{Ce}$	6.0	( $e, e'$ )	$19 \pm 6$	present work
$^{208}\text{Pb}$	—	( $a, a'$ )	—	91
$^{208}\text{Pb}$	-5.4	( $e, e'$ )	$14 \pm 5$	73

a)  $E_x \cdot B(E3)/EWSR(E3, \Delta T = 0) \cdot 100$

b) three states at 6.07, 6.85 and 7.55 MeV

c) two concentrations of strength at 6.75 and 8.05 MeV

Table 9 Known  $E4$  (isoscalar  $\pi\pi$ ) continuum excitations

	$E_x$ (MeV)	$E_x(A-1/3\text{MeV})$	$R^b$	$E_x$ (MeV)	$E_x(A-1/3\text{MeV})$	$R^b$	$E_x$ (MeV)	$E_x(A-1/3\text{MeV})$	$R^b$
$^{58}\text{Ni}^a)$	37	$5 \pm 2$	11.4	43	$3 \pm 2$	7.4	38	$7 \pm 3$	
$^{140}\text{Ce}$	58	$40 \pm 15$	14.9	58	$20 \pm 10$	-12 c)	-62 c)	$20 \pm 10\text{c})$	
$^{60}\text{Ni}^a)$	40	$150 \pm 75$	31	40	$161$	$80 \pm 40$			
$^{15.1}$	58	$150 \pm 75$	-25 c)	-25 c)	$-130\text{c})$	$60 \pm 30\text{c})$			

b)  $R = E_x(E4)/EWSR(E4, \Delta T = 0)$

a) ref. 92

c) inferred from difference to  $E2$  form factor

TABLE 10

$E_x$ (MeV)	$E_{A-1/3}$ (MeV)	$T$ (MeV)	$E_A$ AT $B_{exp}$ ( $\text{fm}^{-2}\text{sr}^{-1}$ )	$T_0$ (eV)	$R_b$	Std. Dev.	Total Error
TABLE 10							
6.0 ± 0.2	31	1.7 ± 0.2	3 0	1.3 10 <sup>-5</sup>	2.0 10 <sup>-3</sup>	19	± 3
10.0 ± 0.2	52	1.8 ± 0.2	2 0	4.30	7.6	9	± 2
12.0 ± 0.2	62	2.8 ± 0.2	2 0	2.5 10 <sup>-3</sup>	10.0	8.7	± 5
15.3 ± 0.2	79	4.4 ± 0.2	1 1	4.1	5.1 10 <sup>-4</sup>	12.9	± 12
22	+ 1	114	5 ± 1	3 0	3.7 10 <sup>-4</sup>	4.9	+ 2
25	+ 1	130	6.5 ± 1	2 1	1.3 10 <sup>-3</sup>	2.1 10 <sup>-3</sup>	+ 8
34	- 38	175	7 - 10	3 0	1.2 10 <sup>-5</sup>	6.8 10 <sup>-2</sup>	+ 10
		195			0 1	2.8 10 <sup>-3</sup>	- 20

- a) For the monopole the measured quantity is  $|M_{12}^{12}|^2 (\text{fm}^4)$
- b)  $R = E_x \cdot B(E_2)/EMSR(E_2, AT) \cdot 100$
- c) The error given (in units of  $R$ ) is the standard deviation of the average sum rule exhaustion and is, therefore, more a measure for the fit to a certain model than a measure for the total uncertainty.
- d) The total error (in units of  $R$ ) is based on the maximum and minimum values found for the areas under the curves during the many attempts to fit the spectra.
- e)  $C_{T2} = 1.0$ .
- f)  $C_{T2} = 0.95$ .
- g) MS model with  $a = 0.76$ .
- h) GT model.
- i) MS model with  $a = 1.0$ .

Results in units of the reduced transition probabilities ( $B$ -values), ground state radiation width ( $r_\gamma^0$ ), and energy weighted sum rule exhaustion, for the major resonances found in this experiment. Some results for weaker states, and those inferred from differences between cross sections and DWBA calculation, are, together with the appropriate discussion, scattered in the text. The isospin assignments are not determined by this experiment, but were taken from comparison with other experiments and theory.

### References

- by R. Becker, C. Goodman, P. Stelson, and A. Zucker  
(Academic, New York, 1967).
1. S.S. Hanna, in "Proceedings of the International School on Electro- and Photonuclear Reactions", edited by S. Costa and C. Scharf, published in "Lecture Notes in Physics", Vol. 61, Springer (Berlin, Heidelberg, New York) 1977.
  2. Rainer Pittman, *Z. Physik* **260**, 283 (1973).
  3. R. Pittman and Th. Walcher, *Phys. Letters* **36B**, 563 (1971); *Z. Naturforsch.* **27a**, 1683 (1972).
  4. R. Pittman, F.R. Buskirk, E.B. Daily, J.N. Dyer, and X.K. Maruyama, *Phys. Rev. Letters* **33**, 849 (1974); **34**, 848 (1975).
  5. O. Hansen and O. Nathan, *Comments on Nuclear and Particle Physics* **5**, 165 (1972).
  6. M. Danos, *Ann. Physik (Leipzig)* **10**, 18 (1952).
  7. Ben Mottelson, Nobel Prize Talk, *Fysisk Tidsskrift* **74**, 97 (1976); *Rev. Mod. Phys.* **48**, 375 (1976); *Science* **193**, 287 (1976).
  8. G.E. Brown and M. Bolsterli, *Phys. Rev. Letters* **3**, 472 (1959); G.E. Brown, L. Castillejo, and J.A. Evans, *Nucl. Phys.* **22**, 1 (1961).
  9. B.R. Mottelson, in Proceedings of the International Conference on Nuclear Structure, Kingston, 1960, edited by D.A. Bromley and E.W. Vogt (Univ. of Toronto Press, Toronto/North-Holland, Amsterdam, 1960); A. Bohr, in *Nuclear Physics: An International Conference*, edited by R. Becker, C. Goodman, P. Stelson, and A. Zucker (Academic, New York, 1967).
  10. I. Hanamoto, in *Proceedings of the International Conference on Nuclear Structure Studies Using Electron Scattering and Photoreaction*, Sendai, 1972, edited by K. Shoda and H. Ui (*Suppl. Res. Rep. Nucl. Sci. Tohoku Univ.*, **5**, 205 (1972)).
  11. A. Bohr and B.R. Mottelson, "Nuclear Structure" (Benjamin, Reading, Mass., 1975) Vol. II.
  12. R. Pittman, to be published in *Physics Reports*.
  13. D.H. Youngblood, J.M. Moss, C.M. Rozsa, J.D. Bronson, A.D. Bacher, and D.R. Brown, *Phys. Rev. C13*, 994 (1976).
  14. J.M. Moss, *Bull. Am. Phys. Soc.* **22**, 574 (1978) (Washington Meeting).
  15. Yung-Su Tsai, *Rev. Mod. Phys.* **46**, 815 (1974).
  16. R. Pittman, F.R. Buskirk, E.B. Daily, J.O. Shannon, and W.H. Smith, *Phys. Rev. C16*, 970 (1977).
  17. E.P. Gordon and R. Pittman, *Nucl. Instr. Methods* **145**, 569 (1977).
  18. F.E. Bertrand, *Ann. Rev. Nucl. Sci.* **26**, 457 (1976).
  19. D.H. Youngblood, C.M. Rozsa, J.M. Moss, D.R. Brown, and J.D. Bronson, *Phys. Rev. Letters* **39**, 1188 (1977).
  20. H. Miura and Y. Torizuka, *Phys. Rev. C16*, 1588 (1977).
  21. A. Richter, in "Proceedings of the Sendai Conference on Electro- and Photoexcitations", Sendai 1977 [Res. Report. Lab. Nucl. Science. Tohoku Univ. **10**, (Suppl.), 195 (1977)].

22. J. Schwinger, Phys. Rev. 76, 760 (1949).
  23. W.C. Barber, F. Berthold, G. Fricke, and F.E. Gudden, Phys. Rev. 120, 2081 (1960).
  24. L.C. Maximon, Rev. Mod. Phys. 41, 193 (1969).
  25. L.W. Mo and Y.S. Tsai, Rev. Mod. Phys. 41, 205 (1969).
  26. Y.S. Tsai, in "Nuclear Structure", edited by R. Hofstadter and L.I. Schiff (Stanford University Press, 1964), p. 221.
  27. L.C. Maximon and D.B. Isabelle, Phys. Rev. 136, B674 (1964).
  28. Leonard C. Maximon, "Electromagnetic Interactions from 5 to 500 Mev and Nuclear Research - A Position Paper as of March 1977", NBS Technical Note 955.
  29. A. Schwierzinski, Dissertation, Technische Hochschule Darmstadt, 1976 (unpublished).
  30. E.S. Ginsberg and R.H. Pratt, Phys. Rev. 134, B773 (1964).
  31. Yung-Su Tsai, SLAC-PUB-848, 1971 (unpublished).
  32. F.R. Buskirk, H.D. Gräf, R. Pithan, H. Theissen, O. Titze, and Th. Walcher, Phys. Letters 42B, 194 (1972).
  33. T. de Forest and J.D. Walecka, Adv. Physics 15, 1 (1966).
  34. A. Migdal, J. Phys. USSR 8, 331 (1944).
  35. W. Bothe and W. Gentner, Z. Physik 106, 263 (1937); Z. Physik 112, 45 (1939).
  36. H. Bethe and R. Bacher, Rev. Mod. Phys. 8, 82 (1936).
  37. M. Goldhaber and E. Teller, Phys. Rev. 74, 1046 (1948).
  38. H. Steinwedel and H. Jensen, Z. Naturforsch. 5a, 413 (1950).
  39. B.L. Berman and S.C. Fultz, Rev. Mod. Phys. 47, 713 (1975).
  40. H. Überall, "Electron Scattering from Complex Nuclei" (Academic, New York 1971).
  41. W.D. Myers, W.J. Swiatecki, T. Kodama, L.J. El-Jaick, and E.R. Hilf, Phys. Rev., C15, 2032 (1977).
  42. W.D. Myers and W.J. Swiatecki, Ann. Phys. (NY), 55, 395 (1969).
  43. N. Marty, M. Morlet, A. Willis, V. Comparat, and R. Frascaria, in "Proc. of the Intern. Symp. on Highly Excited States in Nuclei", Jülich, 1975, edited by A. Faessler, C. Mayer-Börcke, and P. Turek (KFA Jülich, 517 Jülich, W. Germany, 1975).
  44. D.H. Youngblood, C.M. Rosza, J.M. Moss, D.R. Brown, and J.D. Bronson, Phys. Rev. Letters, 39, 1188 (1977).
  45. L. Meyer-Schützmeister, Z. Vager, R.E. Segel, and P.P. Singh, Nucl. Phys. A108, 180 (1968).
  46. C.-P. Wu, F.W.K. Firk, and T.W. Phillips, Nucl. Phys. A147, 19 (1970).
  47. R.B. Watson, D. Branford, J.L. Black, and W.J. Caelli, Nucl. Phys. A203, 209 (1973).
  48. G.S. Foote, D. Branford, D.C. Weisser, N. Shikazono, R.A.I. Bell, and F.C.P. Huang, Nucl. Phys. A263, 349 (1976).
  49. S. Fukuda and Y. Torizuka, Phys. Letters 62B, 146 (1976).
- An earlier account of these data, with differing results, appeared in Phys. Rev. Letters 29, 1109 (1972).
50. Mamiko Sasa and Y. Torizuka, Phys. Rev. C15, 217 (1976).

51. A. Richter, Contributed paper to the IVth Seminar on "Electromagnetic Interactions of Nuclei at Low and Medium Energies", Moscow, December 1977.
52. S.T. Tuan, L.E. Wright, and D.S. Onley, Nucl. Instrum. Methods 60, 70 (1968).
53. N. Grossmann and C. Toepffer, Nucl. Phys. A161, 330 (1971).
54. R. Pitthan, Dissertation, Technische Hochschule Darmstadt, 1972 (unpublished).
55. D.S. Onley and D.L. Wright (unpublished).
56. R. Pitthan, Laboratory Report 44, Institut für Technische Kernphysik, Technische Hochschule Darmstadt 1971 (unpublished).
57. Y. Kawazoe, Res. Rep. Lab. Nucl. Sci. Tohoku Univ. 6, 211 (1973).
58. D.G. Ravenhall, D.R. Yennie, and R.N. Wilson, Phys. Rev. 95, 500 (1964).
59. A. Leprêtre H. Beil, R. Bergère, P. Carlos, J. Pagot, A. de Mniac, A. Veysiere, and H. Miyase, Nucl. Phys. A258, 350 (1976).
60. Z.M. Szalata, K. Itoh, G.A. Peterson, J. Flanz, S.P. Fivozinsky, F.J. Kline, J.W. Lightbody, X.K. Maruyama, and S. Penner, Phys. Rev. C17, 435 (1978).
61. B.L. Berman, "Atlas of Photoneutron Cross Sections", Preprint UCRL-78482, Lawrence Livermore Laboratory, 1976 (unpublished).
62. A. Schwierczinski, R. Frey, E. Spamer, H. Theissen and Th. Walcher, Phys. Letters 55B, 171 (1975).
63. Th. H. Schucan, Nucl. Phys. 61, 417 (1965).
64. G.R. Satchler, Part. Nucl. 5, 105 (1973).
65. M.N. Harakeh, K. Van der Borg, T. Ishimatsu, H.P. Morsch, A. Van der Woude, and P.E. Bertrand, Phys. Rev. Letters 38, 75 (1977).
66. A. Goldmann, Z. Physik 234, 144 (1970).
67. F.H. Lewis and J.D. Walecka, Phys. Rev. 133B, 849 (1964).
68. P. Paul, in Proceedings of the International Symposium on Highly Excited States in Nuclei, Jülich, 1975, edited by A. Faessler, C. Mayer-Börcke, and P. Turek, (KFA Jülich, 517 Jülich, W. Germany, 1975), Vol. 2.
69. R. Pitthan and F.R. Buskirk, Phys. Rev. C16, 983 (1977).
70. A. Richter, ref. 1.
71. G.L. Moore, F.R. Buskirk, E.B. Dally, J.N. Dyer, X.K. Maruyama and R. Pitthan, Z. Naturforsch. 31a, 668 (1976).
72. R.S. Hicks, I.P. Auer, J.C. Bergström, and H.S. Caplan, Nucl. Phys. A278, 261 (1977).
73. J.F. Ziegler and G.A. Peterson, Phys. Rev. 165, 1337 (1968).
74. G.F. Bertsch and S.F. Tsai, Phys. Reports (Phys. Letters C) 18, 126 (1975).
75. T.J. Deal and S. Falleros, Phys. Rev. C7, 1709 (1973).
76. A. Schwierczinski, R. Frey, A. Richter, E. Spamer, H. Theissen, O. Tritze, Th. Walcher, S. Krewald, and S. Rosenfelder, Phys. Rev. Letters 35, 1244 (1975).

77. S. P. Kamerdzhev, Yad. Fiz. 15, 676 (1972) [transl.: Sov. J. Nucl. Phys. 15, 379 (1972)].
78. S.P. Kamerdzhev, Phys. Letters 47B, 147 (1973).
79. P. Ring and J. Speth, Phys. Letters 44B, 477 (1973).
80. G.F. Bertsch, Phys. Rev. Letters 31, 121 (1973).
81. K.F. Liu and G.E. Brown, Nucl. Phys. A265, 385 (1976).
82. E.C. Halbert, J.B. McGrory, G.R. Satchler, and J. Speth, Nucl. Phys. A245, 189 (1975).
83. J. Ahrens, H. Borcher, K.H. Czock, H.B. Eppler, H. Gimmler, M. Kröning, P. Riehn, G. Sita Ram, A. Zieger, and B. Ziegler, Nucl. Phys. A251, 479 (1975).
84. R. Pittman, F.R. Buskirk, J.N. Dyer, E.E. Hunter, and G. Pozinsky, to be published in Phys. Rev. C.
85. W. Thomas, Naturwissenschaften 13, 627 (1923); F. Reiche and W. Thomas, Z. Physik 34, 510 (1925); W. Kuhn, Z. Physik 33, 408 (1925).
86. E.G. Fuller and E. Hayward (eds.), "Photonuclear Reactions", Benchmark Papers in Nuclear Physics (Dowden, Hutchinson and Ross, Stroudsbury, Pennsylvania) 1976, p. 391.
87. M. Gell-Mann, M.L. Goldberger, and W.E. Thirring, Phys. Rev. 95, 1612 (1954).
88. J. Ahrens, H. Heil, R. Bergeire, P. Carlos, P. Daujat, T. Fagot, P. Gardanne, U. Kneissl, A. Leprêtre, A. de Miniac, and A. Vevsiere, Compte Rendu d'Activité, 1976-1977, CEN Saclay, France, p. 71.
89. W. Weisse, Phys. Reports (Phys. Letters C), 13, 54 (1974).
90. J.M. Moss, D.H. Youngblood, C.M. Rosza, D.R. Brown, and J.D. Bronson, Phys. Rev. Letters 37, 816 (1976).
91. J.M. Moss, D.R. Brown, D.H. Youngblood, C.M. Rosza, and J.D. Bronson, to be published.
92. R. Pittman, G.M. Bates, J.S. Beachy, F.R. Buskirk, E.B. Daily, D.H. Dubois, J.N. Dyer and S.J. Kowalick, to be published in Phys. Rev. C.
93. W.A. Houk, R.W. Moore, F.R. Buskirk, J.N. Dyer, and R. Pittman, Bull. Am. Phys. Soc. 22, 542 (1977), and to be published.
94. T. Suzuki, Nucl. Phys. A217, 182 (1973).
95. F.E. Bertrand and D.C. Kocher, Phys. Rev. C13, 2241 (1976).
96. S. Rahaman, M. Mizumoto, G.G. Slaughter, and R.L. Macklin, Phys. Rev. Letters 40, 1306 (1978).
97. M. Nagao and Y. Torizuka, Phys. Rev. Letters 30, 1068 (1973).
98. A. Bohr and B.R. Mottelson, private communication.

## DISTRIBUTION LIST

	No. Copies
1. National Science Foundation Division of Grants and Contracts Washington, D.C. 20550	2
2. Dr. William Rodney National Science Foundation Washington, D.C. 20550	1
3. Library Code 0142 Naval Postgraduate School Monterey, California 93940	2
4. Dean of Research Naval Postgraduate School Monterey, California 93940	2
5. Professor Fred Buskirk Department of Physics and Chemistry Naval Postgraduate School Monterey, California	8
6. Dr. Rainer Pitthan Department of Physics and Chemistry Naval Postgraduate School Monterey, California 93940	2
7. Professor K. E. Woehler Chairman Department of Physics and Chemistry Naval Postgraduate School Monterey, California	1
8. Defense Documentation Center Cameron Station Alexandria, Virginia 22314	2